CORROSION FATIGUE OF A MARINE ALUMINUM ALLOY (5456-H343) IN THE PRESENCE OF SHALLOW CRACKS.

Terrence L. Tinkel

SECURITY CLASSIFICATION OF THIS PAGE (When Data Entered)

REPORT DOCUMENTATION PAGE		READ INSTRUCTIONS BEFORE COMPLETING FORM
1. REPORT NUMBER	2. GOVT ACCESSION NO.	3. RECIPIENT'S CATALOG NUMBER
4. TITLE (and Subtitle) CORROSION FATIGUE OF A MARINE ALUMINUM ALLOY (5456-H343) IN THE PRESENCE OF SHALLOW CRACKS		5. TYPE OF REPORT & PERIOD COVERED THESIS
		6. PERFORMING ORG. REPORT NUMBER
7. AUTHOR(s) TINKEL, TERRENCE L.		8. CONTRACT OR GRANT NUMBER(s)
9. PERFORMING ORGANIZATION NAME AND ADDRESS MASS. INST. OF TECHNOLOGY		10. PROGRAM ELEMENT, PROJECT, TASK AREA & WORK UNIT NUMBERS
11. CONTROLLING OFFICE NAME AND ADDRESS Code 031 NAVAL POSTGRADUATE SCHOOL MONTEREY, CALIFORNIA, 93940		12. REPORT DATE JUN 78
		13. NUMBER OF PAGES 145
14. MONITORING AGENCY NAME & ADDRESS (if different from Controlling Office)		15. SECURITY CLASS. (of this report) UNCLASS
		15a. DECLASSIFICATION/DOWNGRADING SCHEDULE

16. DISTRIBUTION STATEMENT (of this Report)

APPROVED FOR PUBLIC RELEASE: DISTRIBUTION UNLIMITED

17. DISTRIBUTION STATEMENT (of the abstract entered in Block 20, if different from Report)

18. SUPPLEMENTARY NOTES

19. KEY WORDS (Continue on reverse side if necessary and identify by block number)

CORROSION FATIGUE, ALUMINUM ALLOY, SHALLOW CRACKS

20. ABSTRACT (Continue on reverse side if necessary and identify by block number)

SEE REVERSE

DD FORM 1 JAN 73 1473 EDITION OF 1 NOV 65 IS OBSOLETE
(Page 1) S/N 0102-014-6601 |

UNCLASS

SECURITY CLASSIFICATION OF THIS PAGE (When Data Entered)

CORROSION FATIGUE OF A MARINE ALUMINUM ALLOY (5456-H343) IN THE PRESENCE OF SHALLOW CRACKS

by

TERRENCE L. TINKEL
Lieutenant Commander, United States Navy

B.S., University of Oklahoma, (1967)

Submitted in Partial Fulfillment

of the Requirements for the Degrees of

Ocean Engineer

and

Master of Science in Materials Engineering

at the

Massachusetts Institute of Technology

June, 1978

CORROSION FATIGUE OF A MARINE ALUMINUM ALLOY (5456-H343) IN THE PRESENCE OF SHALLOW CRACKS

by

TERRENCE L. TINKEL

Submitted on May 12, 1978, to the Department of Materials Science and Engineering in partial fulfillment of the requirements for Master of Science Degree in Materials Engineering and to the Department of Ocean Engineering in partial fulfillment of the requirements for the Professional Degree, Ocean Engineer.

ABSTRACT

Marine aluminum alloy 5456-H343 is a candidate primary structural material for naval high performance ships. This material in the form of 1/8 inch sheet was used to obtain σ_i v N_f data in air and salt water. Room temperature tests were performed using deflection controlled fully reversed bending at 30 Hz. Data was obtained for smooth and shallow, sharply notched specimens for fatigue lives up to 1×10^7 cycles. Notches were semi-elliptical surface cracks with depths equal to .002 in., .0115 in., and .025 in. with a mean root radius of .0015 - .002 in.

5456-H343 showed excellent corrosion fatigue resistance in salt water, with increasing environmental sensitivity in the range of 10^6 - 10^7 cycles. The material exhibits some notch sensitivity at a fatigue life of 1×10^7 cycles. At this fatigue life notch sensitivity increases with increasing initial notch depth, and notch sensitivity is greater in salt water than in air.

Data analysis results suggest that an effective notch depth of .0005 in. can be attributed to a smooth specimen surface. A simple analytical and graphical analysis based on linear elastic fracture mechanics was used to obtain $d\ell/dn$ v ΔK_i data. Threshold stress intensities of 1.25 and 1 Ksi-$\sqrt{in}$ for air and salt water respectively were estimated at $d\ell/dn = 1 \times 10^{-9}$ in/cycle.

Results were used to develop the following fatigue design/failure criterion:

1. for shallow cracks less than .001 in. deep, the maximum fatigue stress is determined by endurance limit or fatigue strength of smooth specimens.

2. for shallow cracks greater than .020 in. deep, the maximum fatigue stress is determined by the threshold or allowable stress intensity factor of notched specimens.

Thesis Supervisor: Regis M. Pelloux

Title: Professor of Materials Engineering
Department of Materials Science
and Engineering

ACKNOWLEDGEMENTS

I would like to thank the U.S. Navy for sponsoring my studies at M.I.T. and specifically the Office of Naval Research for providing a grant for this work. I would like to thank Mr. Ernie Czyryca at the Naval Ship Research and Development Center, Annapolis, Md., for his help in providing the alloy material, background information, and technical assistance. The help of Mr. Robert Bausha of M.I.T. is appreciated for assistance in designing the notch machining tool and manufacturing the fatigue test specimens. I would like to thank Professor R. M. Pelloux, my thesis advisor, and Professor K. Masubuchi, my thesis reader. Finally, I would like to thank my wife, Carol, who, besides being a busy, working housewife and mother, found time to type the drafts of this work.

TABLE OF CONTENTS

LIST OF TABLES

LIST OF FIGURES

SI CONVERSIONS

1 inch (in.)	=	.0254 meter (m.)
1 pound (lb.)	=	4.448 Newton (N)
1 psi (lb./in.^{2})	=	7100 $\frac{N}{m^2}$ (Pa)
1 mil.	=	.0254 Millimeter (mm)
1 in.	=	.0254 x 10^6 micron (μ)

SYMBOLS

2a	surface length of cracks/notches
C	compliance
E(k)	elliptic integral of the second kind
k	elliptic integral parameter: $k = (1 - \frac{\ell^2}{a^2})$
k'	specimen spring constant in bending
K_t	theoretical stress concentration factor
K_f	fatigue notch factor
K	stress intensity factor
ΔK	stress intensity range
ΔK_i	initial stress intensity range
ΔK_{iALL}	Initial allowable stress intensity range
ΔK_{th}	threshold stress intensity range
ℓ	depth of surface crack/notch
ℓ_o	initial depth of surface crack/notch
$\frac{d\ell}{dn}$	crack propagation rate
M	applied beam bending moment
M_B	stress intensity magnification factor for front and back surface
n	cycles
N_f	cycles to failure
$N_f\|_s$	cycles to failure for smooth specimen
$N_f\|_{\ell_o}$	cycles to failure for a notched specimen with initial notch depth ℓ_o
$N_p\|_s^{\ell}$	cycles to propagate a notch/crack to a depth ℓ from a smooth surface condition
P	applied beam end load

q	notch sensitivity factor
R	stress ratio
r_p^*	plastic zone radius
s	surface width of cracks/notches at midpoint
t	specimen (sheet) thickness
x,y,z	coordinates for fatigue specimen geometry
x',y',z'	coordinates for notch geometry
δ	beam end deflection
ε_o	initial smooth specimen surface strain at test section
σ_o	initial smooth specimen surface stress at test section
σ	alternating surface stress
σ_i	initial alternating surface stress
σ_{iALL}	initial allowable alternating surface stress
σ_{END}	endurance limit
σ_Y	yield strength
ϕ	beam end rotation
γ_C	compliance correction parameter
γ_G	stress intensity correction parameter for front and back surface intensification
γ_P	stress intensity correction parameter for plastic zone size
γ	stress intensity correction parameter for surface intensification and plastic zone size

Note: Any symbols not listed here are explained in the text.

I. INTRODUCTION

A. Background

Series 5xxx aluminum-magnesium alloys are used in many ocean engineering applications because they exhibit high strength-to-weight ratios, high toughness, and good corrosion resistance in sea water. Additionally, these alloys are easy to form and can be readily welded.

Fatigue continues to be one of the most common causes of service failures in engineering equipment. The cyclic loads which are present in most ocean engineering applications are due to random forces from wind and sea and to periodic forces from installed propulsion and auxiliary equipment. Cyclic loading due to surfacing and submerging is an additional factor that must be considered in hull structural design of submersibles.

In ocean structures and in large displacement type ships which are not weight critical, fatigue service failures should normally be prevented by keeping the stress levels below the endurance limit. This approach cannot be used, however, for high performance ships which are weight critical. Such vehicles usually necessitate very efficient structural design; consequently, high stresses and low design margins are usually required. Under tnese design conditions a good understanding of the fatigue characteristics of the alloys to be used in the structure is required.

Any material selected for an ocean engineering application will normally have to be cut, formed, drilled, and welded before it becomes a permanent part of the structure. Thus, a finished product may contain flaws, cracks, or other defects introduced during material processing and fabrication. With some initial defects present at the beginning of service life, fatigue failure prevention becomes a process of controlling and limiting crack growth rather than preventing crack initiation.

Linear elastic fracture mechanics (LEFM) methods have been extensively and successfully applied to predict the service life of components where the components contain relatively long (deep) cracks (>.1 in.). For shallow (short) cracks or notches, however, the validity of the fracture mechanics methods has not been clearly demonstrated. A knowledge gap exists between the two basic fatigue design approaches:

1. design based on endurance limit of smooth or notched (K_f) specimens using σ v N_f data.
2. design based on fatigue crack growth from an initially sharp crack or defect using $d\ell/dn$ v ΔK data.

B. Purpose of Investigation

Since marine aluminum alloy 5456-H343 is a candidate material for application in naval high performance ships, it is mandatory to have good design data and a good

understanding of the performance of this material in a salt water environment. Czyryca [1] has compiled a summary of aluminum alloy fatigue information, including some data for 5456-H343. Chu [2] has obtained some data on crack propagation rate ($d\ell/dn$) versus stress intensity (ΔK) over a limited $d\ell/dn$ range from 7×10^{-7} to 2×10^{-5} in/cycle.

The aim of the present investigation was to extend and expand the fatigue information currently available for alloy 5456-H343. Specific objectives were:

1. to obtain σ v N_f data for both smooth and surface notched specimens in both air and salt water environments, with emphasis on shallow (short) surface cracks.
2. to develop additional $d\ell/dn$ v ΔK data for this material, with emphasis on shallow surface cracks and low crack growth rates.
3. to determine the threshold stress intensity factors.
4. to derive a fatigue design/failure criterion for components containing shallow surface cracks.

II. EXPERIMENTAL PROCEDURES

A. Material

1. 5456-H343 Aluminum Alloy

The material used in this investigation was in the form of 1/8" sheet and was provided by the Naval Ship Research and Development Center (NSRDC) in Annapolis, Md. It is the same material used for the testing conducted by Chu [2].

Temper designation H343 indicates the material is a special strain hardened and stabilized alloy with a low temperature anneal [3,4]. Degree of hardness is about half-way between the annealed and full hard condition.

Chemical composition and strength properties were available [2] and are summarized in Table 1:

Table 1

Chemical Composition and Strength Properties of Material under Investigation

5456-H343 Aluminum Alloy

Nominal composition weight %				.2% yield strength (ksi)	ultimate tensile strength (ksi)
Mg	Mn	Cr	Al	40.3	56.4
5.25	.8	.1	balance		

2. Heat Treatment and Surface Finish

All testing was accomplished using material in the as-received condition. This condition was selected since it represents the typical condition of the alloy following construction, except for weld metal and material in weld heat affected zones (HAZ).

Surface finish on the test specimens was essentially the same as the as-received material. The surface was slightly oxidized and contained light surface scratches and nicks. The specimens were wiped with acetone following manufacture to remove residual dirt and machining oil. Figure 1 shows the as-received material surface finish. Figure 2 shows the as-received material microstructure after polishing and etching.

B. Fatigue Specimens

1. Specimen Geometry

The specimen geometry used for all fatigue tests is shown in Figure 3. The dimensions and configuration of the specimen are the results of a design tradeoff. The main objective was to select a geometry, maximizing specimen end deflection (δ) for a given specimen surface stress, consistent with the fatigue machine limitations and the 1/8" thickness of the sheet material. Detailed considerations associated with selecting this geometry are given in Appendix A.

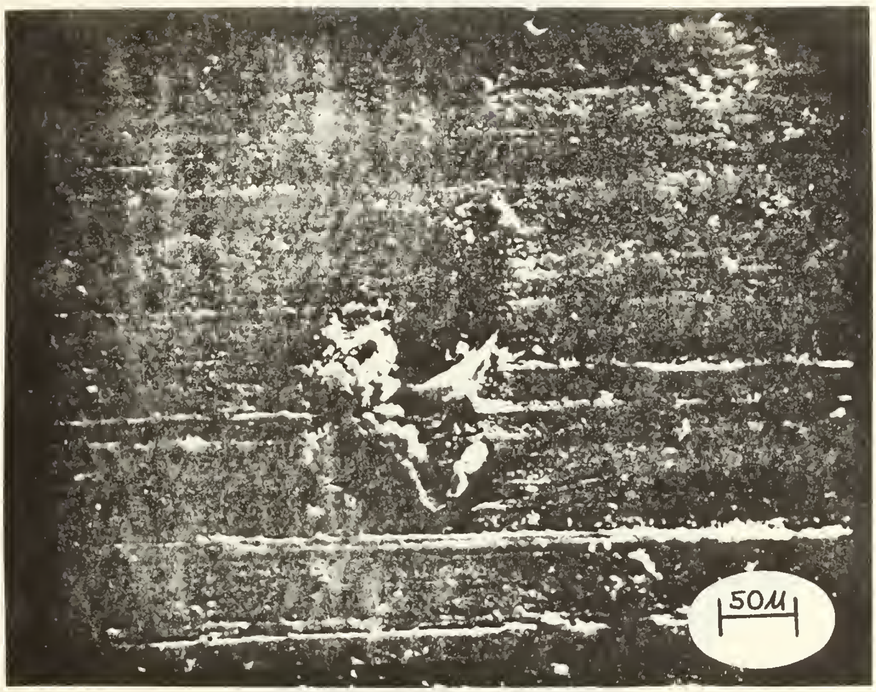

Figure 1: As-received material surface condition. Note mill marks and surface pit. 200X.

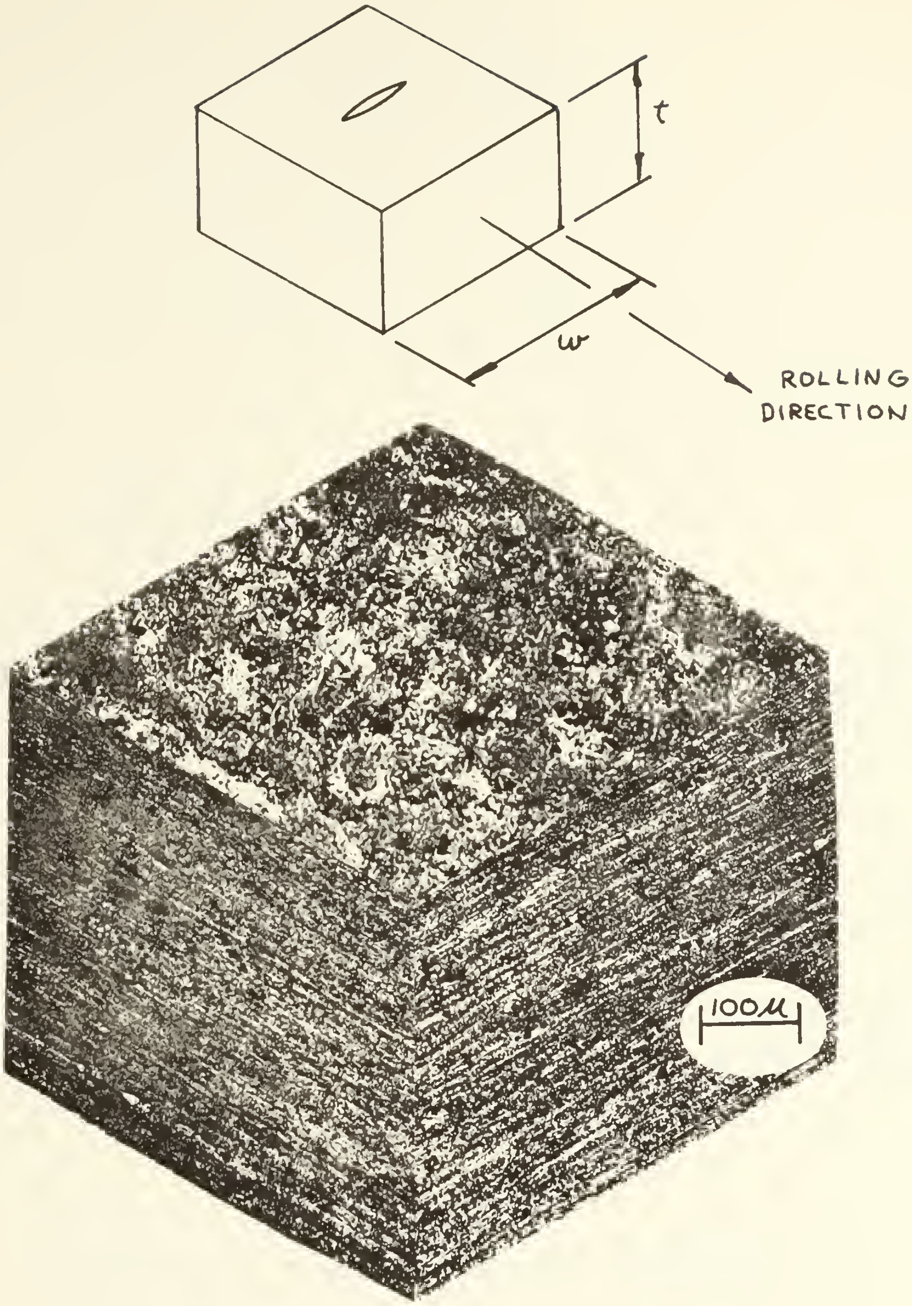

Figure 2: Composite photomicrograph of as-received material polished and etched (Keller's) to show microstructure on principal planes. 128X.

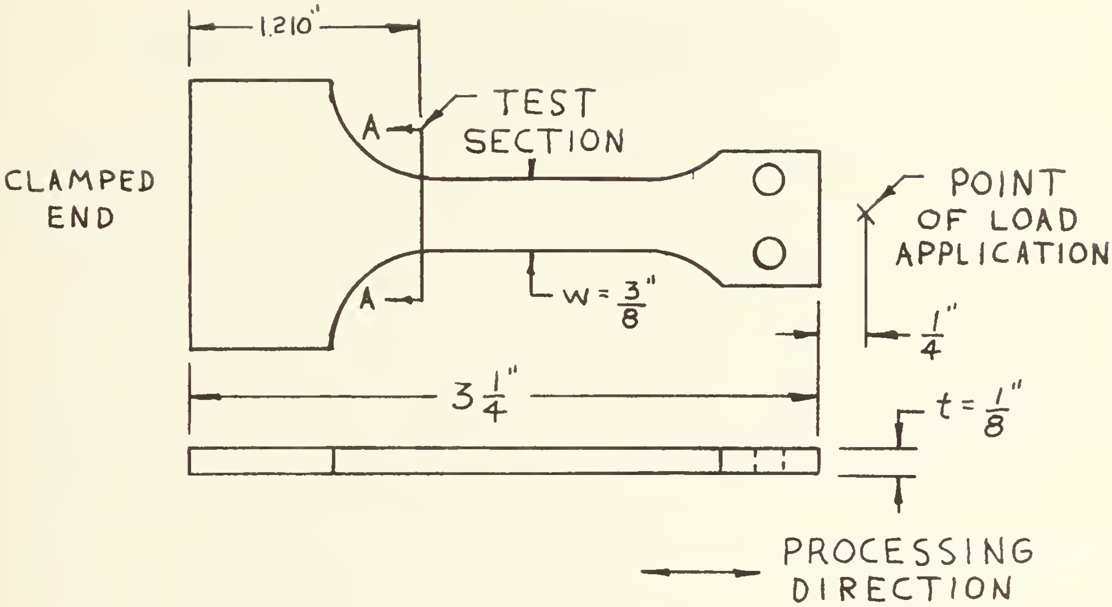

Figure 3: Fatigue specimen geometry

2. Material Processing Direction

Specimens were cut from the as-received sheet with the long specimen dimension parallel to the rolling direction. This orientation was selected so that fatigue cracks would grow in the short transverse direction (i.e., thickness direction) of the sheet.

3. Transverse Section of Maximum Stress

Because the specimen is a loaded cantilever beam, the bending moment increases with distance from the loaded end. The stress at a particular location then depends upon the applied moment, the cross-sectional area, and the distance from the neutral axis. Using information given in reference [5], the section of maximum stress (A-A in Figure 3) was located. This location is referred to throughout this report as the test section of the specimen. Calculations involved with locating the test section are given in Appendix C. All specimen stresses refer to the surface stress at this location, unless otherwise noted.

4. Machined Notches

For test runs aimed at investigating notch sensitivity of the material, sharp notches (cracks) were machined into one side of the specimen at the test section. The geometry of the machined notches is shown in Figure 4. This geometry

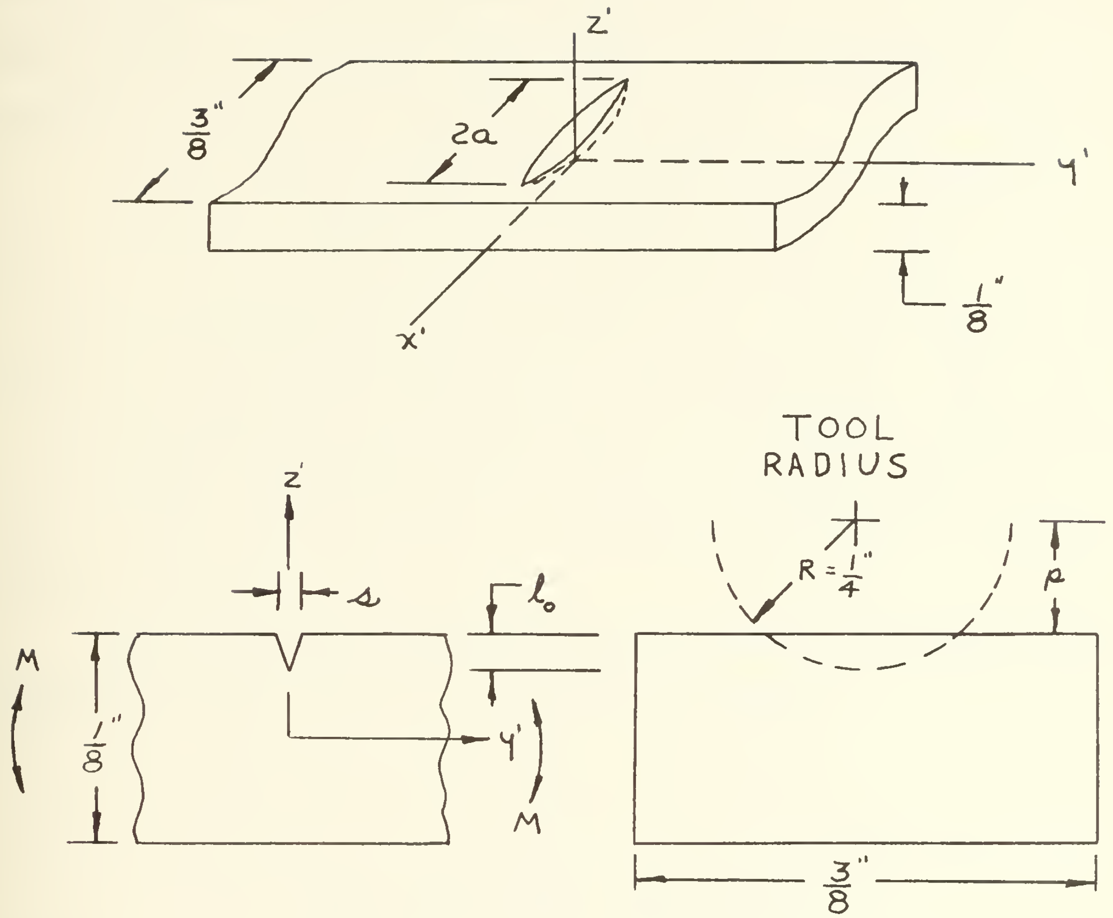

Figure 4: Machined notch geometry.

was selected because it approximates a semi-elliptical surface crack (notch), the characteristics of which have been studied extensively by various investigators [6-10]. Also, the machining method for introducing this notch configuration is quite simple. Various notch depths (ℓ_o) can be made with the same tool set-up by varying the dimension "p" in Figure 4.

Three different machined notch depths were used: ℓ_o = .002 in., .0115 in., and .025 in. For a given notch geometry, ℓ_o varies depending upon the location on the periphery of the semi-ellipse under consideration. For this investigation the depth dimension of interest is the depth $\ell_o = \ell(x'=0)$ measured at the mid-point of the semi-elliptical major axis.

The principal dimensions of the three machined notch configurations used are presented in Table 2.

Table 2

Machined Notch Dimensions

Notch depth (ℓ_o)	Surface width max. (s) in.	Surface length (2a) in.	Approximate root radius in.
.002"	.001	.063	.0015-.002
.0115"	.004	.150	.0015-.002
.025"	.009	.218	.0015-.002

The .002 in. depth is the minimum depth that could be machined within the accuracy of the machining method. The

.025 in. depth is the maximum depth that could be attained with the tool design while still maintaining the same notch geometry. The .0115 in. geometry was selected as an intermediate depth. Figure 5 compares the three machined notch depths (ℓ_o). Figure 6 shows the .025 in. machined notch. The machined root radius obtained for all notch depths is about .0015 - .002 in., which is very close to the initial objective of .001 in.

5. Notch Machining Method

Two methods for making the machined notches were considered: mechanical machining and electrical discharge machining (EDM). An initial group of specimens were manufactured with mechanically machined notches. A preliminary evaluation of the data from these specimens indicated that residual compressive stresses around the machined notch were introduced during the machining operation. The possibility of using EDM to form the notches was considered as a way of ensuring residual compressive stresses would not be introduced. However, EDM was rejected because it could not give a high degree of crack configuration reproducibility. Good reproducibility was considered essential to reduce data scatter and experimental error.

The method finally adopted for introducing notches was to use the same machining tool as was used in the original

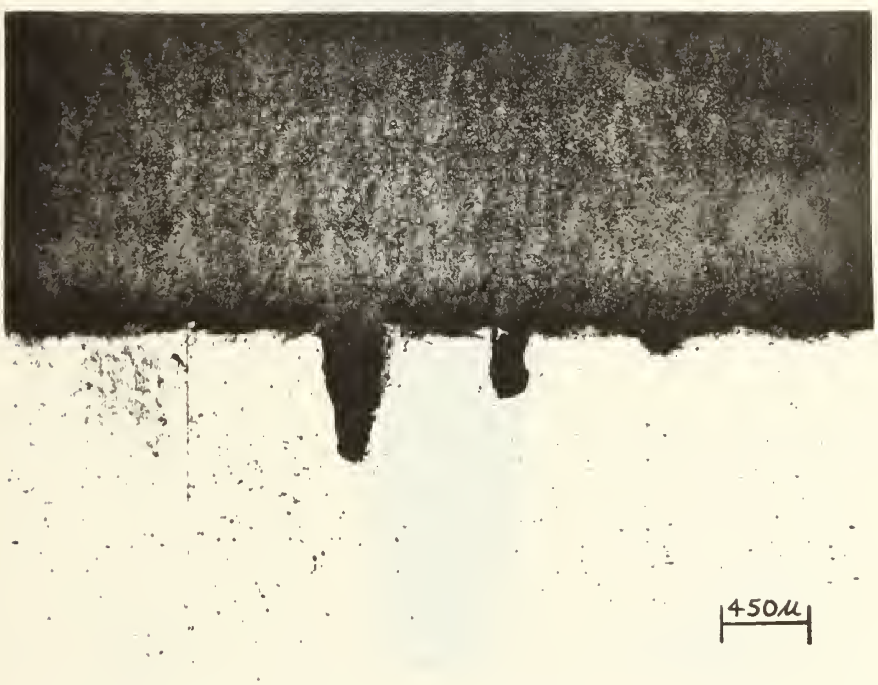

Figure 5: Comparison of machined notch depths. Left to right: .025 in., .0115 in., .002 in. 26X.

Figure 6: Deepest machined notch (.025 in.). Mean root radius is .0015 - .002 in. 128X.

method, but with a stepped rather than a continuous material removal procedure. Subsequent test results indicated the stepped procedure proved satisfactory. Details associated with the machining method finally selected are presented in Appendix B.

6. Fatigue Machines

All fatigue testing was performed using two identical machines similar to model CSS-40 manufactured by Fatigue Dynamics, Inc. The machines are constant displacement and constant speed (1750 - 1800 RPM). Displacement adjustments are made by positioning a cam which controls the connecting rod stroke. The connecting rod attaches to the unclamped end of the specimen. An automatic device shuts off the machine when the test specimen breaks. The connecting rod is configured so that the actual point of load application is 1/4-inch away from the end of the specimen (see Figure 3). The actual point of load application is not important if strain gages are used to set the initial stress level. But, location of this point is important if the stress is determined using end deflection measurements. Limitations and constraints of these machines are discussed further in Appendix A.

7. Determination of Initial Surface Stress

The load applied to the specimen depends upon the cam setting and the specimen compliance. Once the specimen

geometry is fixed, a calibration curve can be developed relating cam setting to stress. This approach was used for the first few test runs but was discarded in favor of strain gage measurements to improve test accuracy.

Strain gages were mounted at the test section on both the upper and lower surfaces of a smooth specimen. These gages were used to determine initial surface strain for a smooth specimen (ε_o) for a given end deflection (δ) using equation (1).

$$\varepsilon_o = \frac{\varepsilon_{max} - \varepsilon_{min}}{2} \tag{1}$$

Initial surface stress for a smooth specimen was calculated using

$$\sigma_o = E\varepsilon_o \tag{2}$$

where

$$E = 10.3 \times 10^6 \text{ psi}$$

Details associated with determining initial surface stress are presented in Appendix C.

8. Salt Water Apparatus

The artificial sea water solution (3.5% sodium chloride (NaCl) plus distilled water) for the corrosion fatigue tests was stored in a 5 gallon plastic bottle elevated a few feet above the fatigue machines. A felt wick, attached to the upper side of the specimen by plasticine, kept the specimen surface wet with salt water throughout a test. The solution flowed

from the bottle to the wick through 1/16 inch diameter plastic tubing. Clip valves attached to the tubing regulated the solution flowrate. The lower end of the tubing was mounted so that the solution would drip directly onto the wick. This arrangement proved to be simple and effective, and the operation of the automatic shut-off device on the machine was not restricted.

C. Test Procedure

The number of cycles to failure (N_f) were measured versus initial stress (σ_i) for both air and salt water at room temperature. For this investigation failure was defined to occur with complete specimen fracture.

A smooth specimen with strain gages attached was used to set the end deflection (δ) for a test. The necessary end deflection was obtained by adjusting the fatigue machine cam setting. Strain was read directly from a conventional strain indicating instrument in units of micro-inches. Once the required end deflection was attained, the cam setting was locked into position. The strain gaged specimen was removed and replaced by a specimen to be tested. After completing a series of tests at a particular stress level (cam setting), the strain gaged specimen was again installed to verify that the previous stress/strain setting had not changed.

The presence of a notch increases notched specimen compliance compared to a smooth (unnotched) one. The amount

of compliance change depends upon notch depth (ℓ_o). A compliance correction parameter (γ_c) was developed for various notch/crack depths. Selected values for γ_c are presented in Table 3. Details associated with determining γ_c are presented in Appendix C. The initial surface stress (σ_i) for a notched specimen was determined using

$$\sigma_i = \gamma_c \sigma_o \tag{3}$$

where

$$\gamma_c = \gamma_c[\ell_o]$$

Table 3

Compliance Correction Parameters (γ_c) for Machined Notch Geometry

ℓ_o	.002 in.	.0115 in.	.025 in.
ℓ_o/t	.016	.092	.200
γ_c	.992	.957	.909

All testing was planned to be accomplished in fully reversed bending with

$$R = \frac{\sigma_{min}}{\sigma_{max}} = -1 \tag{4}$$

The mean strain/stress was checked each time a strain gage reading was taken. Although initial mean strain was set at zero, subsequent measurements indicated some positive mean

strain was present during all testing. The amount measured varied from about 80 - 190 μ in., with 140 μ in. (144 psi stress) being a representative average. This amount of mean strain/stress was considered negligible for this investigation because a low tensile mean stress has little or no effect on fatigue crack growth rate in 5456 aluminum alloy [2].

For ease of observation and to facilitate application of salt water, all machined notch specimens were placed on test with the notched surface facing up. The presence of positive mean stress increased the local stress on the upper surface around the notch. This increased the propensity that crack initiation or initial crack propagation would occur at the test section on the upper surface.

Once a particular test was started, it was run until the specimen failed (i.e., broke) or until 1×10^7 cycles were reached. The range of initial surface stresses (σ_i) used for this investigation varied from 10 to 45 Ksi. The lower stress corresponds to the fatigue strength at 1×10^7 cycles in salt water. The upper stress is approximately yield for the material. Test frequency for the entire investigation was 30 Hz which corresponds to the normal 1800 RPM speed of the fatigue test machines.

A few of the specimens completing 1×10^7 cycles without failure were subjected to additional testing at a higher stress range of about 40 Ksi in air until failure. This exposed the fracture surface for subsequent examination and permitted

measurements to be made of crack propagation during the first 1×10^7 cycles. σ_i for these specimens was used to approximate fatigue strength at 1×10^7 cycles. Although aluminum does not strictly exhibit an endurance limit, fatigue strength at 1×10^7 cycles is reported as an endurance limit for this investigation.

III. RESULTS

A. Fatigue Tests

Results from σ_i v N_f tests conducted during this investigation are summarized in Figures 7 through 10. Results are for tests using smooth and machined notch (.002 in., .0115 in., and .025 in.) specimens in both air and a 3.5% NaCl solution. The stress (σ_i) used for plotting these curves is the initial alternating surface stress at the test section (section of maximum stress). Detailed curves presenting σ_i v N_f data are presented in Appendix D.

Endurance limit (fatigue strength at 1 x 10^7 cycles) was approximated using data from specimens completing 1 x 10^7 cycles without failure. A summary of these results is presented in Table 4.

Table 4

Endurance Limit - Ksi

(Fatigue Strength at 1 x 10^7 Cycles)

Notch depth (ℓ_o) / Environment	Smooth	.002 in.	.0115 in.	.025 in.
Air	19.2	18.5	15.3*	13.2
Salt water	15.2	13.7	11.3	10*

* Corrected value (see Appendix H for explanation).

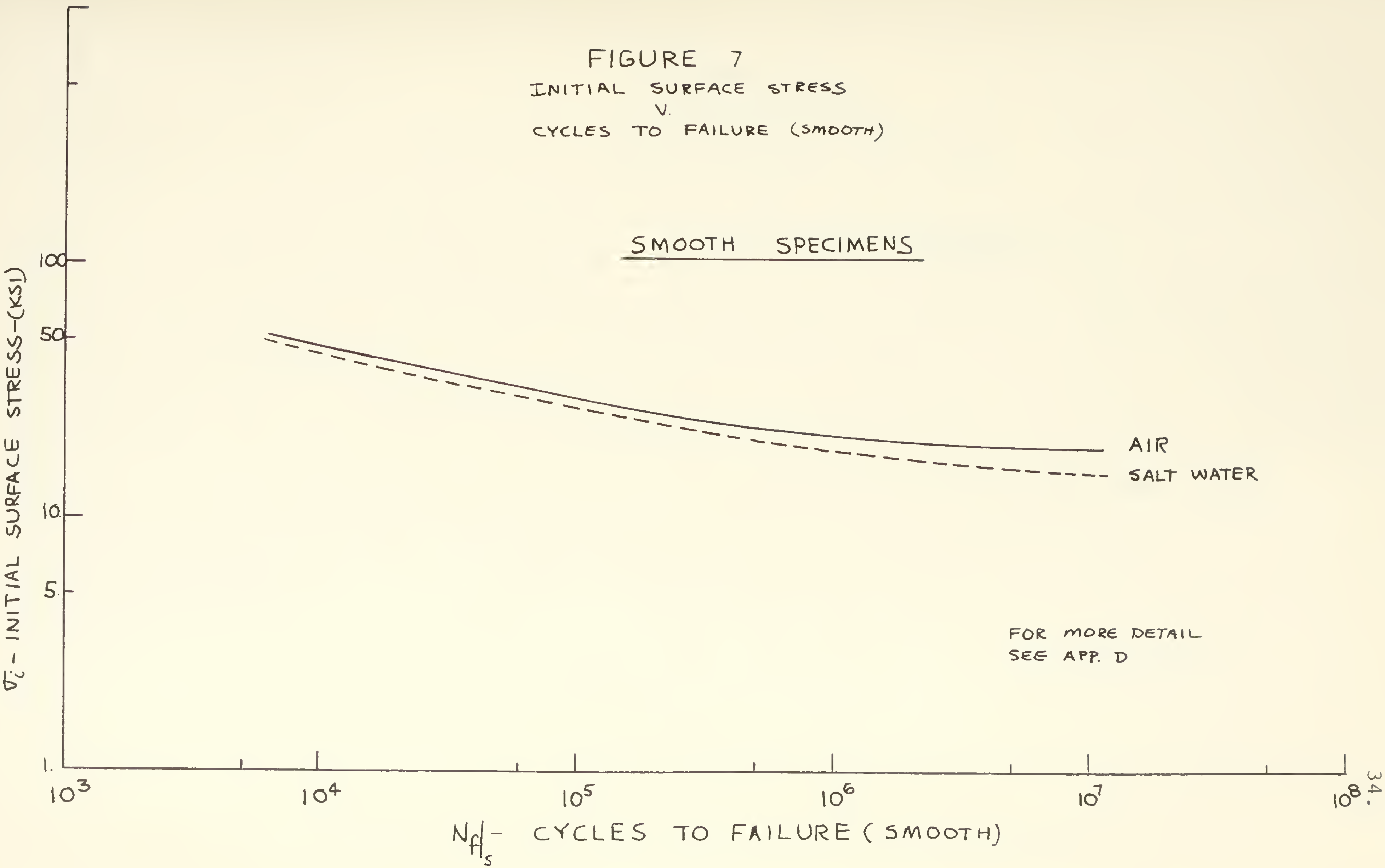

FIGURE 7
INITIAL SURFACE STRESS
V.
CYCLES TO FAILURE (SMOOTH)

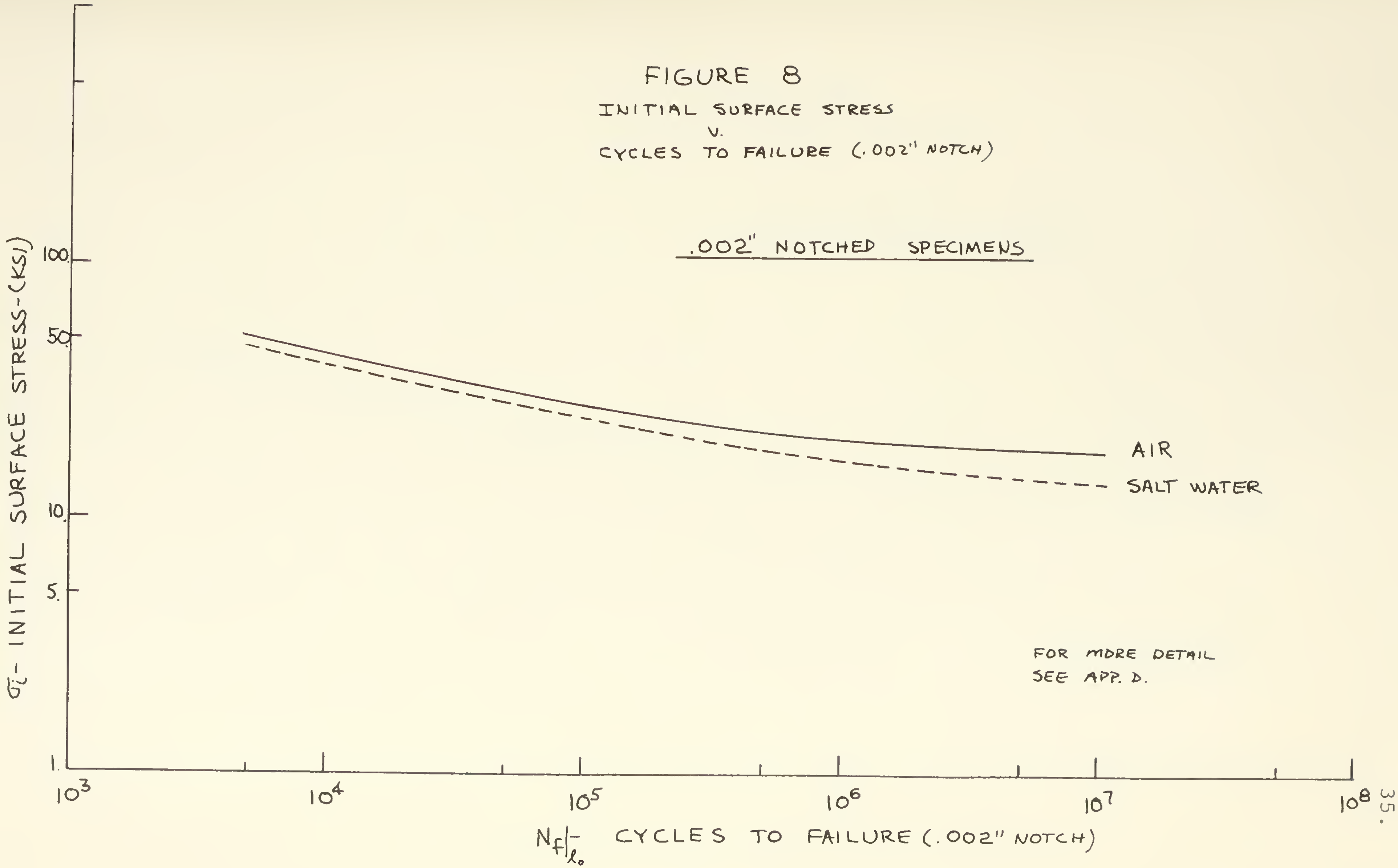

FIGURE 8

INITIAL SURFACE STRESS
v.
CYCLES TO FAILURE (.002" NOTCH)

FIGURE 9

INITIAL SURFACE STRESS v. CYCLES TO FAILURE (.0115" NOTCH)

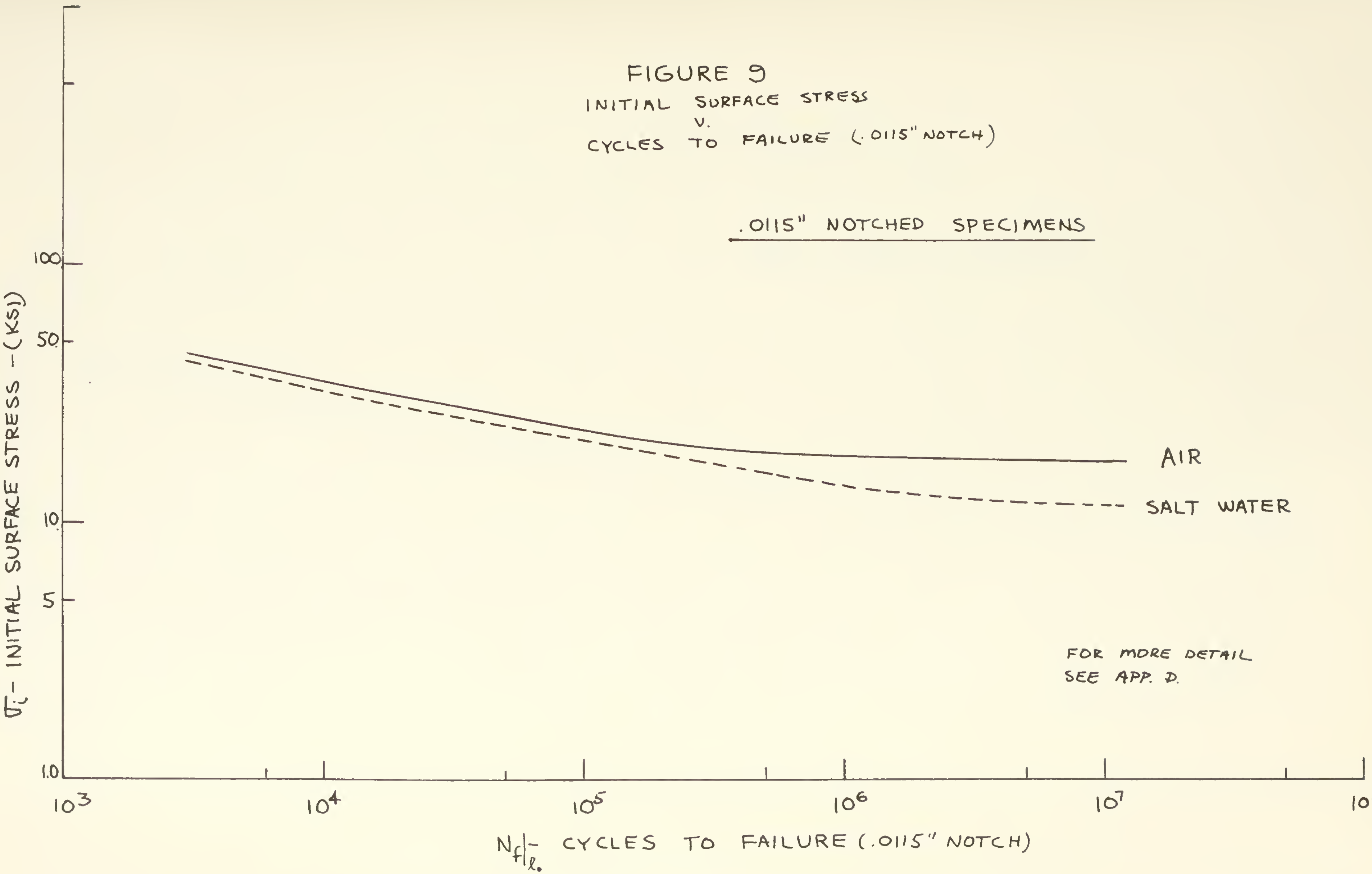

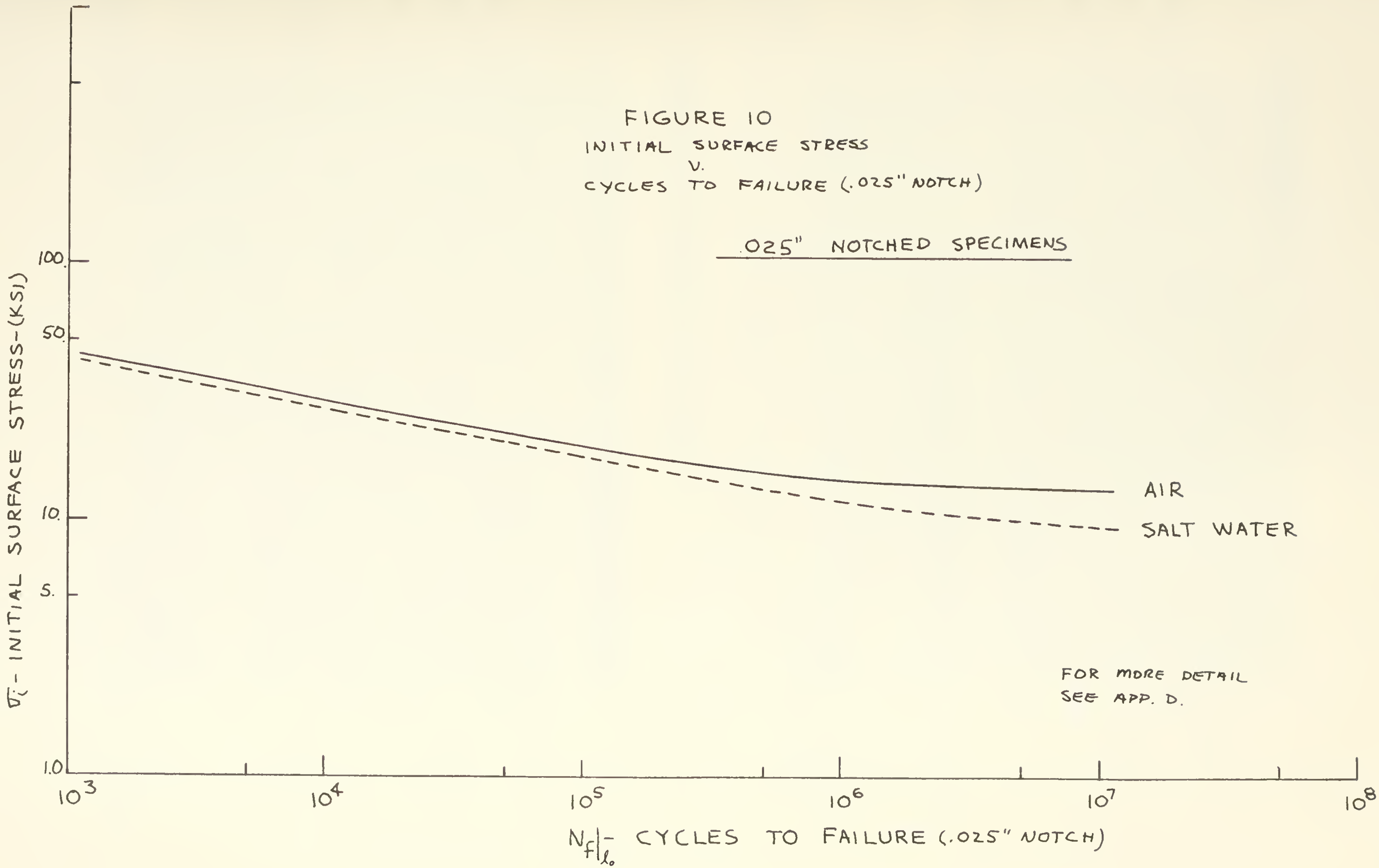

FIGURE 10
INITIAL SURFACE STRESS
v.
CYCLES TO FAILURE (.025" NOTCH)

B. SEM Examination

A number of failed test specimens were selected for examination using a scanning electron microscope (SEM). Specimens were selected from both air and salt water tests. The photographs in Figures 11 through 27 are representative of the various features observed on surfaces of failed specimens.

Information in Metals Handbook, Volume 10 [11] was used to guide examination of the fracture surface.

SEM examination provided a means of measuring cumulative crack growth that occurred during 1×10^7 cycles of testing. This information is presented in Appendix D.

C. Results of Test Data Analysis

1. Effective Notch Depth of Smooth Specimens

During data analysis, curves of ℓ_o v N_f were plotted for various constant values of σ_i between 20 and 45 Ksi. These curves suggest crack propagation started with a small, but finite, notch on the smooth specimens. This effective notch depth was graphically determined for each of the selected values of σ_i. For air tests the value of ℓ_o ranged from .00048 in. to .00072 in. For salt water tests ℓ_o ranged from .0006 in. to .001 in.

If an effective notch depth exists as suggested by the data, then it will be a function of the smooth specimen surface

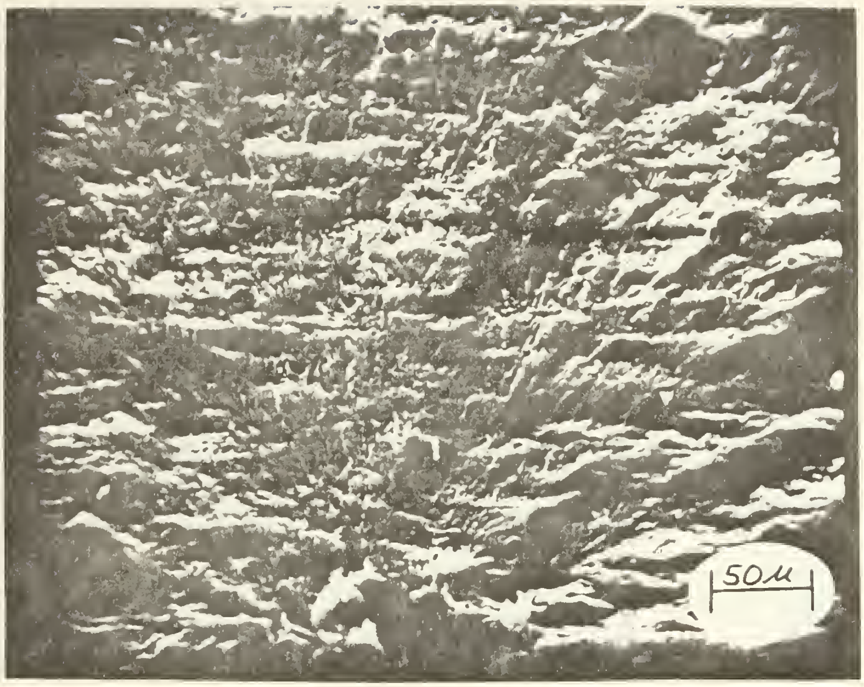

Figure 11: Fracture surface. Smooth specimen (air #115). σ_i = 20,137 psi. Natural notch depth (bottom center of photo) is .0015 in. 260X.

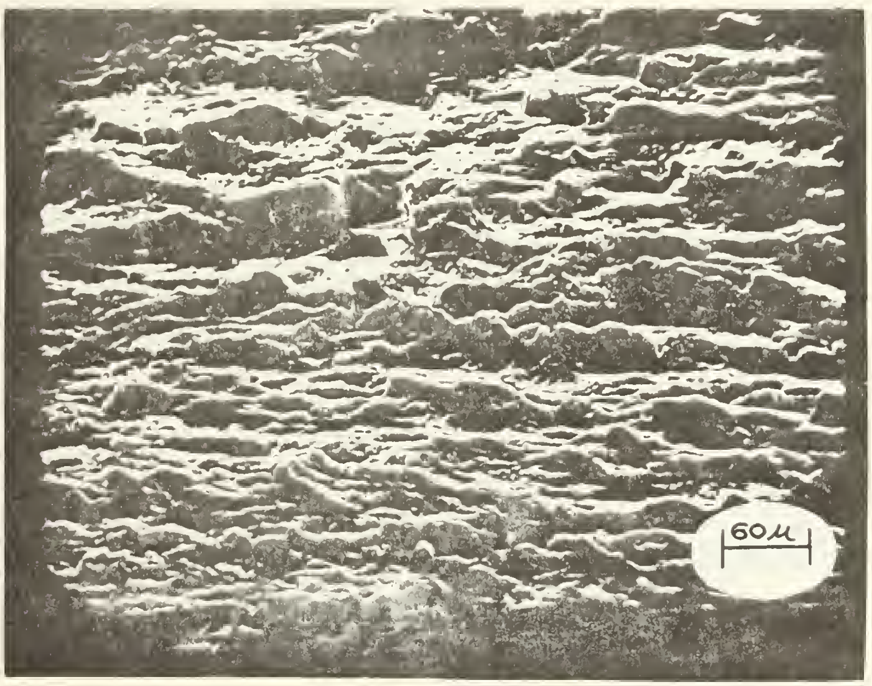

Figure 12: Fracture surface. Smooth specimen (salt water #87). σ_i = 20,240 psi. Natural notch depth (bottom center of photo) is .0003 in. 188X.

Figure 13: Fracture surface. Smooth specimen (air #16). σ_i = 17,768 psi. Note fatigue origin on specimen (lower edge middle) with diverging river marks. 20X.

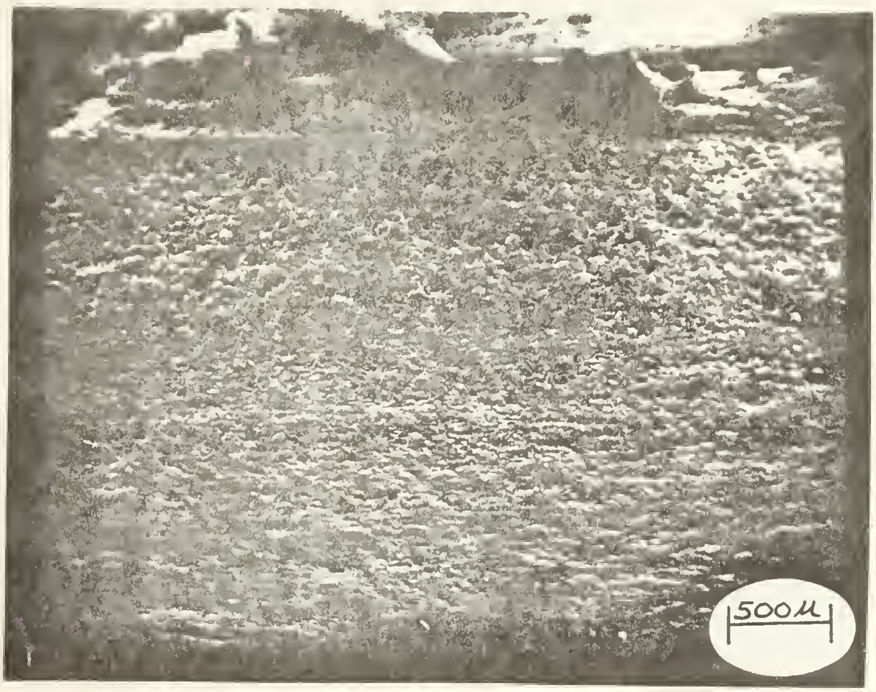

Figure 14: Fracture surface. Notched .002 in. specimen (air #48). σ_i = 21,713 psi. Notch on lower specimen edge. 26X.

Figure 15: Fracture surface. Notched .0115 in. specimen (salt water #69). σ_i = 11,947 psi. Note irregular surface indicative of multiple crack origins. 22X.

Figure 16: Fracture surface. Notched .0115 in. specimen (salt water #68). σ_i = 38,295 psi. Notch on specimen lower edge. Note river markings are obscured by corrosion product. 21X.

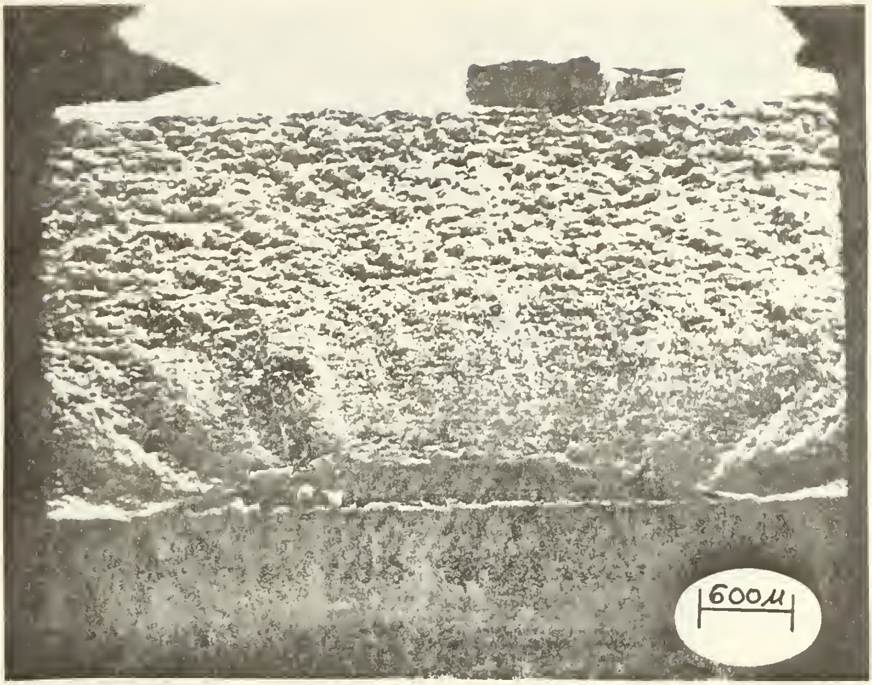

Figure 17: Fracture surface. Notched .0115 in. specimen (salt water/air #106). Completed 1.02×10^7 cycles at σ_i = 11,385 psi in salt water followed by 5.4×10^3 cycles at σ_i = 38,591 psi in air. Total crack propagation in 1.02×10^7 cycles $\cong$ .0035 in. 20X.

Figure 18: Fracture surface. Notched .025 in. specimen (air #109). σ_i = 36,375 psi. Transition from stage 2 fatigue propagation (smooth appearance) to ductile/ fast fracture (rough appearance). Transition occurred at ℓ = .052 in. 22X.

Figure 19: Fatigue striations (air #106). 5200X.

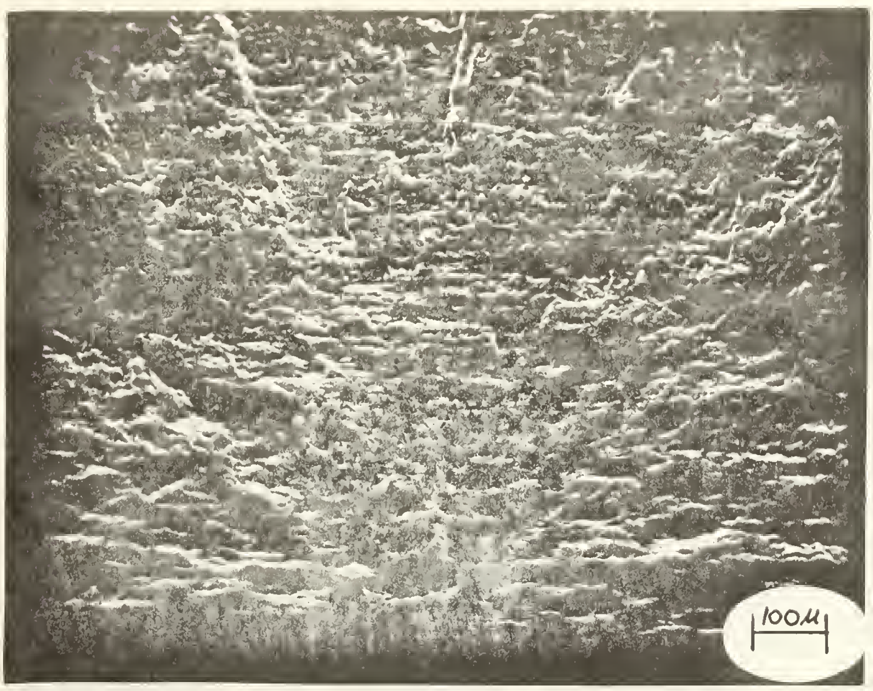

Figure 20: Fracture surface. Smooth specimen (air #16). Completed 1.27×10^7 cycles at $\sigma_i = 17{,}768$ psi in air followed by 7.8×10^3 cycles at $\sigma_i = 40{,}325$ psi. Total crack propagation in 1.27×10^7 cycles $\cong .013$ in. Depth of natural origin discontinuity is .0037 in. 100X.

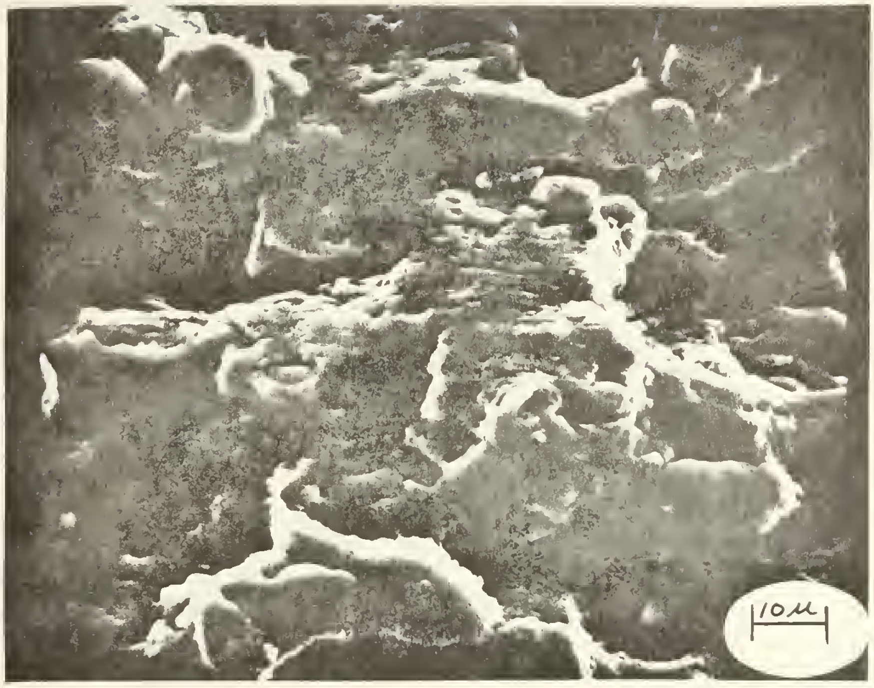

Figure 21: Fracture surface. Smooth specimen (air #114). Stage 2 crack propagation. Completed 9.89×10^6 cycles at σ_i = 19,004 psi in air followed by 1.65×10^4 cycles at σ_i = 40,325 psi. Total crack propagation in 9.89×10^6 cycles $\cong$ .0043 in. 1000X.

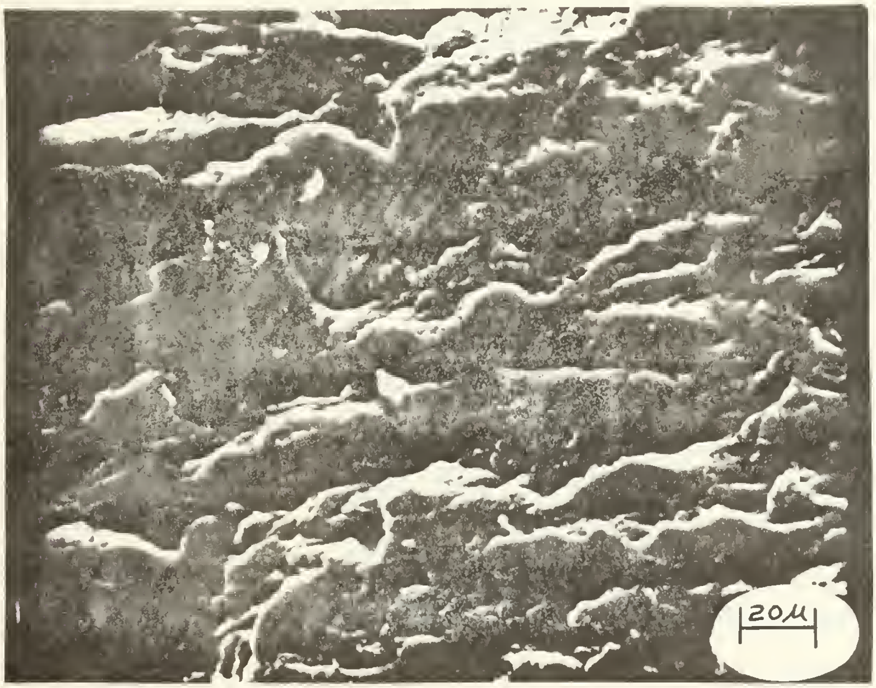

Figure 22: Fracture surface. Smooth specimen (salt water #87). σ_i = 20,240 psi. Stage 2 fatigue crack propagation. 500X.

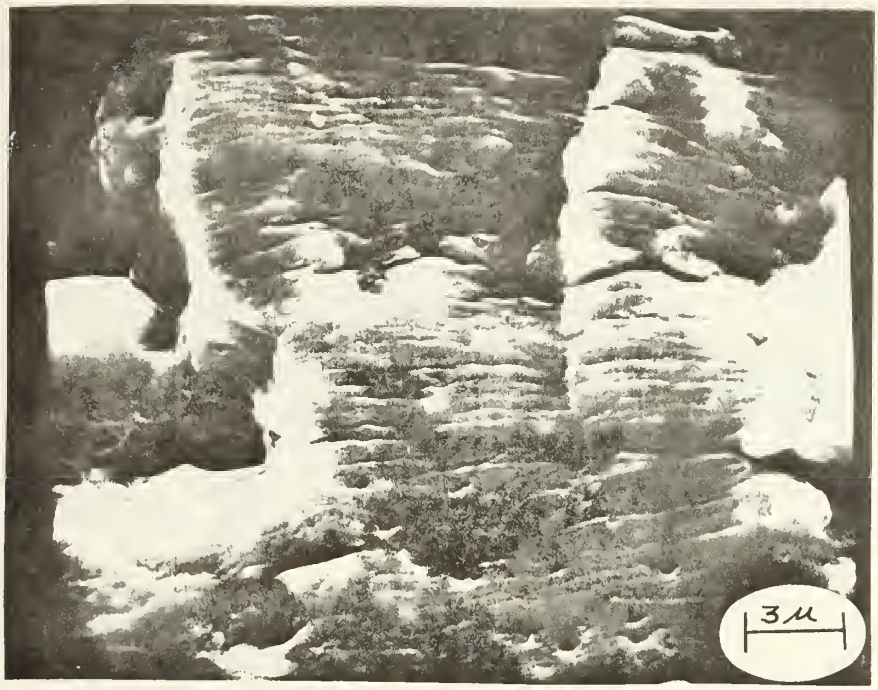

Figure 23: Fracture surface. Notched .025 in. specimen (salt water #94). Completed 1.02×10^7 cycles at σ_i = 9,410 psi in salt water followed by 2.5×10^3 cycles at σ_i = 36655 psi in air. Stage 2 fatigue crack propagation. Note striations. Total crack propagation in 1.02×10^7 cycles ≅ .001 in. 4300X.

Figure 24: Fracture surface. Notched .025 in. specimen (air #111). Completed 1.51×10^7 cycles at σ_i = 12,968 psi in air followed by 2.6×10^3 cycles at σ_i = 36,655 psi in air. Transition from stage 2 crack propagation to ductile/fast fracture. Total crack propagation in 1.51×10^7 cycles ≅ .0026 in. 1000X.

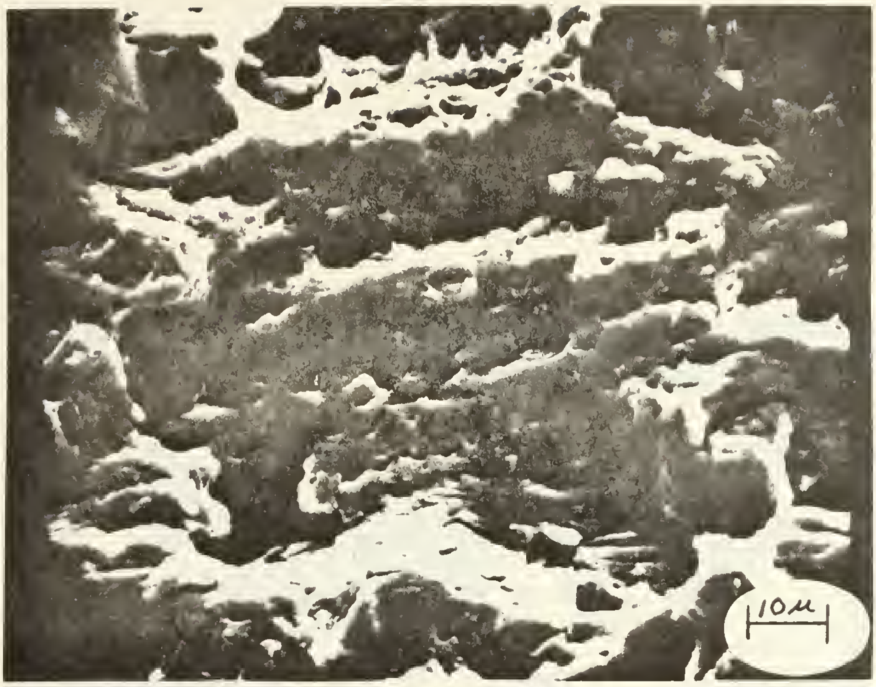

Figure 25: Fracture surface. Smooth specimen (salt water #89). σ_i = 40,016 psi. Transition from stage 2 fatigue propagation to ductile/fast fracture. 1040X.

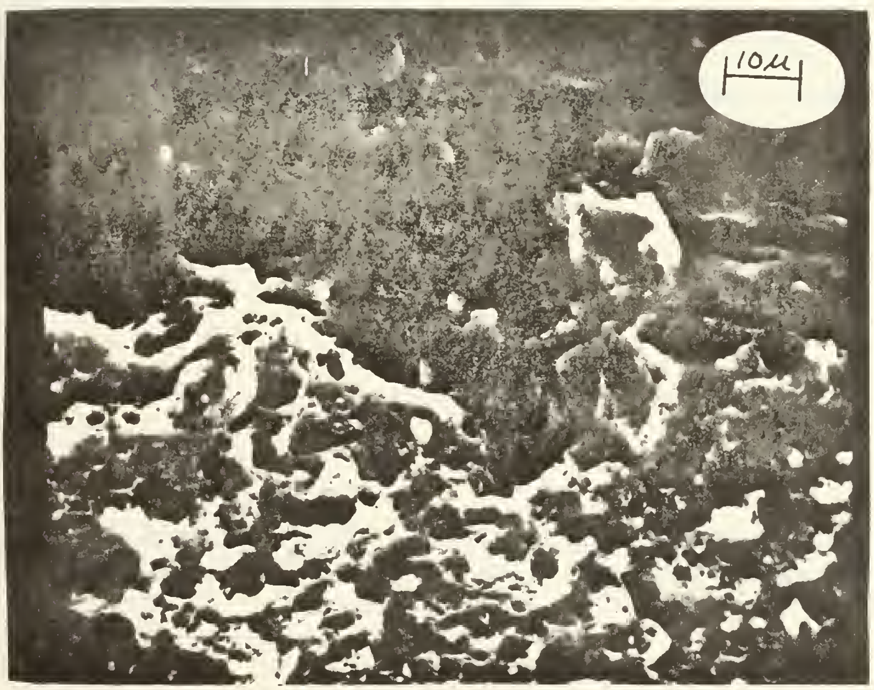

Figure 26: Fracture surface. Notched .002 in. specimen (salt water #74). σ_i = 22,019 psi. Transition from ductile/fast fracture to shear at base of shear lip. 1000X.

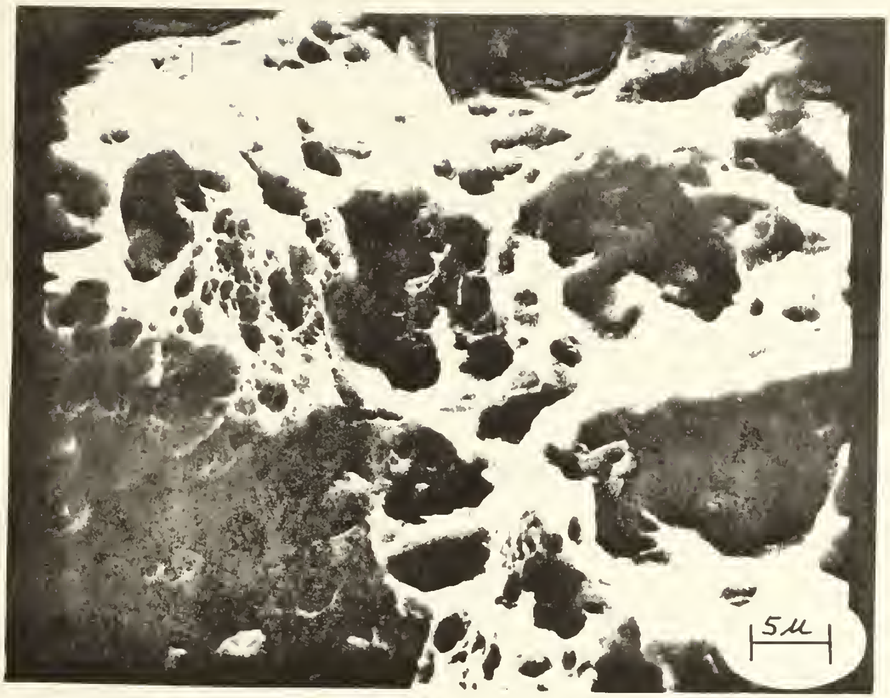

Figure 27: Fracture surface. Notched .025 in. specimen (air #112). σ_i = 13,763 psi. Ductile/fast fracture region. Note dimples and holes. 2050X.

finish. An ℓ_o value of .0005 in. was found to be representative of the smooth surface effective notch depth for this material and surface finish. Details associated with this determination are presented in Appendix E.

2. Notch Sensitivity

The theoretical stress concentration factor (K_t) was calculated for each of the machined notches using information collected by Peterson [12]. The data in Table 4 was used to calculate the fatigue-notch factor (K_f) for both air and salt water. Notch sensitivity at 1×10^7 cycles was then determined using equation (5), which is an expression taken from Dieter [13],

$$q = \frac{K_f - 1}{K_t - 1} \qquad (5)$$

where q is a notch sensitivity factor. Results are summarized in Table 5 and plotted in Figure 28.

Table 5

5.a Notch Sensitivity - Air

Notch depth / Factors	.002 in.	.0115 in.	.025 in.
K_t	3.54	3.71	4.00
K_f	1.038	1.255	1.455
q	.0150	.0941	.1517

FIGURE 28

NOTCH SENSITIVITY AND STRESS CONCENTRATION AND FATIGUE NOTCH FACTOR
V.
INITIAL NOTCH DEPTH

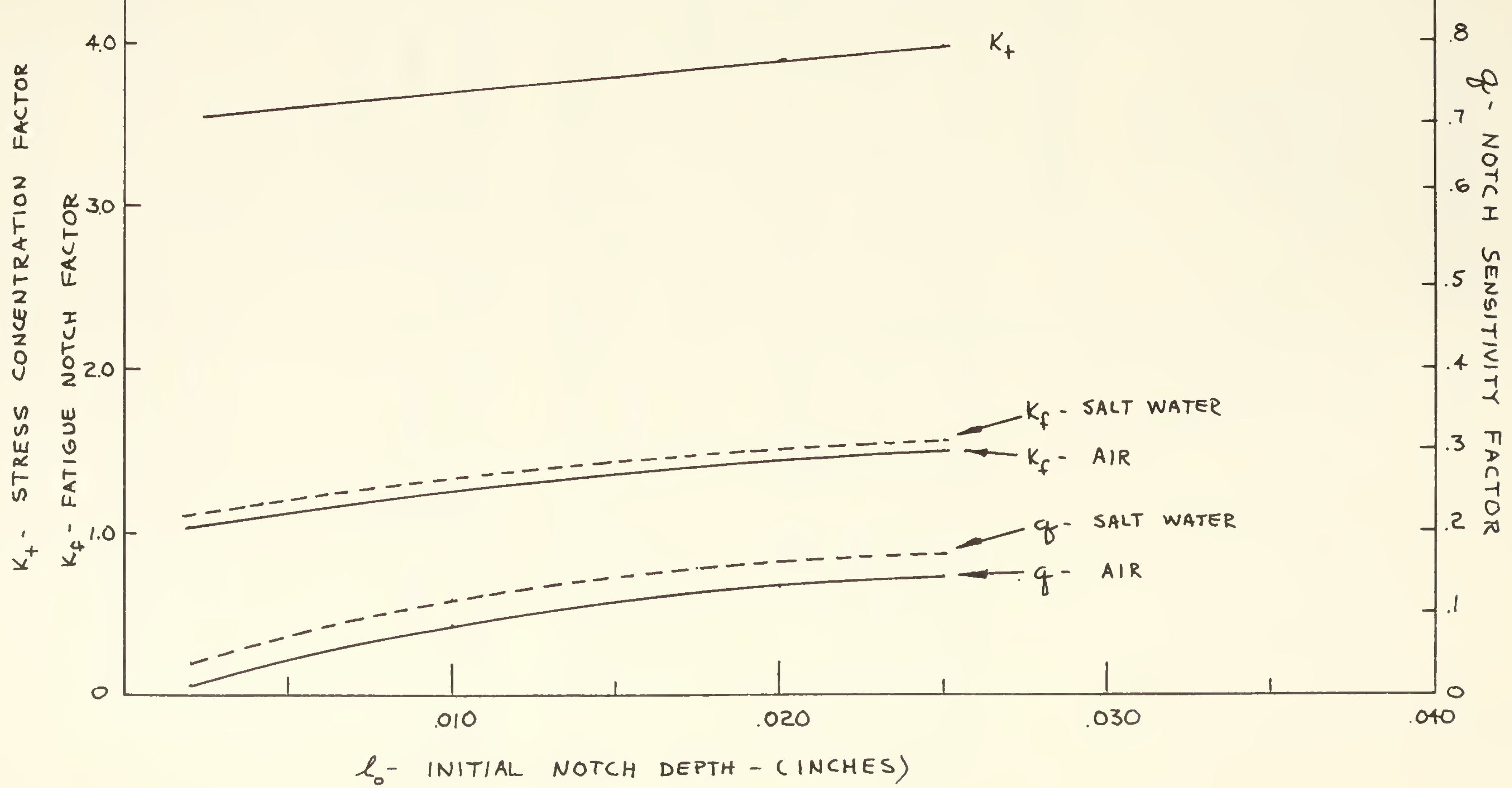

5.b Notch Sensitivity - Salt Water

Notch depth / Factors	.002 in.	.0115 in.	.025 in.
K_t	.354	3.71	4.00
K_f	1.110	1.345	1.520
q	.0433	.1273	.1733

3. Crack Propagation

The σ_i v N_f and N_f v ℓ_o data were used to develop crack propagation data σ_i v $N_p|_s^{\ell}$ where $N_p|_s^{\ell}$ is the number of cycles to propagate a crack from the smooth surface condition to a depth ℓ. Equation (6) was used to determine $N_p|_s^{\ell}$.

$$N_p|_s^{\ell} = N_p = n = N_f|_s - N_f|_{\ell_o} \qquad (6)$$

Plots of σ_i v N_p are presented in Figures 29 and 30 for air and salt water, respectively. Additional details are presented in Appendix F.

Fracture mechanics was then used to correlate the data. Values of $d\ell/dn$ were determined and associated stress intensity factors were calculated using

$$\Delta K_i = \gamma\sigma_i \sqrt{\pi\ell} \qquad (7)$$

σ_i rather than $2\sigma_i$ was used to calculate ΔK_i because crack propagation was assumed to occur only during the tension part of the cycle.

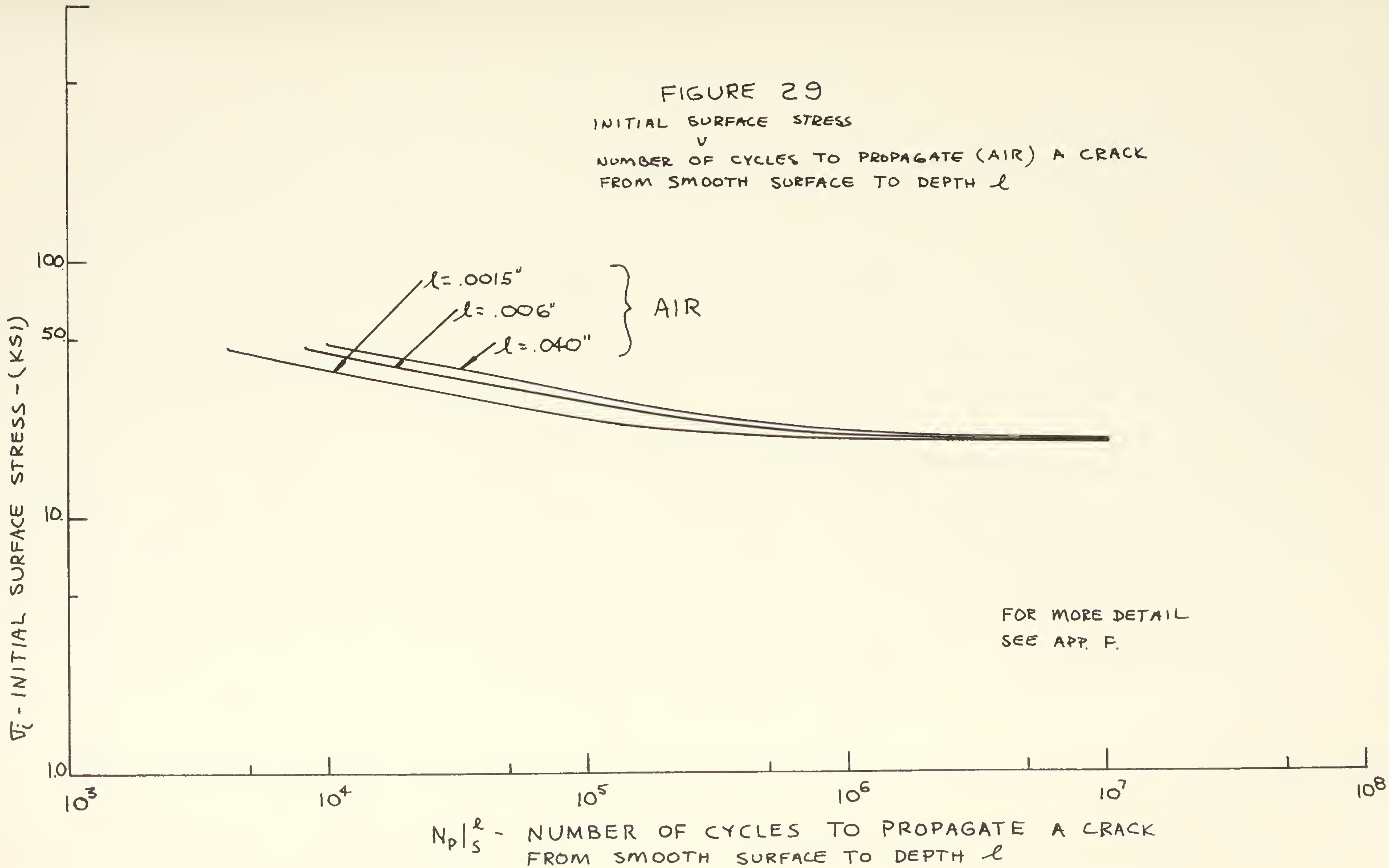
FIGURE 29
INITIAL SURFACE STRESS
V
NUMBER OF CYCLES TO PROPAGATE (AIR) A CRACK
FROM SMOOTH SURFACE TO DEPTH ℓ
ℓ = .0015"
ℓ = .006"
ℓ = .040"
AIR
FOR MORE DETAIL
SEE APP. F.
σi - INITIAL SURFACE STRESS - (KSI)
100.
50.
10.
1.0
10^3
10^4
10^5
10^6
10^7
10^8
Np|ℓ s - NUMBER OF CYCLES TO PROPAGATE A CRACK
FROM SMOOTH SURFACE TO DEPTH ℓ

FIGURE 30

INITIAL SURFACE STRESS
V.
NUMBER OF CYCLES TO PROPAGATE (SALT WATER) A CRACK FROM SMOOTH SURFACE TO DEPTH ℓ.

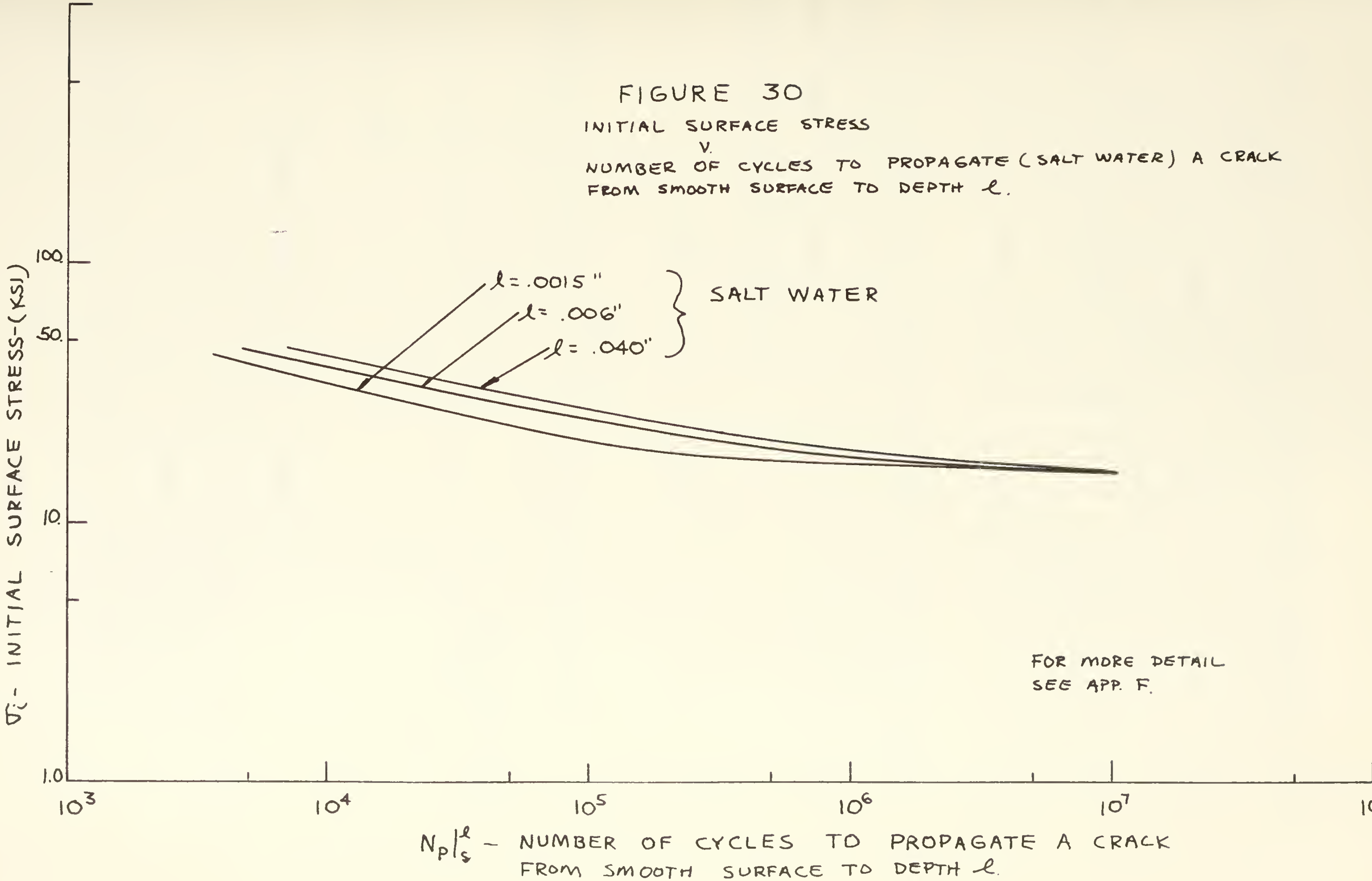

$d\ell/dn$ v ΔK_i was plotted. A safe crack propagation curve was drawn using the lowest value of ΔK_i for each value of $d\ell/dn$. Results are summarized in Figure 31 for air and salt water. Additional data concerning the fracture mechanics correlation are presented in Appendix F. Details associated with calculating stress intensities are presented in Appendix G. The crack propagation data reported by Chu [2] is indicated in Figure 31.

Equation (8) is a modified version of the Paris crack propagation law [14,15] and was used to describe the safe curves drawn in Figure 31. The empirical constants for this equation are given in Table 6.

$$\frac{d\ell}{dn} = A\,(\Delta K - \Delta K_{th})^n \tag{8}$$

Table 6

Empirical Constants for Crack Propagation Equation

	A(in/cycle)	n	ΔK_{th} (Ksi-$\sqrt{in}$)
air	1×10^{-7}	2.2	1.25
salt water	1.1×10^{-7}	2.6	1

4. Fatigue Design/Failure Criterion

The σ_i v N_f curves were used to develop ℓ_o v σ_i data for various constant values of N_f. Stress intensity factors corresponding to particular ℓ_o and σ_i values were also

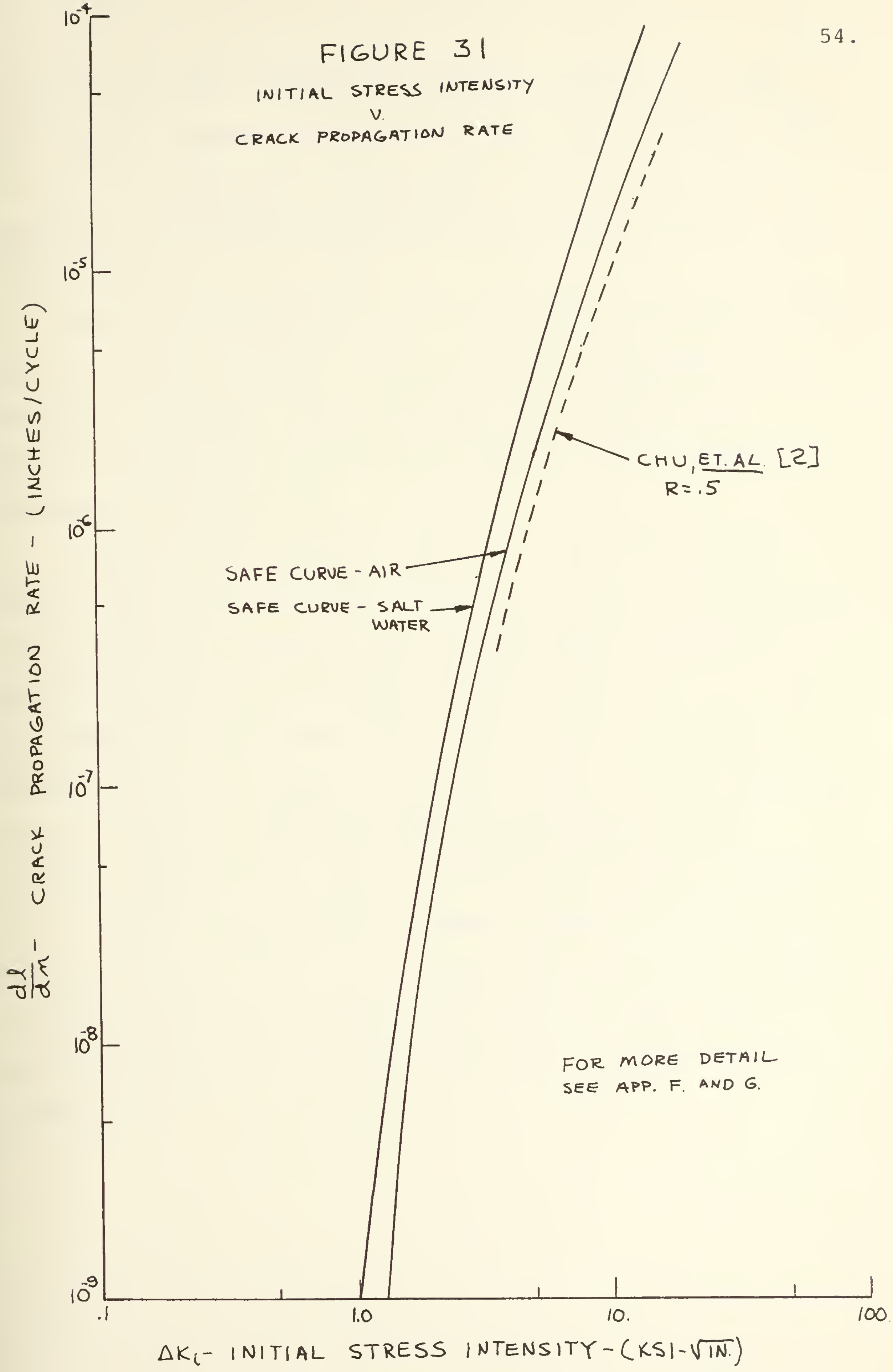
FIGURE 31
INITIAL STRESS INTENSITY
V.
CRACK PROPAGATION RATE
CHU, ET. AL. [2]
R=.5
SAFE CURVE - AIR
SAFE CURVE - SALT WATER
FOR MORE DETAIL SEE APP. F. AND G.
dl/dn - CRACK PROPAGATION RATE - (INCHES/CYCLE)
10^-4
10^-5
10^-6
10^-7
10^-8
10^-9
.1
1.0
10.
100.
ΔK_i - INITIAL STRESS INTENSITY - (KSI-√IN.)

calculated. This information was used to plot σ_i v ℓ_o and ΔK_i v ℓ_o for constant values of N_f equal to 5×10^3, 1×10^4, 1×10^5, 1×10^6, and 1×10^7 cycles. These curves are summarized in Figures 32 and 33 for air and salt water, respectively.

The curves show that σ_i is independent of initial notch depth ℓ_o for $\ell_o \lesssim .001$ in. and increasingly dependent for larger ℓ_o. Further, the curves show ΔK_i is independent of initial notch depth (ℓ_o) for $\ell_o \gtrsim .020$ in. and increasingly dependent for smaller ℓ_o.

These curves provide a convenient tool for fatigue design using this material. For $\ell_o \lessgtr .001$ in., the endurance limit concept for fatigue can be safely used to design for infinite life (non-propagating cracks). Also, for $\ell_o \lessgtr .001$ in., appropriate allowable fatigue strengths can be used to design for finite fatigue life (sub-critical crack propagation). For $\ell_o \gtrsim .020$ in., fracture mechanics threshold stress intensity (ΔK_{th}) can be used to design for infinite fatigue life. Further, appropriate allowable stress intensities can be used to design for finite fatigue life. Allowable fatigue strengths and stress intensities as well as other details associated with developing this criterion are presented in Appendix H.

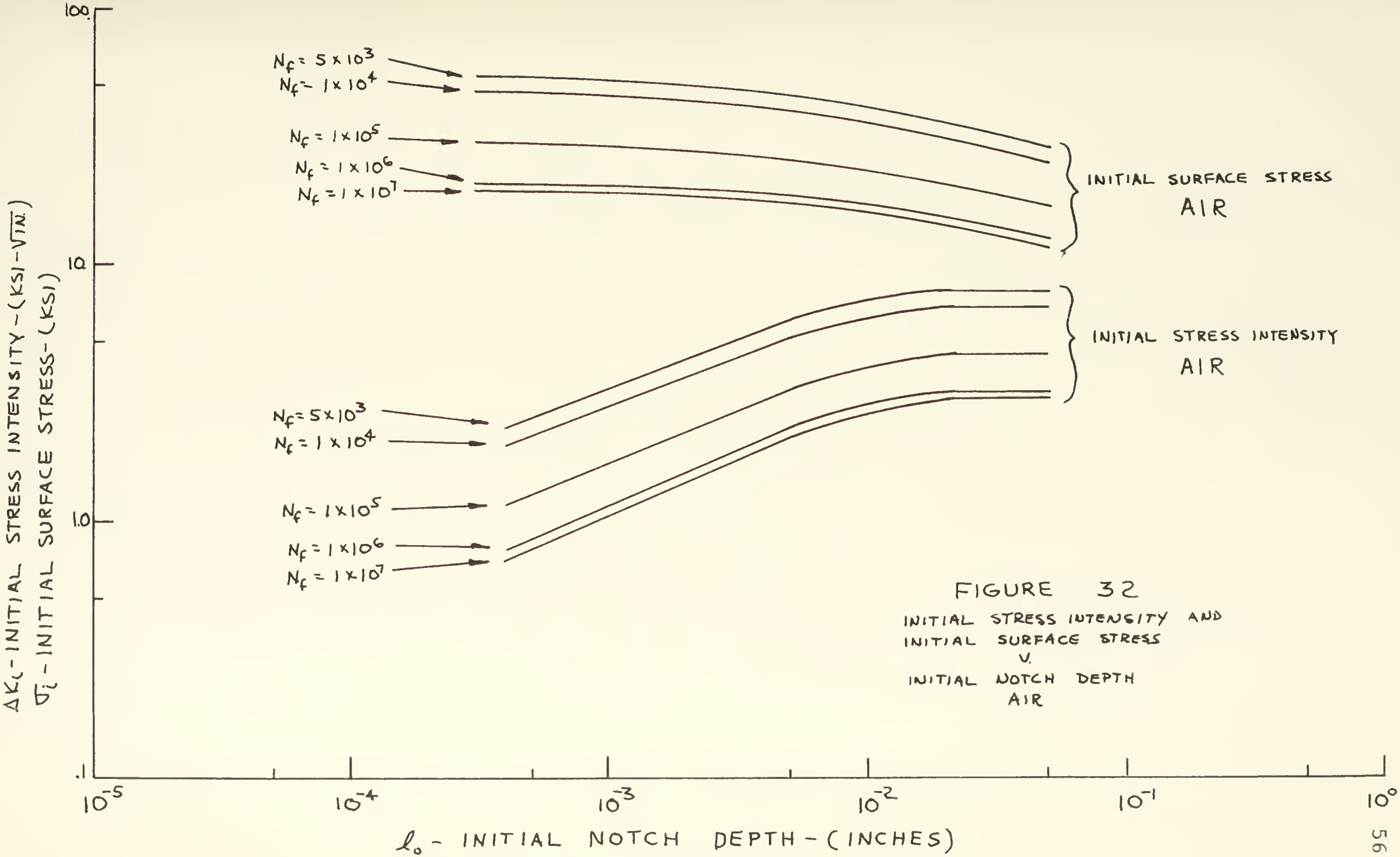

FIGURE 32

INITIAL STRESS INTENSITY AND
INITIAL SURFACE STRESS
V.
INITIAL NOTCH DEPTH
AIR

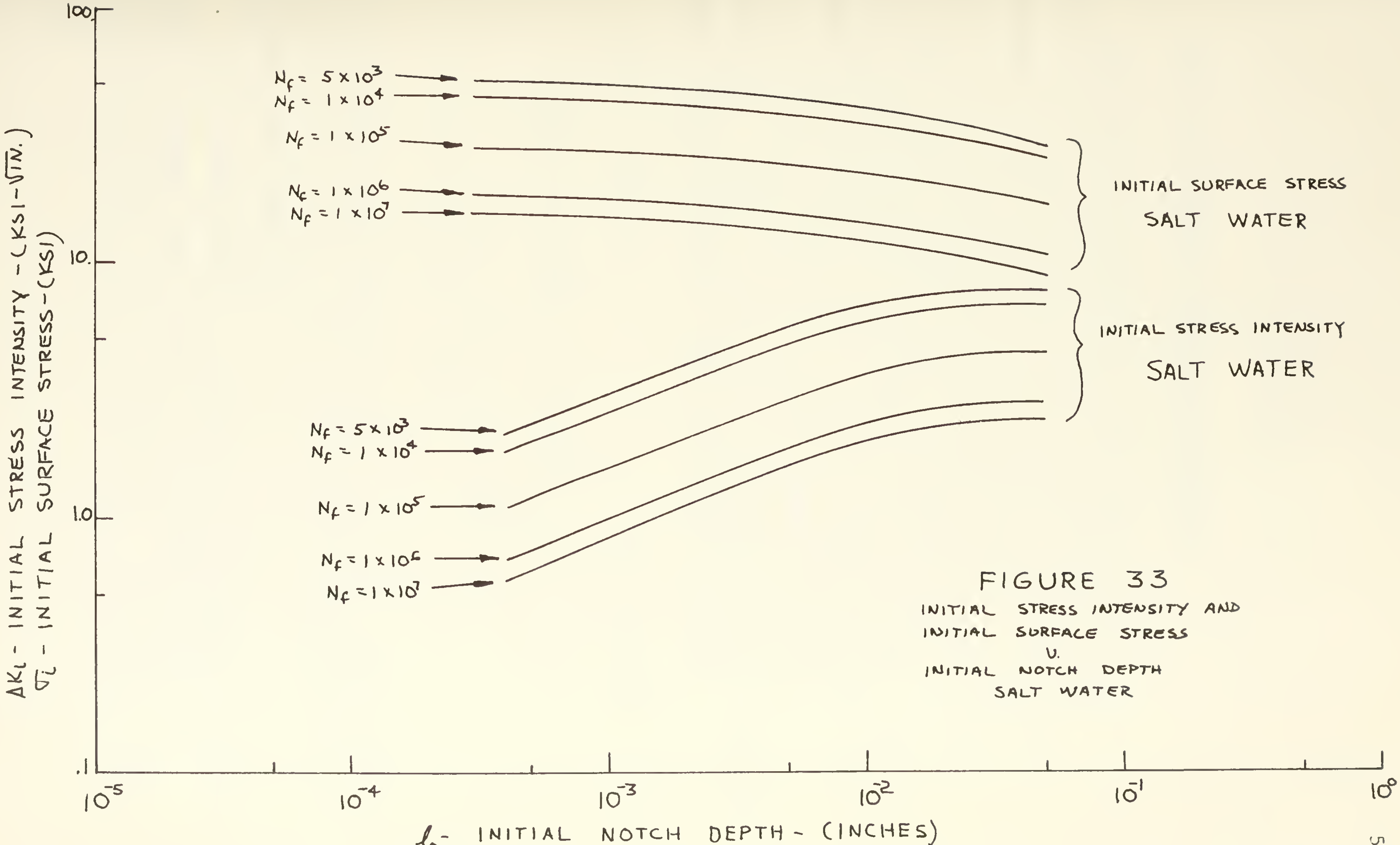

FIGURE 33
INITIAL STRESS INTENSITY AND
INITIAL SURFACE STRESS
v.
INITIAL NOTCH DEPTH
SALT WATER

IV. DISCUSSION

A. Notch Tip Residual Compressive Stress

Preliminary evaluation of data from the first set of machined notch specimens indicated the material becomes increasingly notch insensitive as stress (σ_i) is decreased below 30 Ksi. Specimens from this test series containing the deepest notch tested (.025 in.) completed over 1 x 10^7 cycles without failure at stresses as high as 20 Ksi. The possibility that test stress intensity factors were too low to promote crack growth was initially suggested as an explanation. Later, a method for calculating stress intensity factors was developed and used to analyze this case:

$$\ell_o = .025 \text{ in.} \qquad \sigma_o = 20 \text{ Ksi}$$

$$\Delta K_i = \sigma_i \gamma \sqrt{\pi \ell_o} = \sigma_o \gamma_c \gamma \sqrt{\pi \ell_o}$$

$$= (20)(.909)(.825)\sqrt{\pi(.025)}$$

$$= 4.2 \text{ Ksi} - \sqrt{\text{in.}}$$

Chu [2] provides an estimate of $\Delta K_{th} = 3.6$ Ksi - $\sqrt{\text{in.}}$ This analysis indicated that some other reason was responsible for this unexpected behavior.

As discussed earlier, additional investigation indicated residual stresses were present at the machined notch tip causing the apparent notch insensitivity. The initial notch

machining method was modified to incorporate a stepped material removal procedure as discussed in Appendix B. Subsequent test results indicated residual stress was reduced. However, whether all or the major portion was eliminated remains unknown. The care required for selecting a method of introducing specimen machined notches was clearly evident in this work. An additional point is that the initial set of machined notch test results confirm the already established fact that notch-tip compressive stress can substantially increase fatigue life.

B. σ_i v N_f Evaluation

As mentioned previously, fatigue tests performed for this investigation were deflection controlled. Consequently the stress present at the beginning of a test (σ_i) continually decreased with increasing crack growth because of increasing compliance. Initial stress was corrected to reflect the change based on initial notch depth (ℓ_o). However, no other corrections were made to compensate for additional changes that occurred as ℓ became larger than ℓ_o. If similar tests were performed under load rather than deflection control, shorter fatigue lives would be expected for the same initial stress (σ_i) because σ would not decrease over a test run.

Test results presented in Figures 7 - 10 show 5456-H343 alloy is somewhat sensitive to corrosive effects of NaCl solution. However, its corrosion resistance to fatigue is

considered quite good when compared to some other aluminum alloys, for instance 7075-T6. If similar tests were performed under load rather than deflection control, an increased sensitivity to corrosive environment would probably be observed. A reason for this is that stress around a crack would increase faster with increasing crack length under load control.

Data points for σ_i v N_f salt water tests show more scatter, in general, than the air tests. Thus, results and conclusions based on this data are subject to more error. The multiplicity of crack origins known to be a major feature of corrosion fatigue [11] may be a factor in this regard. The presence of multiple crack origins on surfaces of salt water tested specimens was observed during SEM examination as shown in Figure 15.

Data from two of the three machined notch geometries tested (.002 in. and .025 in.) show a decreased sensitivity to salt water corrosion at high stress (>40 Ksi). Substantial macroscopic plastic deformation associated with high stress amplitudes tends to limit environmental interaction [11]. Data from this work tends to confirm this observation.

C. Smooth Specimen Effective Notch Depth

The effective notch depth for smooth specimens suggested by ℓ_o v N_f for constant σ_i curves is partially confirmed with

SEM examination results. Figures 11, 12 and 20 show crack initiation sites on the surface of smooth specimens. Additionally, a small, randomly selected piece of the as-received material was used to obtain surface roughness data. Measurements were made over about 1 inch surface length. Depths of the larger surface notches observed ranged from .00015 in. to .0004 in. This is slightly lower than that predicted by the data, but not unreasonably so.

D. Crack Propagation Evaluation

Use of σ_i v N_f data and equation (6)

$$N_p = N_p\Big|_s^{\ell} = N_f\Big|_s - N_f\Big|_{\ell_o} \qquad (6)$$

to derive σ_i v $N_p\Big|_s^{\ell}$, where $N_p\Big|_s^{\ell}$ is the number of cycles to propagate a crack, is a simple and practical method to obtain crack propagation information. A primary advantage of this method is that quantitative crack propagation information can be determined from tests conducted on relatively inexpensive equipment. The alternative approach is to run direct crack propagation tests on expensive hydraulic test machines. A comparison of $d\ell/dn$ v ΔK_i data in Figure 31 with available data [2] suggest this approach provides reasonable accuracy for crack propagation rates between 10^{-5} - 10^{-6} in./cycle. But, the degree of accuracy achievable in the lower $d\ell/dn$ ranges cannot be confirmed without additional data becoming available.

One immediate source of error with this crack propagation analysis method is seen in Figures 29 and 30. The curves for all the various notch depths converge to the same point in the high cycle range (10^6 - 10^7 cycles). This is partially due to the experimental decision to limit test cycles to 1 x 10^7 or less to reduce time for data collection. Another reason is that equation (6) is quite susceptible to round-off error when $N_f|_s$ is large and $N_f|_{\ell_o}$ is small.

The stress intensity factor at the beginning of a test (ΔK_i) was used to attempt data correlation using $d\ell/dn$. Smooth specimen data was also used to facilitate correlation using ℓ_o = .0005 in. Correlation results are considered good, although apparent scatter was evident. Part of the scatter appears to be dependent upon the value of σ_i used to calculate ΔK_i. This dependency may be due to using a constant stress (σ_i) rather than a crack depth dependent stress (σ) for calculating ΔK.

The threshold stress intensity factor (ΔK_{th}) predicted by the air curve in Figure 31 of 1.25 Ksi-$\sqrt{in.}$ is less than 3.6 Ksi-$\sqrt{in.}$ estimated by Chu [2]. Possible contributing factors are:

1. the lowest $d\ell/dn$ values found in this work are two orders of magnitude lower than those reported by Chu.
2. deflection controlled, fully reversed bending rather than load controlled testing was performed in this work.

3. initial notch depths (ℓ_o) used in this work are much shorter than the 1.7 in. used by Chu.
4. accuracy of the analysis method used in this investigation, at least in the lower $d\ell/dn$ range required to approximate threshold stress intensity, remains to be validated.
5. σ_i rather than $2\sigma_i$ was used to calculate ΔK_i, and ΔK_i rather than ΔK was plotted against $d\ell/dn$.

The crack propagation equation (8) used to fit the $d\ell/dn$ v ΔK_i data should be used with some caution as discussed below:

$$\frac{d\ell}{dn} = A(\Delta K - \Delta K_{th})^n \tag{8}$$

ΔK depends upon both σ and ℓ. ℓ varies with crack propagation and σ may or may not change depending on loading conditions.

$$\Delta K = \sigma\gamma\sqrt{\pi\ell} \tag{9}$$

but

$$\sigma[\ell] = \gamma_c[\ell] \cdot \sigma_i \tag{10}$$

where $\sigma_i = \sigma[\ell=\ell_o]$ is a constant. For stress controlled situations $\gamma_c = 1$. Load control would require another correction not considered in this work.

Substituting (10) into (9) gives

$$\Delta K = \sigma_i\gamma_c\gamma\sqrt{\pi\ell} \tag{11}$$

Now substituting (11) into (8), rearranging, and integrating gives

$$n_f - n_o = \int_o^f \frac{d\ell}{A(\sigma_i \gamma_c \gamma \sqrt{\pi \ell} - \Delta K_{th})^n} \qquad (12)$$

To use equation (12), one must ensure that $\Delta K > \Delta K_{th}$ since the term in brackets breaks down mathematically if $\Delta K < \Delta K_{th}$. Physically, if $\Delta K < \Delta K_{th}$, $n_f - n_o \to \infty$ indicating a non-propagating crack situation. Values for A, ΔK_{th}, and n are given in Table 6. Methods for determining γ_c (deflection controlled case) and γ are given in Appendix C and G.

E. Design/Failure Criterion Evaluation

The curves in Figures 32 and 33 provide a design tool and suggest limitations for fatigue analysis.

1. For $\ell_o \leq .001$ in. Maximum initial stress ($\sigma_{i\ max}$) should be determined using smooth specimen data endurance limit or fatigue strength. Specifically:
   a. If $N_{required} \geq 1 \times 10^7$ cycles
      then $\sigma_{i\ max} \leq \sigma_{iALL} = \sigma_{iEND}$
   b. If $N_{required} < 1 \times 10^7$ cycles
      then $\sigma_{i\ max} \leq \sigma_{iALL}$
2. For $\ell_o \geq .020$ in. Maximum initial stress ($\sigma_{i\ max}$) should be determined using notched specimen data maximum initial stress intensity ($\Delta K_{i\ max}$).
   a. If $N_{required} \geq 1 \times 10^7$ cycles
      then $\Delta K_{i\ max} \leq \Delta K_{th}$
      and $\sigma_{i\ max} = \Delta K_{i\ max}/\gamma\sqrt{\pi \ell_o}$

b. If $N_{required} < 1 \times 10^7$ cycles

then $\Delta K_{i\ max} \leq \Delta K_{iALL}$

and $\sigma_{i\ max} = \Delta K_{i\ max}/\gamma\sqrt{\pi \ell_o}$

The values of γ are given in Appendix G. To further simplify (2a) and (2b) above, γ can be set equal to .93 for $\ell_o \geq .020$ in. to provide a lower bound on $\sigma_{i\ max}$.

V. SUMMARY AND CONCLUSIONS

1. σ_i v N_f data was obtained for 5456-H343 in air and in a 3.5% salt water environment. Room temperature fatigue tests were performed in fully reversed bending at 30 Hz on smooth and sharply notched specimens for fatigue lives up to 1 x 10^7 cycles. The notched specimens contained semi-elliptical shaped machined surface notches with depths of .002 in., .0115 in., and .025 in. and a mean root radius of .0015 - .002 in.
2. 5456-H343 shows excellent corrosion fatigue resistance in salt water, with increasing environmental sensitivity in the range of 10^6 - 10^7 cycles. Susceptiblity to corrosion is minimal at stresses above $\pm$ 40 Ksi. This is probably due to macroscopic plastic deformation and short fatigue life at high stress levels.
3. 5456-H343 is slightly notch sensitive for the range of shallow notches tested at a fatigue life of 1 x 10^7 cycles. The alloy is more notch sensitive in salt water than air. Notch sensitivity was found to increase slightly with initial notch depth for both air and salt water.
4. A fatigue crack propagation analysis technique provided $d\ell/dn$ v ΔK_i information over the range $10^{-8} < d\ell/dn < 10^{-5}$ in./cycle. Available $d\ell/dn$ v ΔK data from other investigators over the range $10^{-6} < d\ell/dn < 10^{-5}$ in./cycle are in agreement with the results of this work.

5. The crack propagation information obtained from the smooth (ℓ_o = .0005 in.) and machined notch (.002 in., .0115 in., and .025 in.) specimens can be correlated using linear elastic fracture mechanics. Some of the scatter in the data is most likely due to experimental error, but most of the scatter appears to be dependent upon the value of σ_i used to calculate ΔK_i. This may be a result of using a constant stress (σ_i) rather than a crack depth dependent stress (σ) to calculate stress intensity for correlation.

6. The threshold stress intensity value of ΔK_{th} = 1.25 Ksi-$\sqrt{in.}$ predicted by the $d\ell/dn$ v ΔK_i plots for air is less than the ΔK_{th} = 3.6 Ksi-$\sqrt{in.}$ estimated in other available work. Additional data will be required to determine the correct value of ΔK_{th}.

7. A fatigue design/failure criterion for propagating and non-propagating cracks was developed. For $\ell_o \lesssim .001$ in., the endurance limit concept for fatigue should be used to design for infinite life (non-propagating cracks). Additionally, appropriate allowable fatigue strengths can be used to design for finite life (propagating cracks). Endurance limit and allowable fatigue strengths are determined from smooth specimen data. For $\ell_o \gtrsim .020$ in. the fracture mechanics threshold stress intensity factor should be used to design for infinite life. Appropriate allowable stress

intensity factors can be calculated to design for finite life. Threshold and allowable stress intensity factors are determined from notched specimen data.

VI. RECOMMENDATIONS FOR FURTHER WORK

1. Additional σ_i v N_f testing should be done to investigate factors not evaluated in this investigation. Specifically, the effects of the following factors should be investigated.
    - a. Mean stress
    - b. Microstructure
    - c. Surface finish
    - d. Load versus deflection control.
2. $d\ell/dn$ v ΔK testing should be conducted using shallow cracks to check the low range (1×10^{-8} to 1×10^{-9} in./cycle) validity of the crack propagation analysis technique used in this work and to check the accuracy of threshold stress intensities estimated from this information.
3. The fatigue design/failure criterion developed in this work should be re-evaluated to incorporate the results of the additional work proposed in (1) above.
4. Additional work should be performed to identify analytical/empirical expressions for the fatigue design curves developed in this work.

REFERENCES

1. Czyryca, E. J., et al., "A Compilation of Fatigue Information for Aluminum Alloys", NSRDC Report 3856, (June 1973).

2. Chu, H. P., et al., "Fatigue-Crack Propagation in Aluminum-Alloy Stiffened Panels under Uniform Lateral Loading", Paper D-23 presented at the 1977 SESA Meeting, Dallas, Texas, (15-20 May 1977).

3. Aluminum Standards and Data, published by the Aluminum Association, (1976).

4. "A Guide for the Selection and Use of Aluminum Alloys for Structure of Ships of the United States Navy", NAVSHIPS 0900-029-9010, Naval Ship Engineering Center, (July 1971).

5. McClintock, F. A., "A Criterion for Minimum Scatter in Fatigue Testing", Paper No. 55-APM-26 presented at the National Applied Conference (ASME), Troy, New York, (16-18 June 1955).

6. Collipriest, J. E., Jr., "An Experimentalist's View of the Surface Flaw Problem", The Surface Crack: Physical Problems and Computational Solutions, presented at the Winter Annual ASME Meeting, New York, New York, (26-30 November 1972).

7. Shah, R. C., and Kobayashi, A. S., "On the Surface Flaw Problem", The Surface Crack: Physical Problems and Computational Solutions, presented at the Winter Annual ASME Meeting, New York, New York (26-30 November 1972).

8. Burck, L. H., "Fatigue Growth of Surface Cracks in Bending", Engineering Fracture Mechanics, 9, (1977).

9. Rice, J. R., and Levy, N., "The Part-Through Surface Crack in an Elastic Plate", Journal of Applied Mechanics, (March 1972).

10. Smith, F. W., and Sorensen, D. R., "The Semi-elliptical Surface Crack - A Solution by the Alternating Method", International Journal of Fracture, 12 (1976).

11. Metals Handbook, 10, ASTM.

12. Peterson, R. E., Stress Concentration Factors, John Wiley and Sons, New York, (1974).

13. Dieter, G. E., Mechanical Metallurgy, McGraw-Hill, (1976).

14. Paris, P. C., in Proceedings, 10th Sagamore Army Materials Research Conference, Syracuse University Press, (1964).

15. Chu, H. P., "Effect of Mean Stress Intensity on Fatigue Crack Growth in 5456-H117 Aluminum Alloy", ASTM STP 559, (1974).

16. McClintock, F. A., "Check List for Bending Tests Using SF-2 Fatigue Machine", unpublished, (June 1963).

17. Broek, D., Elementary Engineering Fracture Mechanics, Noordhoff International Publishing Co., Leyden, (1974).

APPENDIX A

Selection of Fatigue Specimen Geometry

The following constraints and limitations were used to guide the fatigue specimen geometry selection:

1. Fatigue machine connecting rod load capacity is 0 - 40 lb.
2. Fatigue machine crank stroke range is 0 - 1 inch. Thus, for fully reversed bending and no mean stress, maximum end deflection is $\pm$ 1/2 inch.
3. Maximum specimen length between clamp edge and drill holes in unclamped end is 2-1/4 inches (without modifying machines).
4. Specimen thickness is constrained to 1/8 inch thickness of as-received sheet material.
5. Specimen geometry should permit attaining surface stresses at least as high as yield at the test section (i.e., section of maximum stress).
6. Specimen geometry should ensure test section will not be located at the clamped edge to prevent possible fretting and crevice corrosion effects.
7. When yield stress is attained at the test section, end deflection should be as large as possible without exceeding $\pm$ 1/2 inch to maximize sensitivity to cam setting adjustment increment.

A number of possible configurations were briefly evaluated using the following simple strength of material

relationships for a constant, rectangular cross-section, cantilevered beam. The sketch in Figure A1 describes the important characteristics.

$$\delta = \frac{4Py^3}{Ewt^3} \tag{A1}$$

$$\sigma = \frac{6Py}{wt^2} \tag{A2}$$

Through a process of trial and error, the geometry in Figure A2 evolved as one that would satisfy the basic requirements.

Prior to final specimen design, a simple load versus deflection test was performed for one of the candidate geometries to examine the validity of the ideal load versus deflection model. This geometry was similar to the one finally selected. The test was conducted by applying known loads to the specimen and measuring deflection with a dial indicator. Results from two test runs were averaged and are plotted in Figure A3. These results indicated the model provides a fair approximation of the actual case. The degree of accuracy can be improved by a judicious choice of y in Figure A1, the length over which unconstrained bending actually occurs.

A load (P) versus surface strain (ε_o) test was performed for the specific geometry selected for this investigation. A smooth specimen with strain gages located at the test section was used. The results of two separate loading and unloading cycles were averaged and used to plot the curve shown in Figure A4.

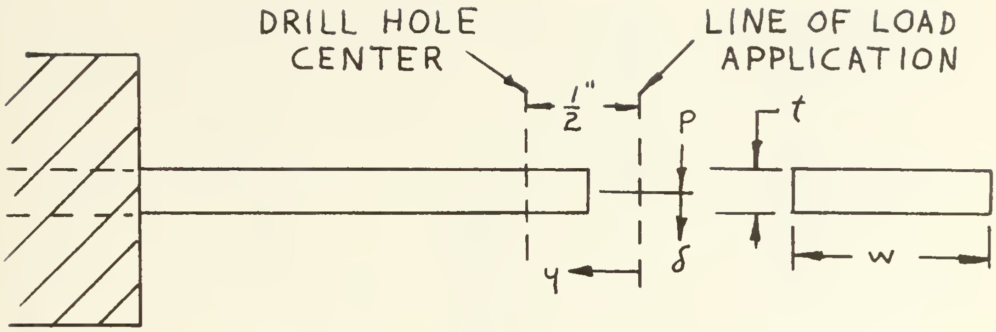

Figure A1: Important Characteristics of Cantileveled Beam.

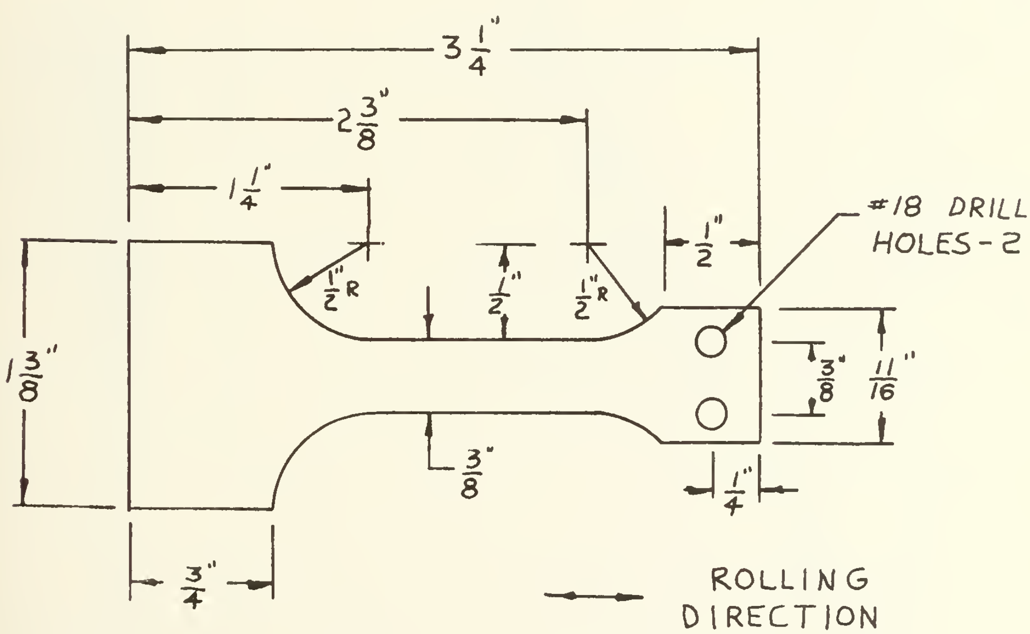

Figure A2: Fatigue specimen geometry.

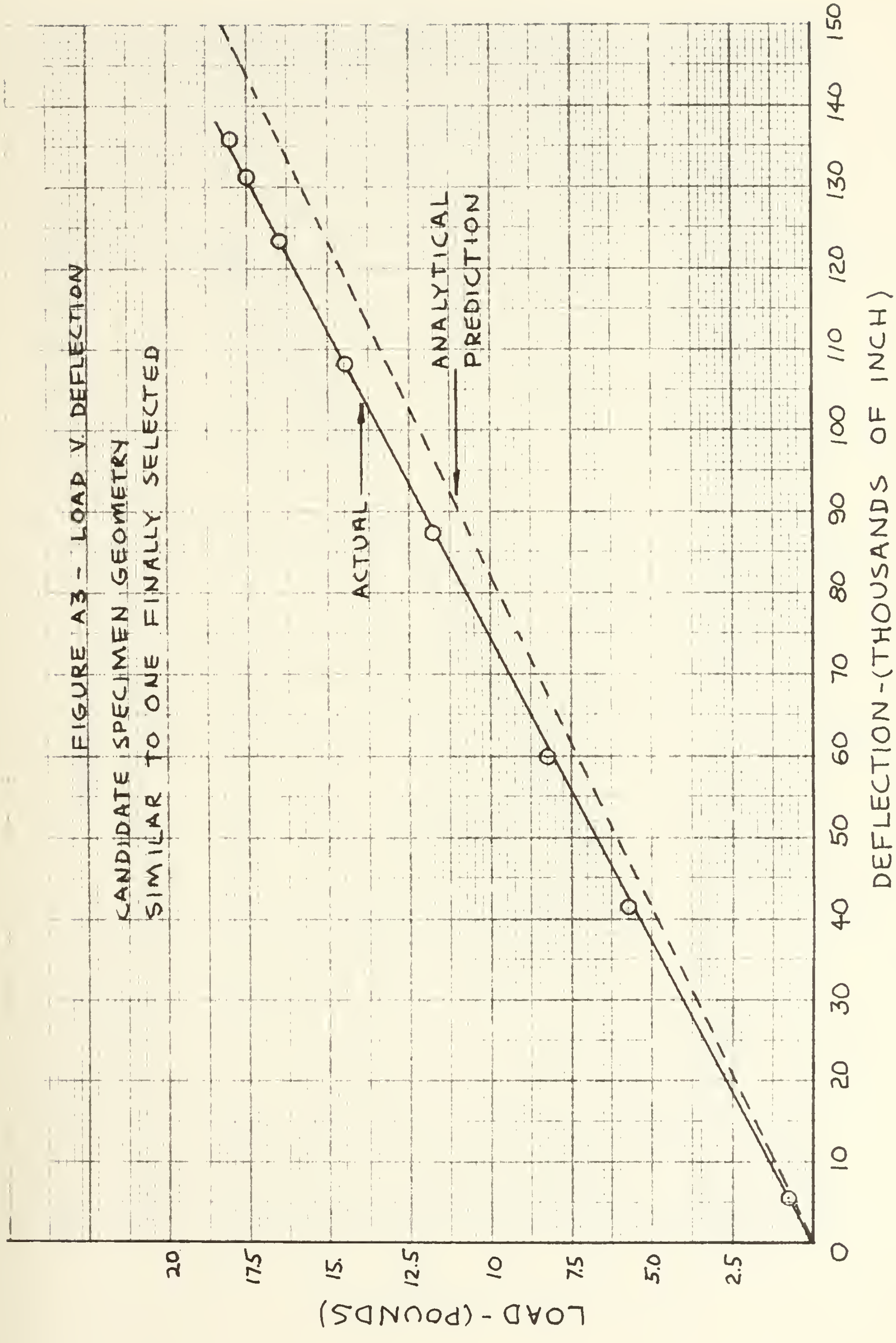
FIGURE A3 - LOAD V. DEFLECTION
CANDIDATE SPECIMEN GEOMETRY
SIMILAR TO ONE FINALLY SELECTED
ACTUAL
ANALYTICAL PREDICTION
LOAD - (POUNDS)
20
17.5
15.
12.5
10
7.5
5.0
2.5
0
10
20
30
40
50
60
70
80
90
100
110
120
130
140
150
DEFLECTION-(THOUSANDS OF INCH)

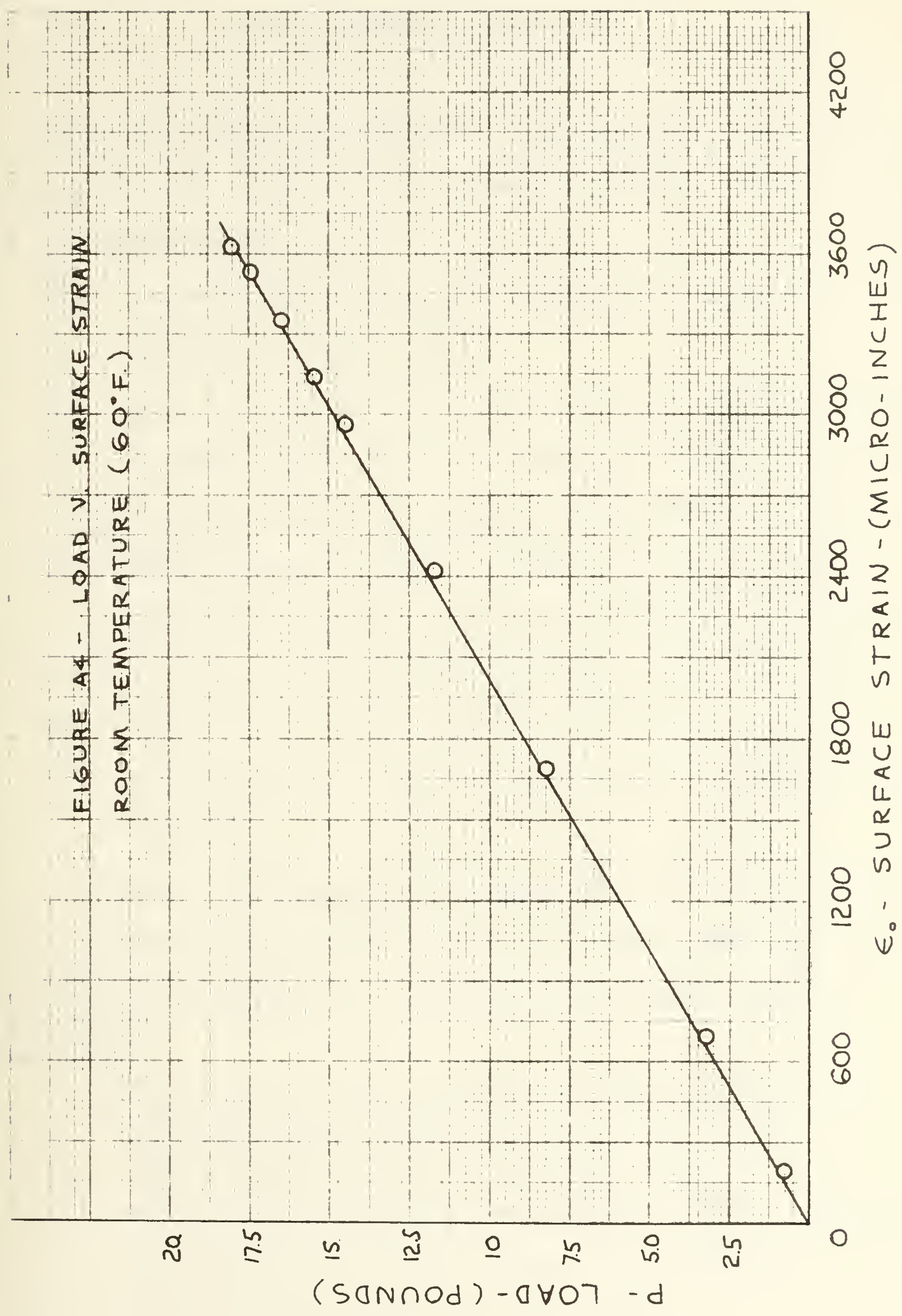
FIGURE A4 - LOAD V. SURFACE STRAIN
ROOM TEMPERATURE (60°F.)
P - LOAD - (POUNDS)
2.5
5.0
7.5
10
12.5
15
17.5
20
0
600
1200
1800
2400
3000
3600
4200
ϵ_o - SURFACE STRAIN - (MICRO-INCHES)

APPENDIX B

Notch Machining Method

The following factors were used to guide the method and tool design used to machine the shallow surface notches into the fatigue specimens:

1. Surface width of notches should be narrow to simulate a real crack.
2. Root radius of the notch should be small to simulate a sharp crack, with an objective being .001 inch.
3. A large number of separate cuts would be needed. Good reproducibility of the notch configuration from one specimen to the next would be required.
4. The surface ligament distance between the crack edge and specimen edge should be as large as practicable for the deepest notch to minimize edge effects.

Machine shop personnel recommended modifying a conventional slitting saw blade to make the notch machining tool. The following limitations concerning the tool were also suggested:

1. To provide sufficient tool strength, saw blade width should be at least .010 inches.
2. Minimum tool cutting tip radius is .001 - .002 inch.
3. Minimum tool cutting radius is .25 inches.
4. Minimum tool cutting angle is 20°.

A sketch of the cutting tool geometry selected is shown in Figure B1.

The following geometrical relationships were used to determine the desired notch principal dimensions.

$$\ell_o + p = R = .25 \text{ in.} \tag{B1}$$

$$\frac{\theta}{2} = \cos^{-1} [\frac{p}{R}] \tag{B2}$$

$$2a = 2R \sin(\frac{\theta}{2}) \tag{B3}$$

$$s = 2\ell_o \tan 10° \tag{B4}$$

Principal dimensions for a number of different notch depths are presented in Table B1.

Table B1

Principal Dimensions for Various Notch Depths

ℓ_o	2a	s
.0015	.055	.0005
.002	.063	.001
.004	.089	.0014
.0115	.150	.004
.025	.218	.009
.040	.2713	.010

Notches were machined on one side of the specimen at the test section (section of maximum stress). The orientation

of the machined notches in the specimen is further described in Figure B2.

An initial group of specimens had notches machined using one continuous material removal cut. Test results indicated this approach left residual compressive stresses in the material adjacent to the notch. The machining procedure was changed to use three rather than one continuous material removal step. The first step removed material to within .004 inches of the desired depth. The second removed material to within .002 inches of the desired depth. The third removed material to the desired depth. This procedure was modified in the case of the .002 inch notches. In this case about .001 inch was removed on the first step and the remaining .001 inch on the second step.

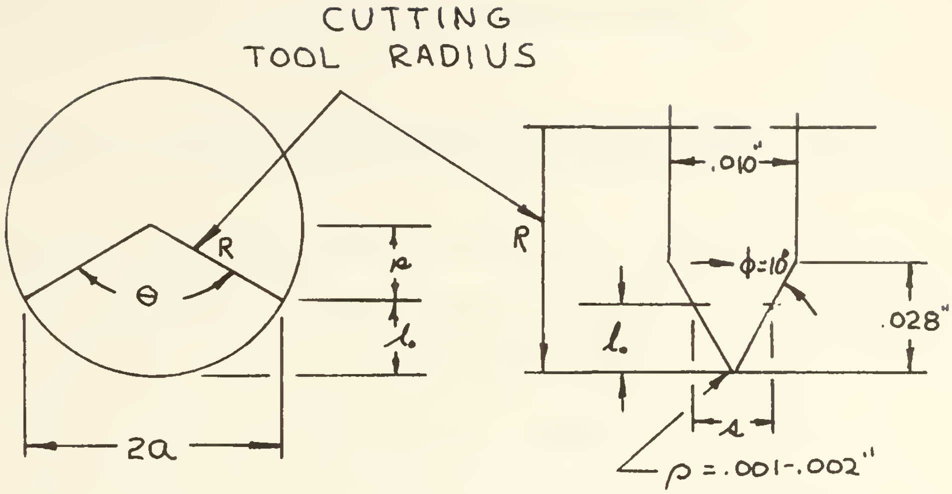

Figure B1: Notch cutting tool geometry.

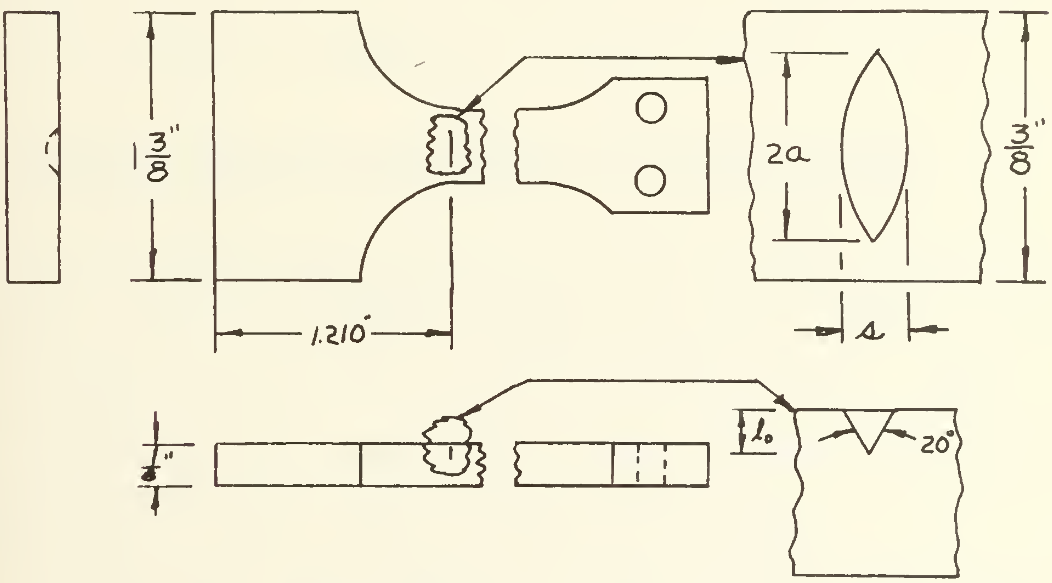

Figure B2: Orientation of machined notches in specimens.

APPENDIX C

Specimen Surface Stress Determination

1. Location of Section of Maximum Stress (Test Section)

The section of maximum stress (test section) in the fatigue specimens was located using information developed by McClintock [5]. For reference purposes a sketch of the specimen is presented in Figure Cl. The section of maximum stress is at $y = y_o + y_m = 2.29$ in. located at Section A-A.

$$y_m = \frac{wR}{2y_o} - \frac{w^2R^2}{8{y_o}^3} \qquad \text{(Cl)}$$

$$y_m = \frac{(.375 \text{ in.})(.5 \text{ in.})}{2(2.25 \text{ in.})} - \frac{(.375 \text{ in.})^2(.5 \text{ in.})^2}{(8)(2.25 \text{ in.})^3}$$

$$y_m = .0397 \text{ in.}$$

2. Direct/Indirect Determination of Surface Stress

Early in the experimental work, an attempt was made to indirectly obtain the desired specimen surface stress (σ_o) by adjusting the cam dial to a pre-determined setting. This required developing a cam setting versus surface stress/strain calibration curve for each fatigue test machine.

Two BLH SR-4 (Type FAE-12-12-S13L) strain gages (one for the upper surface, one for the lower) were attached to a smooth fatigue specimen at the test section. A series of runs were made recording strain (ε_o) corresponding to various cam

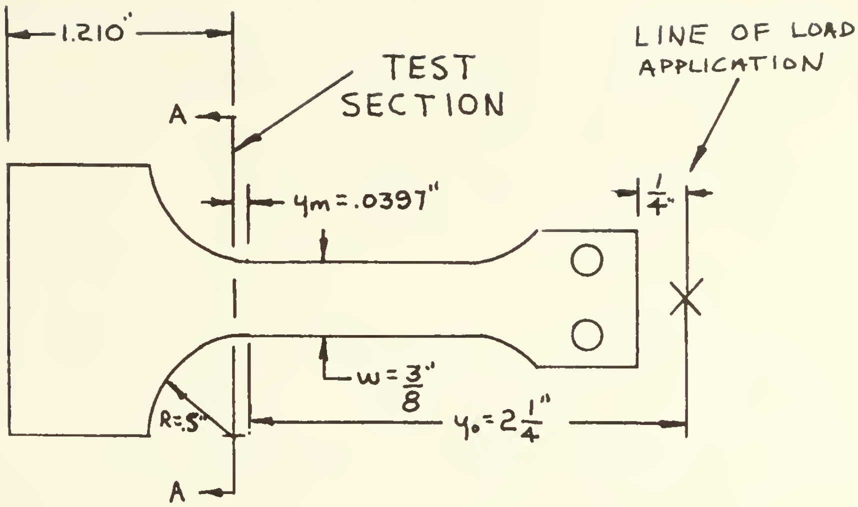

Figure C1: Nomenclature definition for test section location.

settings. Two to three readings were taken for each integral cam setting mark within the range of elastic strains as determined from the strain gages. The strain readings were averaged for each point and were used to plot the calibration curves. No significant difference in results were observed between the two machines within the range of scatter observed. Based on the range of worst scatter, the accuracy of this method was considered to be $\pm$ 750 psi on stress. Figure C2 presents the calibration curve developed for this indirect method of stress determination.

The indirect method of determining surface stress/strain was used for the first few $\sigma_o - N_f$ test runs. Preliminary evaluation of data indicated data scatter could be reduced by directly measuring strain corresponding to each cam setting, after the cam setting adjustment was made and the cam setting locking bolt tightened. This approach required a little more time to use, but the improved accuracy was considered worth the effort. The direct measuring method was used for all remaining test runs.

3. Determination of Compliance Correction Parameter (γ_c) for Notched Specimens

The fatigue test machines used for this investigation are displacement (deflection) controlled. Further, the nominal surface stress (σ_o) that results from a given deflection depends upon the spring constant (k') or conversely the

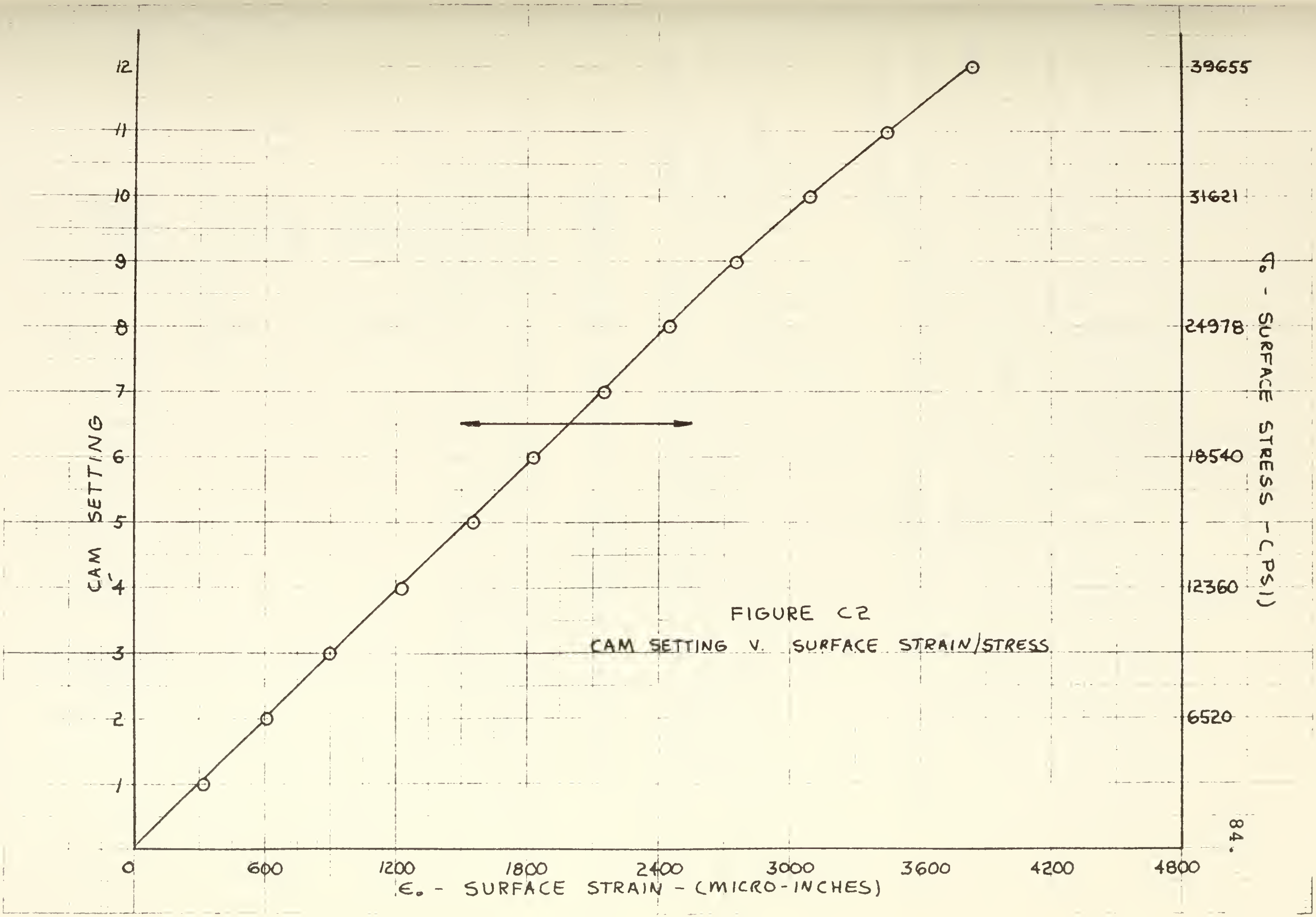

FIGURE C2

CAM SETTING V. SURFACE STRAIN/STRESS

compliance (C) of the specimen. If a strain gaged smooth specimen is used to obtain a particular (σ_o) at a given end deflection (δ), and then a notched specimen is placed in the machine with the same δ, the initial nominal surface stress, (σ_i) present in the notched specimen will be less than σ_o because of the increased notched specimen compliance. Thus, some method of calculating a correction parameter (γ_c) was needed where

$$\gamma_c = \frac{\sigma_i}{\sigma_o} \tag{C2}$$

This correction parameter would permit determining σ_i knowing the corresponding σ_o. Two methods were investigated for calculating γ_c and are discussed in the following section.

a. Method Using McClintock Approximations for a Notched Beam

The following expressions were developed by McClintock [16]. The nomenclature is described in Figure C3.

For a smooth beam

$$\delta = \frac{4Py^3}{Ewt^3} = \frac{P}{k'} \tag{C3}$$

$$k' = \frac{Ewt^3}{4y}$$

For a notched beam

$$\Delta\delta \approx \frac{12Py_n^2}{Ewt_n^3} (\text{lesser of } t_n;\ t - t_n) = \frac{F}{k'_n} \tag{C4}$$

$$k_n' = \frac{Ewt_n^3}{12y_n^2 \text{ (lesser of } t_n;\ t - t_n)}$$

$$\begin{aligned}(\text{lesser of } t_n;\ t - t_n) &= \ell_o && \text{for} \quad \ell_o < t/2 \\ &= t/2 && \text{for} \quad \ell_o = t/2 \\ &= t - \ell_o && \text{for} \quad \ell_o > t/2\end{aligned}$$

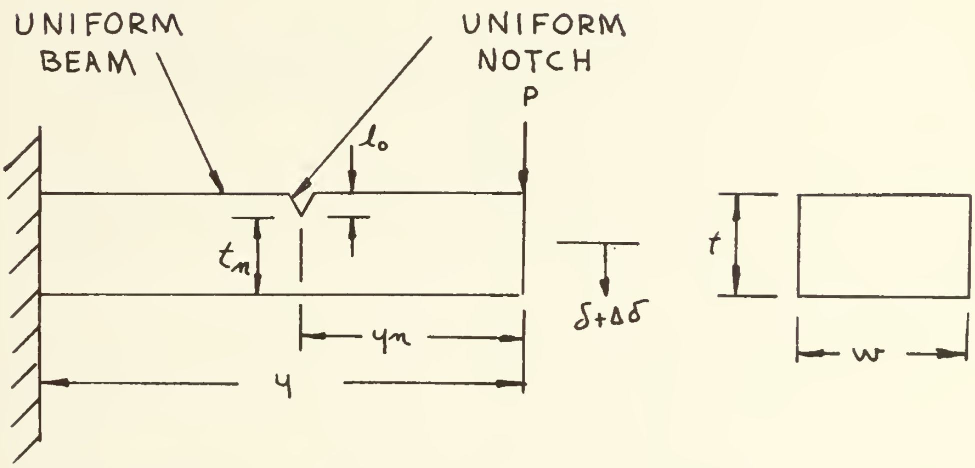

Figure C3: Nomenclature definition for McClintock approximation.

where $\Delta\delta$ is the additional deflection resulting from the presence of a uniform notch across the <u>entire</u> beam width, w. Referring to Figure C4:

$$P_1 = k_n'(\delta + \Delta\delta) \tag{C5}$$

$$k_n' = \frac{P_1}{\delta + \Delta\delta}$$

$$P_n = k_n'\delta \tag{C6}$$

$$P_n = \frac{P_1\delta}{\delta + \Delta\delta} \tag{C7}$$

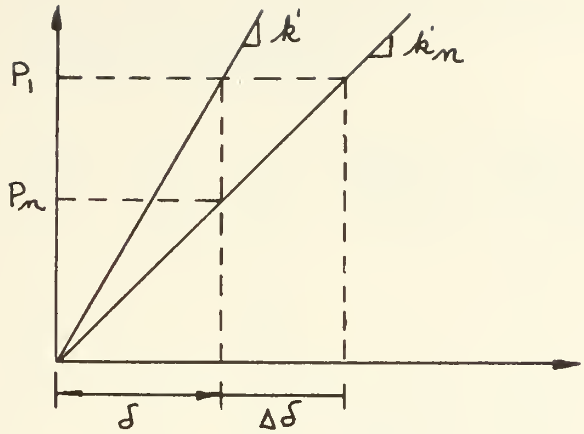

Figure C4: Load versus deflection.

Now since $\sigma \propto P$

$$\frac{P_n}{P_1} = \frac{\delta}{\delta + \Delta\delta} = \frac{\sigma_i}{\sigma_o} = \gamma_c = \frac{1}{1 + \frac{\Delta\delta}{\delta}} \qquad \text{(C8)}$$

$$\frac{\Delta\delta}{\delta} = \frac{3\, y_n^2 t^3 (\text{lesser of } t_n;\ t - t_n)}{t_n^3 y^3}$$

For the specimen geometry used in this investigation

$y = y_n$; $y = 2.046$ in.; $t = .125$ in.

$$\therefore \quad \frac{\Delta\delta}{\delta} = \frac{3t^3\ (\text{lesser of } t_n;\ t - t_n)}{t_n^3 y}$$

$$\text{for} \quad \ell_o < \frac{t}{2} \qquad \frac{\Delta\delta}{\delta} = \frac{3t^3 \ell_o}{y(t-\ell_o)^3} = \frac{2.864\text{x}10^{-3}\ell_o}{(.125-\ell_o)^3} \qquad \text{(C9)}$$

$$\text{for} \quad \ell_o > \frac{t}{2} \qquad \frac{\Delta\delta}{\delta} = \frac{3t^3}{y(t-\ell_o)^2} = \frac{2.864\text{x}10^{-3}}{(.125-\ell_o)^2} \qquad \text{(C10)}$$

Substituting (C9) and (C10) into (C8) gives an approximate expression for γ_c as a function of ℓ_o for this particular specimen geometry.

$$\gamma_c = \frac{1}{1 + \dfrac{2.864 \times 10^{-3}\, \ell_o}{(.125 - \ell_o)^3}} \qquad \ell_o < \frac{t}{2}$$

or

$$\frac{1}{1 + \dfrac{2.864 \times 10^{-3}}{(.125 - \ell_o)^2}} \qquad \ell_o > \frac{t}{2}$$

Expression (C11) was used to derive the compliance correction parameters given in Table C1. These values are also plotted in Figure C6.

The above method is intended to give a rough approximation and would appear to be most valid when $\Delta\delta$ is small compared to δ. Further, because the actual crack does not extend across the entire specimen width, this method tends to overestimate the compliance of the actual specimen for a given ℓ_o and thus underestimate σ_i.

b. Method Using Results of Rice and Levy

The following expression was developed by Rice and Levy [9]. The nomenclature is described in Figure C5.

Table C1

Compliance Correction Parameters Using McClintock Approximation

ℓ	0	.002	.010	.0115	.020	.025	.030	.040	.050	.060
ℓ/t	0	.016	.080	.092	.160	.200	.240	.320	.400	.480
γ_c	1	.997	.982	.978	.953	.933	.909	.843	.747	.615
ℓ		.0625	.070	.080	.090	.100	.110	.120	.125	
ℓ/t		.500	.560	.640	.720	.800	.880	.960	1.00	
γ_c		.577	.514	.414	.300	.179	.073	.009	0	

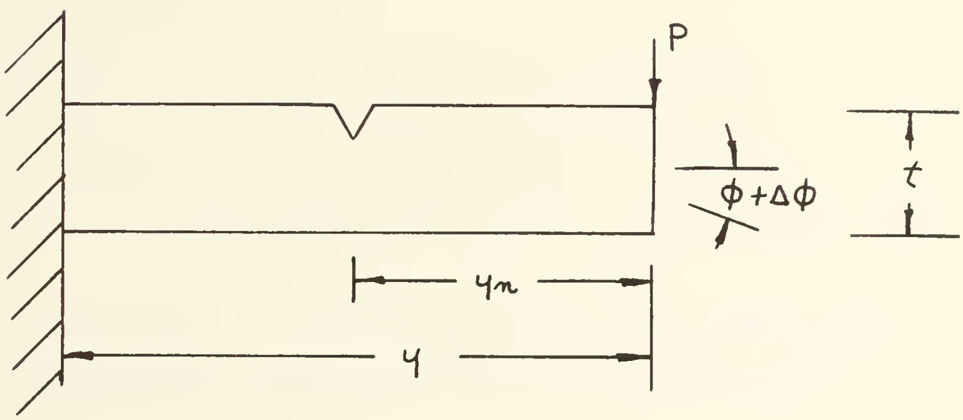

Figure C5: Nomenclature definition for Rice and Levy approximation.

$$\Delta\phi = \frac{12(1-\nu)^2}{E}\alpha_{bb}\left[\frac{6\,Py_n}{wt^2}\right] \qquad (C12)$$

where $\Delta\phi$ is the additional beam rotation due to the presence of a notch.

Now

$$\delta = \phi y = \frac{4Py^3}{Ewt^3} \tag{C13}$$

and

$$\Delta\delta \approx \Delta\phi y \tag{C14}$$

then $$\frac{\Delta\delta}{\delta} = \frac{72(1 - \nu^2)y^2 P\alpha_{bb}}{Ewt^2} \times \frac{Ewt^3}{4Py^3} \tag{C15}$$

$$= \frac{18(1 - \nu^2)t\alpha_{bb}}{y} \tag{C15}$$

where $y = 2.046$ in., $\nu = .3$; $t = .125$ in. and α_{bb} is a factor taken from Figure 4a in [9] and depends upon the ratio ℓ/t. ν is Poisson's ratio.

Substituting values for y, ν, t into (C15)

$$\frac{\Delta\delta}{\delta} = \frac{18(1 - .3^2)(.125 \text{ in.})\alpha_{bb}}{(2.046 \text{ in.})} = 1.007\alpha_{bb} \approx \alpha_{bb}$$

Therefore using (8C) an expression can be obtained for the compliance correction parameter (γ_c) as a function of ℓ/t.

$$\gamma_c = \frac{1}{1 + \alpha_{bb}} \tag{C16}$$

This expression was used to derive the approximate compliance correction parameters given in Table C2. These values are also plotted in Figure C6.

Table C2

Compliance Correction Parameters Using Rice and Levy Approximation

ℓ	0	.002	.010	.0115	.020	.025	.030
ℓ/t	0	.016	.080	.092	.160	.200	.240
α_{bb}	0	.008	.040	.045	.080	.100	.150
γ_c	1	.992	.962	.957	.926	.909	.870
ℓ		.040	.050	.060	.070	.080	.090
ℓ/t		.320	.400	.480	.560	.640	.720
α_{bb}		.200	.300	.500	.800	1.30	2.30
γ_c		.833	.769	.667	.556	.435	.303

Again the above method is intended to provide a rough approximation. The values of α_{bb} were developed for a plate undergoing bending [9], and the values of α_{bb} will be most accurate when the length of the crack (2a) is large compared to t. This is not actually the case for the specimen geometry selected for this investigation.

4. Comparison of Methods

The values for γ_c calculated using each of the above methods are plotted in Figure C6. It can be seen that there is good agreement between the two approximations. No additional effort was spent to further investigate the validity of these results.

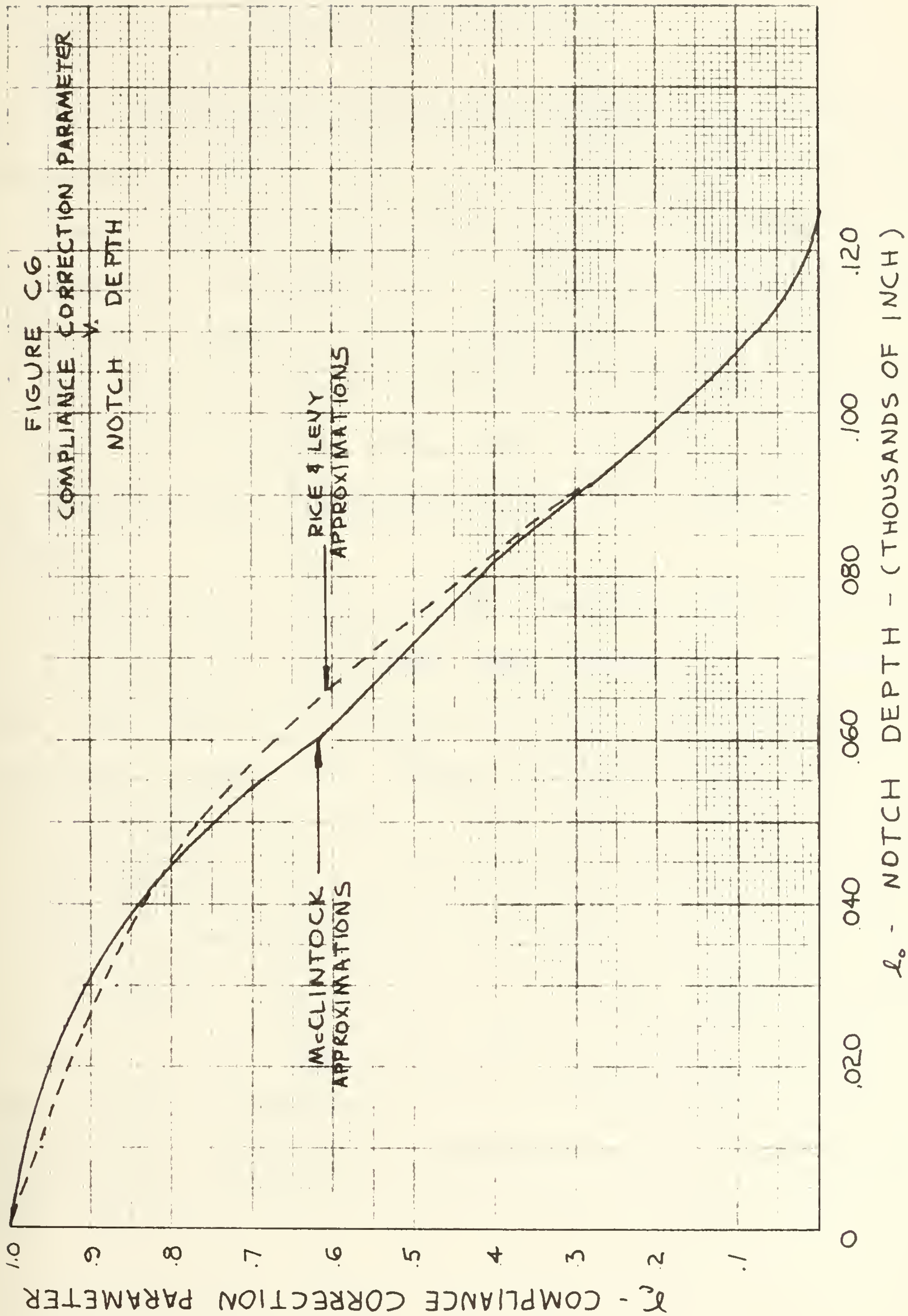
FIGURE C6
COMPLIANCE CORRECTION PARAMETER
V.
NOTCH DEPTH
RICE & LEVY APPROXIMATIONS
McCLINTOCK APPROXIMATIONS
λ - COMPLIANCE CORRECTION PARAMETER
1.0
.9
.8
.7
.6
.5
.4
.3
.2
.1
0
.020
.040
.060
.080
.100
.120
ℓo - NOTCH DEPTH - (THOUSANDS OF INCH)

APPENDIX D

Fatigue Test Results

The raw data obtained from the fatigue investigation is presented in Table D1 for air and Table D2 for salt water.

The initial stress (σ_o) was corrected for compliance (see Appendix C) to obtain (σ_i). σ_i was then plotted against N_f for both environments for a given initial notch depth. The plots for the various notch depths tested are presented in Figures D1 through D4. The data points were connected with smooth curves. No formal curve fitting method was attempted.

Figure D5 shows plots of data obtained when the first set of machined notch specimens were tested in air. Subsequent investigation led to the conclusion that residual compressive stresses were present around the notch tip in these specimens. When data in Figure D5 is compared to the air data in Figures D1 - D4, it can be seen that the presence of residual stress had little or no effect on fatigue life for σ_i > 30 Ksi. For 30 Ksi < σ_i < 20 Ksi, residual compressive stress has an increasing effect, especially for the deeper (.025 in.) notches. For σ_i < 20 Ksi, the material appears to be insensitive to notches, even for the deepest depth, .025 in.

Table D1

Fatigue Test Data - Air

Material: 5456-H343
Cycling Mode: Fully reverse bending @ 30 Hz
Environment: Air

Spec. Ident. No.	Initial notch depth (ℓ_o)	ε_o (μ in.)	σ_o (psi)	σ_i (psi)	N (cycles)	Remarks
3	s	(11-1)*	35432	35432	27600	
4	s	(8-1)	24978	24978	164500	
7	s	(12-1)	39655	39655	20000	
9	s	(6-1)	18540	18540	1542200	
11	s	(7-1)	21836	21836	389800	
13	s	(10-1)	31621	31621	54700	
15	s	1700	17510	17510	12663600	didn't break initially
19	s	1975	20343	20343	514400	
21	s	5160	53000	53000	4900	
17	s	3885	40016	40016	21300	
113	s	2395	24669	24669	236400	
114	s	1845	19004	19004	9889400	didn't break initially
115	s	1955	20137	20137	923800	

* Test run on machine #1

Spec. Ident. No.	Initial notch depth (ℓ_o)	ε_o (μ in)	σ_o (psi)	σ (psi)	N (cycles)	Remarks
5	s	(11-2)**	36462	36462	30800	
6	s	(6-2)	26008	26008	132300	
8	s	(12-2)	40170	40170	17700	
10	s	(6-2)	18952	18952	725500	
12	s	(7-2)	22454	22454	258600	
14	s	(10-2)	32960	32960	49600	
16	s	1725	17768	17768	12664000	didn't break initially
18	s	1980	20394	20394	582500	
20	s	4810	49543	49543	6800	
			Air (1)*			
49	.002	2915	30025	29784	49300	
45	.002	1811	18653	18504	1470600	didn't break at notch
95	.002	3885	40016	39696	11700	
99	.002	2395	24669	24472	171900	
98	.002	1955	20137	19976	371500	didn't break at notch
			Air (2)**			
42	.002	1970	20291	20129	783800	didn't break at notch
44	.002	4675	48153	47768	5300	
46	.002	2415	24875	24676	204200	

* Test run on machine #1
** Test run on machine #2

Spec. Ident. No.	Initial notch depth (ℓ_o)	ε_o (μ in)	σ_o (psi)	σ_i (psi)	N (cycles)	Remarks
50	.002	3990	41097	40768	10800	
48	.002	2125	21888	21713	285000	possible inclusion at notch cross section
96	.002	1785	18386	18239	1259100	
			Air (1)			
33	.0115	2915	30025	28734	24900	
41	.0115	1811	18653	17851	543500	broke prior to .025 notch @ same stress
101	.0115	1212	12484	11947	3238800	discontinued test prior to breaking
103	.0115	3885	40016	38295	5100	
105	.0115	2395	24669	23608	69600	collected visual crack propagation data, good fracture surface
104	.0115	1716	17675	16915	11682000	didn't break
			Air (2)			
32	.0115	1970	20291	19419	392600	
34	.0115	4675	48153	46082	2900	
40	.0115	2415	24875	23805	75000	
38	.0115	1710	17613	16856	10330000	didn't break
36	.0115	3990	41097	39330	5600	

Spec. Ident. No.	Initial notch depth (ℓ_o)	ε_o (μ in)	σ_o (psi)	σ_i (psi)	N (cycles)	Remarks
37	.0115	2125	21888	20947	151800	
102	.0115	1470	15141	14490	10324900	didn't break
			Air (1)			
22	.025	1965	20240	18398	249200	
25	.025	1498	15429	14025	10007800	
27	.025	2915	30025	27293	12800	
29	.025	1811	18653	16956	612300	didn't break at notch
31	.025	1811	18653	16956	479400	didn't break at notch
1	.025	1811	18653	16956	10243800	didn't break initially
55	.025	2410	24823	22564	31800	
57	.025	1965	20240	18398	103800	stepped machining procedure. Crack propagation data
107	.025	1212	12484	11348	9897500	didn't break initially
111	.025	1385	14266	12968	15089100	didn't break initially, broke in 2600 cycles @ 366555

Note: The initial notch machining procedure was used for the following specimens:
.002" - specimen numbers: 42-51
.0115" - specimen numbers: 32-41
.025" - specimen numbers: 22-31

Spec. Ident. No.	Initial notch depth (ℓ_o)	ε_o (μ in)	σ_o (psi)	σ_i (psi)	N (cycles)	Remarks
			Air (2)			
23	.025	970	9991	9082	10000100	didn't break initially, N_f may be in error ± 100
26	.025	4675	48153	43771	1100	
24	.025	2415	24875	22611	55200	observed final failure
2	.025	1710	17613	16010	626200	didn't break at notch apparent inclusion
30	.025	2125	21888	19896	133400	
112	.025	1470	15141	13763	1163600	stepped machining procedure
109	.025	3885	40016	36375	2700	
110	.025	1845	19004	17245	240000	

Note: The initial notch machining procedure was used in the following specimens:
.002" - specimen numbers: 42-51
.0115" - specimen numbers: 32-41
.025" - specimen numbers: 22-31

Table D2

Fatigue Test Data - Salt Water

Material: 5456-H343
Environment: 3.5% NaCl
Cycling Mode; Fully reversed bending at 30 Hz

Spec. Ident. No.	Initial notch depth (ℓ_o)	ε_o (μ in)	σ_o (psi)	σ_i (psi)	N (cycles)	Remarks
			Salt water (1)			
83	s	2410	24823	24823	170500	dull side
87	s	1965	20240	20240	280700	
85	s	1725	17768	17768	1068700	didn't break at max stress section
89	s	3885	40016	40016	12800	
91	s	2395	24669	24669	156700	
116	s	1955	20137	20137	985,500	didn't break at max stress section
			Salt water (2)			
82	s	2880	29664	29664	46900	
84	s	2155	22197	22197	642200	didn't break, discontinued test, dull side
86	s	2155	22197	22197	345300	
88	s	1807	18612	18612	1855900	broke at clamp
90	s	1470	15141	15141	10278500	didn't break
117	s	4690	48307	48307	5800	

Spec. Ident. No.	Initial Notch depth (λ_o)	ε_o (μ in)	σ_o (psi)	σ_i (psi)	N (cycle)	Remarks
			Salt water (1)			
47	.002	1811	18653	18504	1135700	initial 118,800 cycles in air/dist. water
73	.002	2410	24823	24624	114000	
75	.002	1965	20240	20078	293500	
79	.002	1725	17768	17626	619200	
81	.002	1212	12484	12384	6279800	broke at clamp
80	.002	3885	40016	39696	7600	
			Salt water (2)			
51	.002	2125	21888	21713	317700	initial 106,600 cycles in air/dist. water
72	.002	2880	29664	29427	29000	
74	.002	2155	22197	22019	206900	
76	.002	1807	18612	18463	573900	
78	.002	1470	15141	15020	2056100	
100	.002	1345	13854	13743	7132000	didn't break at notch
43	.002	4690	48307	47291	5000	
			Salt water (1)			
63	.0115	2410	24823	23756	54800	
65	.0115	1965	20240	19370	154600	
67	.0115	1725	17768	17004	282600	
69	.0115	1212	12484	11947	1178400	
71	.0115	1212	12484	11947	3077300	s.w. inadvertently stopped for some unkown period prior to 2,273,600 cycles
68	.0115	3885	40016	38295	4400	

Spec. Ident. No.	Initial Notch depth (ℓ_o)	ε_o (μ in)	σ_o (psi)	σ_i (psi)	N (cycles)	Remarks
			Salt Water (2)			
62	.0115	2880	29664	28388	13200	
64	.0115	2155	22197	21243	138500	
66	.0115	1807	18612	17812	267400	
70	.0115	1470	15141	14490	1373600	
106	.0115	1155	11897	11385	10226700	didn't break
			Salt Water (1)			
53	.025	2410	24823	22564	32300	
59	.025	1965	20240	18398	99800	
61	.025	1725	17768	16151	366900	
60	.025	1212	12484	11348	964300	
93	.025	3885	40016	36375	2600	
			Salt Water (2)			
52	.025	2880	29664	26964	8500	
54	.025	2155	22197	20177	70900	
56	.025	1807	18612	16918	266600	
58	.025	1807	18612	16918	215500	
92	.025	1470	15141	13763	481800	
94	.025	1005	10352	9410	10171500	didn't break
108	.025	1155	11897	10814	952800	

Note: The initial notch machining procedure was used for the following specimens:
.002" - specimen numbers: 42-51
.0115" - specimen numbers: 32-41
.025" - specimen numbers: 22-31

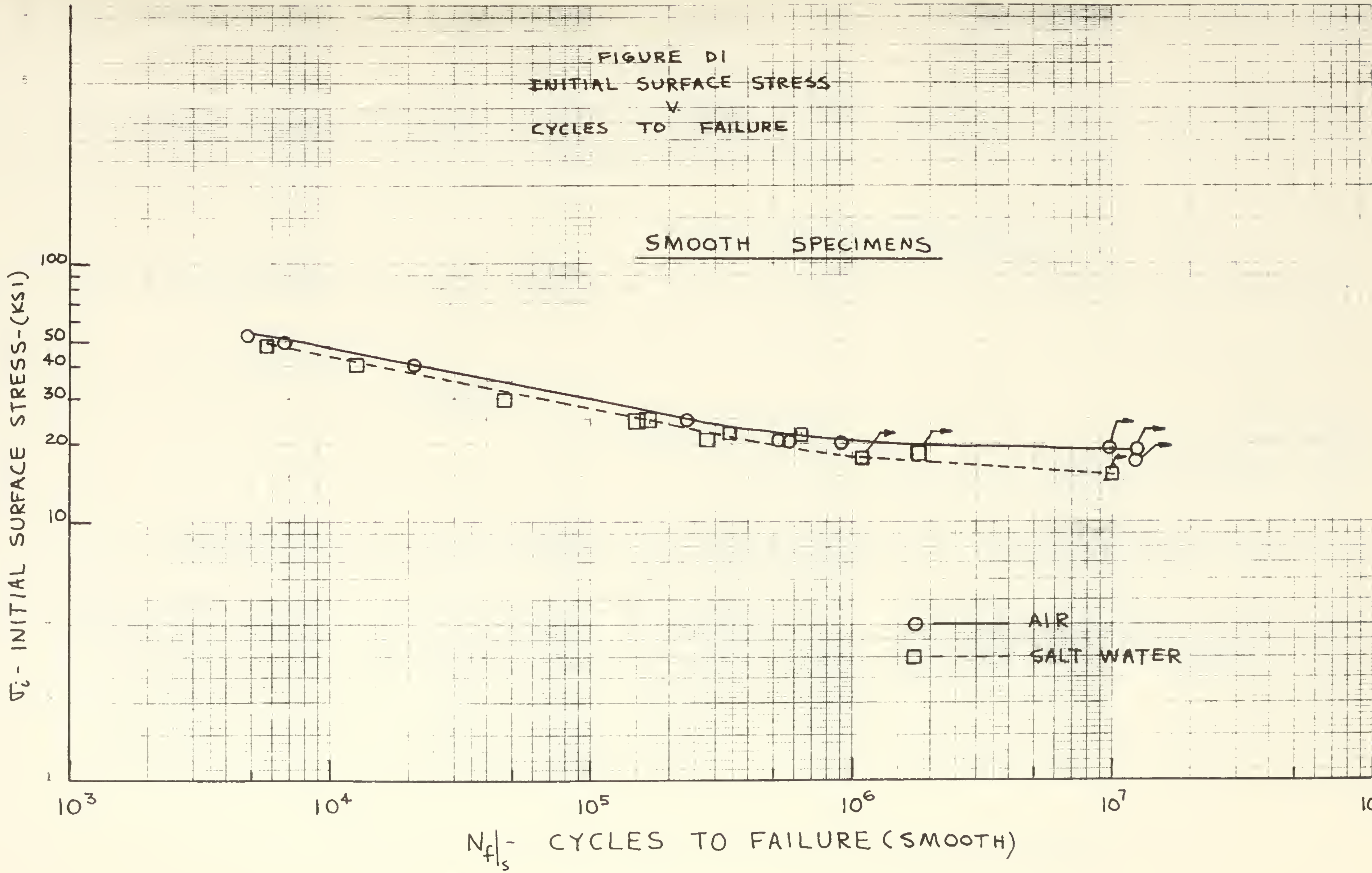
FIGURE D1
INITIAL SURFACE STRESS
V.
CYCLES TO FAILURE
SMOOTH SPECIMENS
100
50
40
30
20
10
σ_i - INITIAL SURFACE STRESS-(KSI)
10^3
10^4
10^5
10^6
10^7
10^8
$N_f|_s$ - CYCLES TO FAILURE (SMOOTH)
AIR
SALT WATER

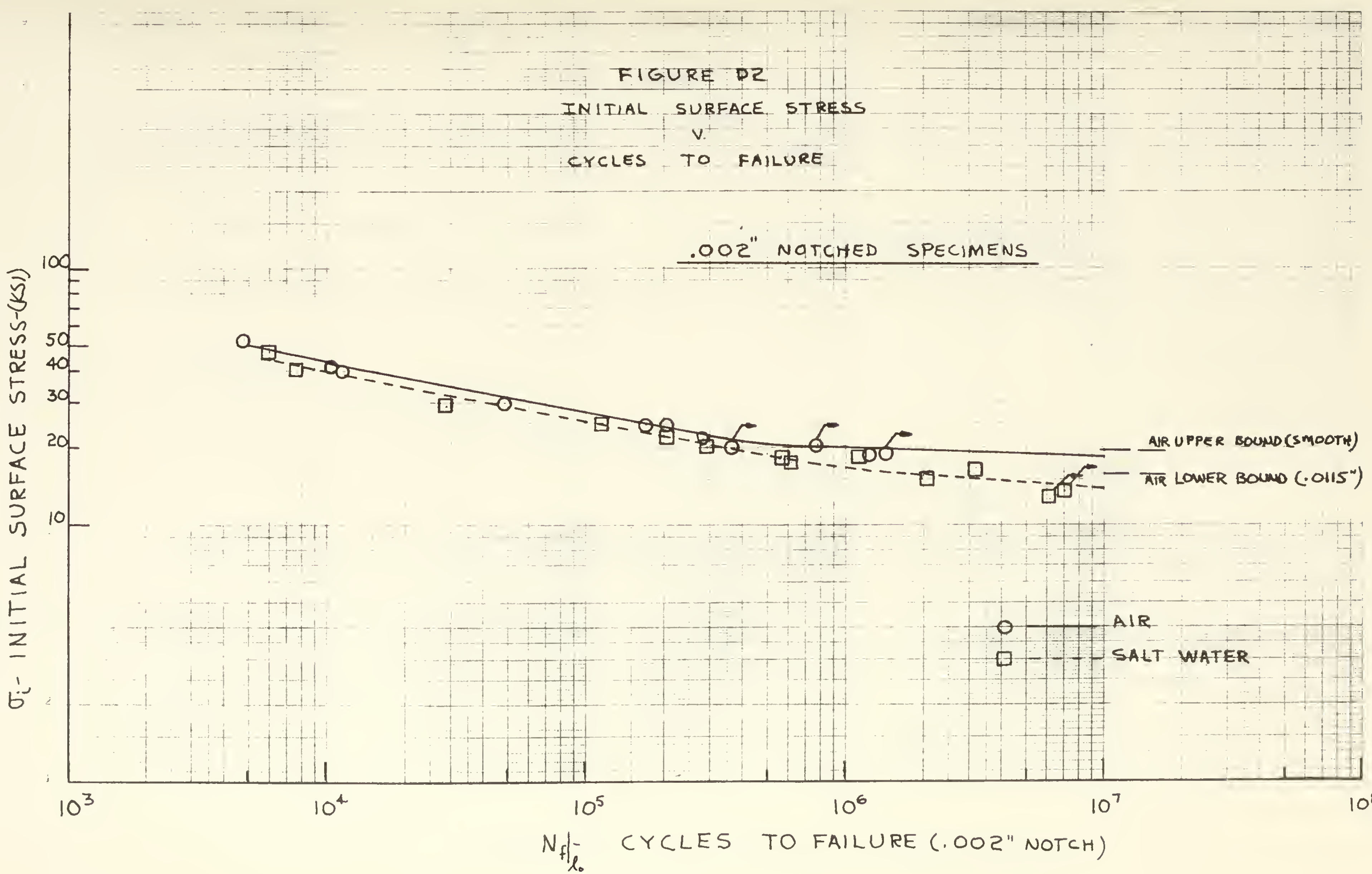
FIGURE D2
INITIAL SURFACE STRESS
V.
CYCLES TO FAILURE
.002" NOTCHED SPECIMENS
100
50
40
30
20
10
AIR UPPER BOUND (SMOOTH)
AIR LOWER BOUND (.0115")
AIR
SALT WATER
σ_i - INITIAL SURFACE STRESS-(KSI)
10^3
10^4
10^5
10^6
10^7
10^8
$N_f|_{\ell_0}$ - CYCLES TO FAILURE (.002" NOTCH)

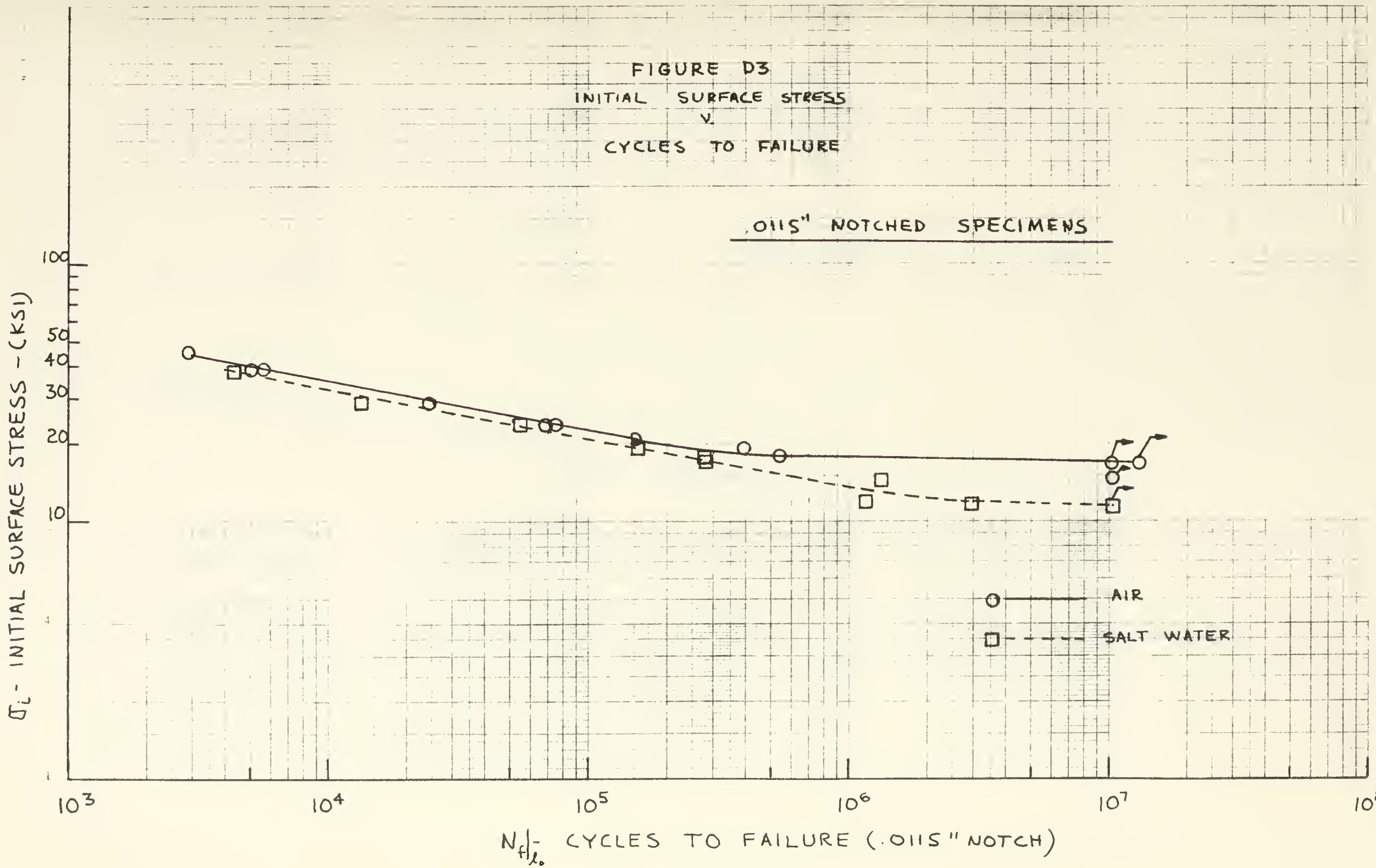

FIGURE D3
INITIAL SURFACE STRESS
V.
CYCLES TO FAILURE

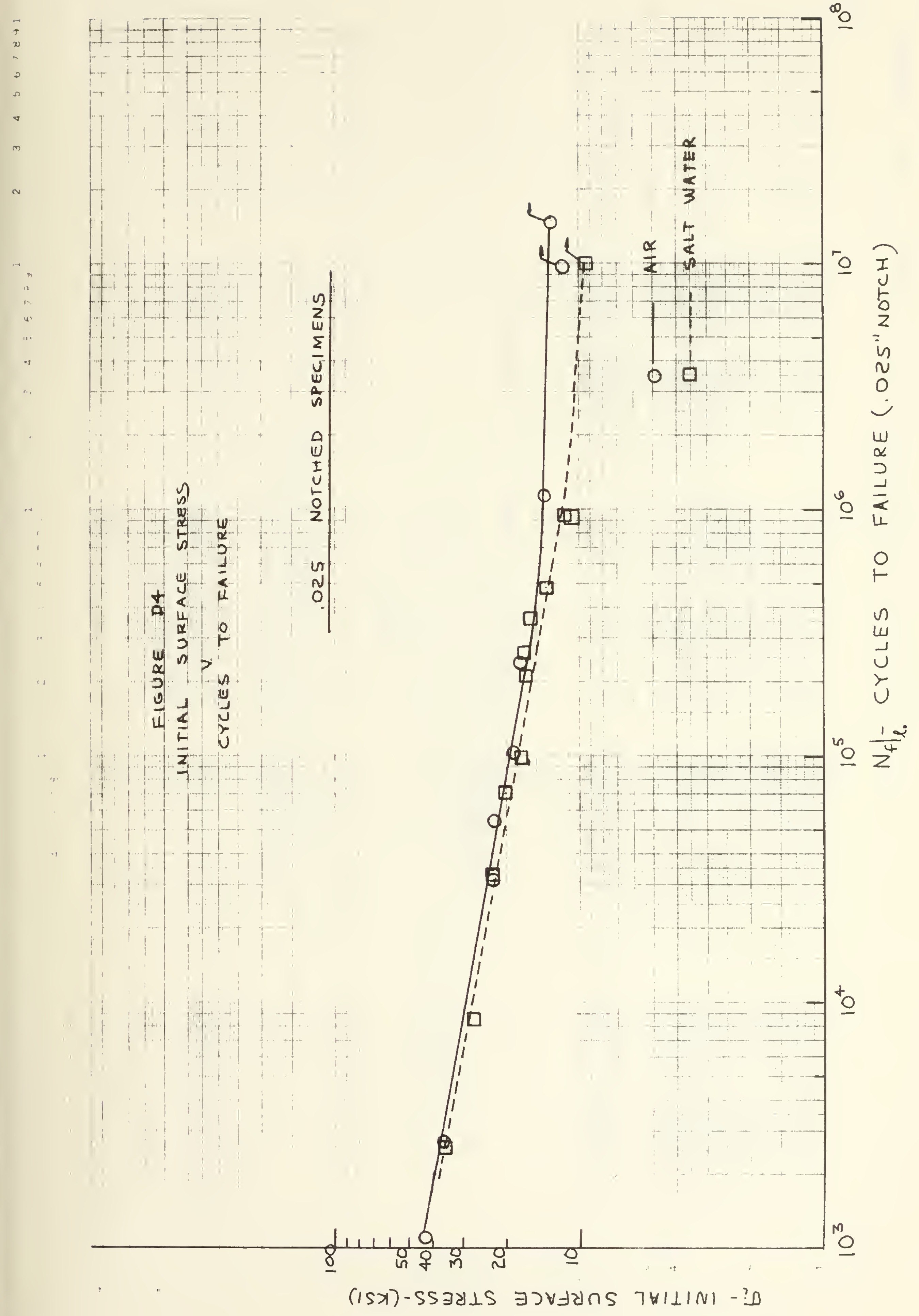
FIGURE D4
INITIAL SURFACE STRESS
V
CYCLES TO FAILURE
.025 NOTCHED SPECIMENS
AIR
SALT WATER
σ_i - INITIAL SURFACE STRESS-(KSI)
100
50
40
30
20
10
10^3
10^4
10^5
10^6
10^7
10^8
$N_f|_{i}$ - CYCLES TO FAILURE (.025" NOTCH)

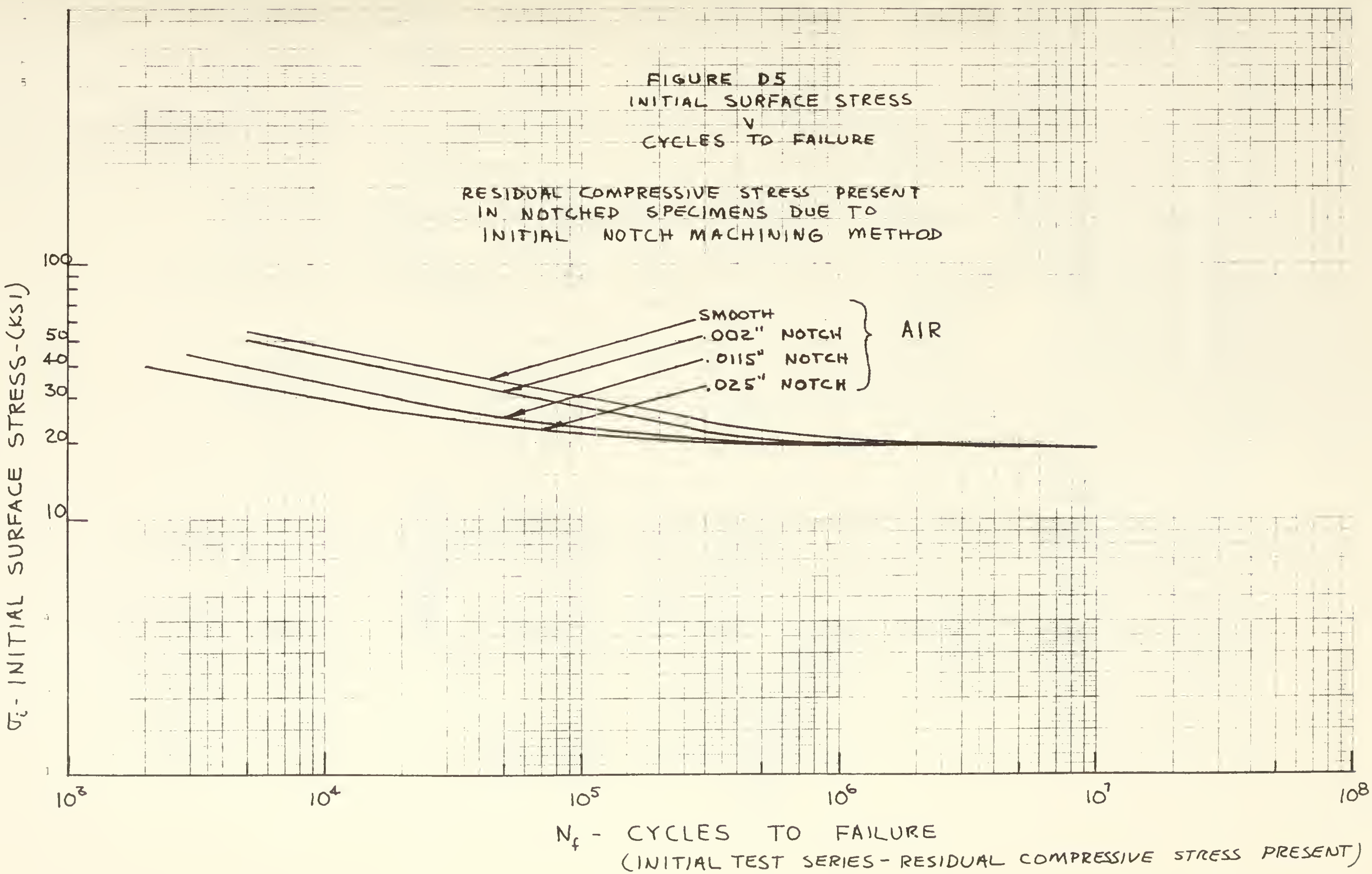
FIGURE D5
INITIAL SURFACE STRESS
V
CYCLES TO FAILURE
RESIDUAL COMPRESSIVE STRESS PRESENT
IN NOTCHED SPECIMENS DUE TO
INITIAL NOTCH MACHINING METHOD
SMOOTH
.002" NOTCH
.0115" NOTCH
.025" NOTCH
AIR
100
50
40
30
20
10
σ_i - INITIAL SURFACE STRESS-(KSI)
10^3
10^4
10^5
10^6
10^7
10^8
N_f - CYCLES TO FAILURE
(INITIAL TEST SERIES - RESIDUAL COMPRESSIVE STRESS PRESENT)

Some specimens completed about 1 x 10^7 cycles without failure. A few were subjected to additional testing at a higher stress of about 40 Ksi in air to cause rapid failure. A summary of these results and the cumulative initial crack propagation measurements made during SEM examination are presented in Table D3.

Table D3

Cumulative Crack Propagation Data for

1 x 10^7 Cycles

Specimen	$\Delta \ell$ (in.)	σ_i initial	N initial	Initial environment
#114(s)	.0043	19004	9,889,400	air
#102(.0115)	not measured	14490	10,324,900	air
#90	not measured	15141	10,278,500	salt water
#106(.0115)	.0035	11385	10,226,700	salt water

σ_i(psi) N(cycles)

Specimen	σ_i final	N_f	Final environment
#114(s)	40325	16500	air
#102(.0115)	38591	5600	air
#90	40325	15000	air
#106(.0115)	38591	5400	air

Specimen	$\Delta \ell$ (in.)	σ_i initial	N initial	Initial environment
#94(.025)	.001	9410	10,171,500	salt water
#16(s)	.013	17768	12,664,000	air
#107(.025)	.0016	11348	9,897,500	air
#111(.025)	.0026	12968	15,089,100	air

σ (psi) N (cycles)

Specimen	σ_i final	N_f	Final environment
#94	36655	2500	air
#16(s)	40325	7800	air
#107(.025)	36655	2700	air
#111(.025)	36655	2600	air

APPENDIX E

Determination of Effective Notch Depth for Smooth Specimen Surface

For selected values of constant stress (σ_i) between 20 and 45 Ksi, ℓ_o v N_f was plotted for constant values of σ_i. Smooth curves were drawn through the data points. For $\ell_o < .002$ in. extrapolation of the curves was accomplished using a straight line approximation with a slope equal to that at $\ell_o = .002$ in. A similar approach was used to extrapolate for $\ell_o > .025$ in.

The value of ℓ_o corresponding to N_f (smooth specimen) was found. This was done for each selected value of σ_i for both air and salt water. The value of ℓ_o for the different values of σ_i ranged from .00048 in. to .00072 in. for air and .0006 in. to .001 in. for salt water.

This suggests that an effective surface notch depth can be attributed to the smooth surface of the as-received material used in this investigation. An average value of $\ell_o = .0005$ in. was selected and used for subsequent analysis. Attributing a notch depth to the smooth surface permits calculating a stress intensity factor for the various smooth specimen data points.

Data used to construct the ℓ_o v N_f curves are presented in Tables E1 and E2 for air and salt water, respectively.

Table E1

N_f v ℓ_o for Constant σ_i (Air)

ℓ_o/σ_i	45 Ksi	40 Ksi	35 Ksi	30 Ksi	25 Ksi	20 Ksi
smooth	1.25×10^4	2.25×10^4	4.5×10^4	9.5×10^4	2.3×10^5	1.6×10^6
.0015	8.2×10^3	1.53×10^4	3.0×10^4	6.5×10^4	1.62×10^5	9.7×10^5
.002	7.4×10^3	1.37×10^4	2.7×10^4	5.9×10^4	1.5×10^5	8.0×10^5
.006	4.3×10^3	7.8×10^3	1.56×10^4	3.45×10^4	9.2×10^4	3.45×10^5
.0115	2.55×10^3	4.8×10^3	9.6×10^3	2.1×10^4	5.5×10^4	1.73×10^5
.025	9.2×10^2	1.75×10^3	3.6×10^3	8.3×10^3	2.2×10^4	7.5×10^4
.040	3.8×10^2	8.4×10^2	1.73×10^3	4.0×10^3	1.0×10^4	4.3×10^4

Table E2

N_f v ℓ_o for Constant σ_i (Salt Water)

ℓ_o/σ_i	45 Ksi	40 Ksi	35 Ksi	30 Ksi	25 Ksi	20 Ksi
smooth	8.4×10^3	1.5×10^4	2.92×10^4	6.5×10^4	1.58×10^5	4.9×10^5
.0015	6.1×10^3	1.11×10^4	2.25×10^4	5.0×10^4	1.25×10^5	4.25×10^5
.002	5.5×10^3	1.0×10^4	2.0×10^4	4.42×10^4	1.12×10^5	3.73×10^5
.006	3.15×10^3	5.7×10^3	1.15×10^4	2.6×10^4	6.65×10^4	2.1×10^5
.0115	1.85×10^3	3.42×10^3	6.9×10^3	1.55×10^4	4.02×10^4	1.26×10^5
.025	8.1×10^2	1.5×10^3	3.1×10^3	7.2×10^3	1.92×10^4	6.4×10^4
.040	4.3×10^2	8.4×10^2	1.81×10^3	4.1×10^3	1.15×10^4	4.0×10^4

Values for smooth, .002 in., .0115 in., and .025 in. machined notch specimens were used to draw the curves. The values for .0015 in., .006 in., and .040 in. notches were obtained by interpolation and extrapolation. The data are plotted in Figures E1 and E2 for air and salt water, respectively.

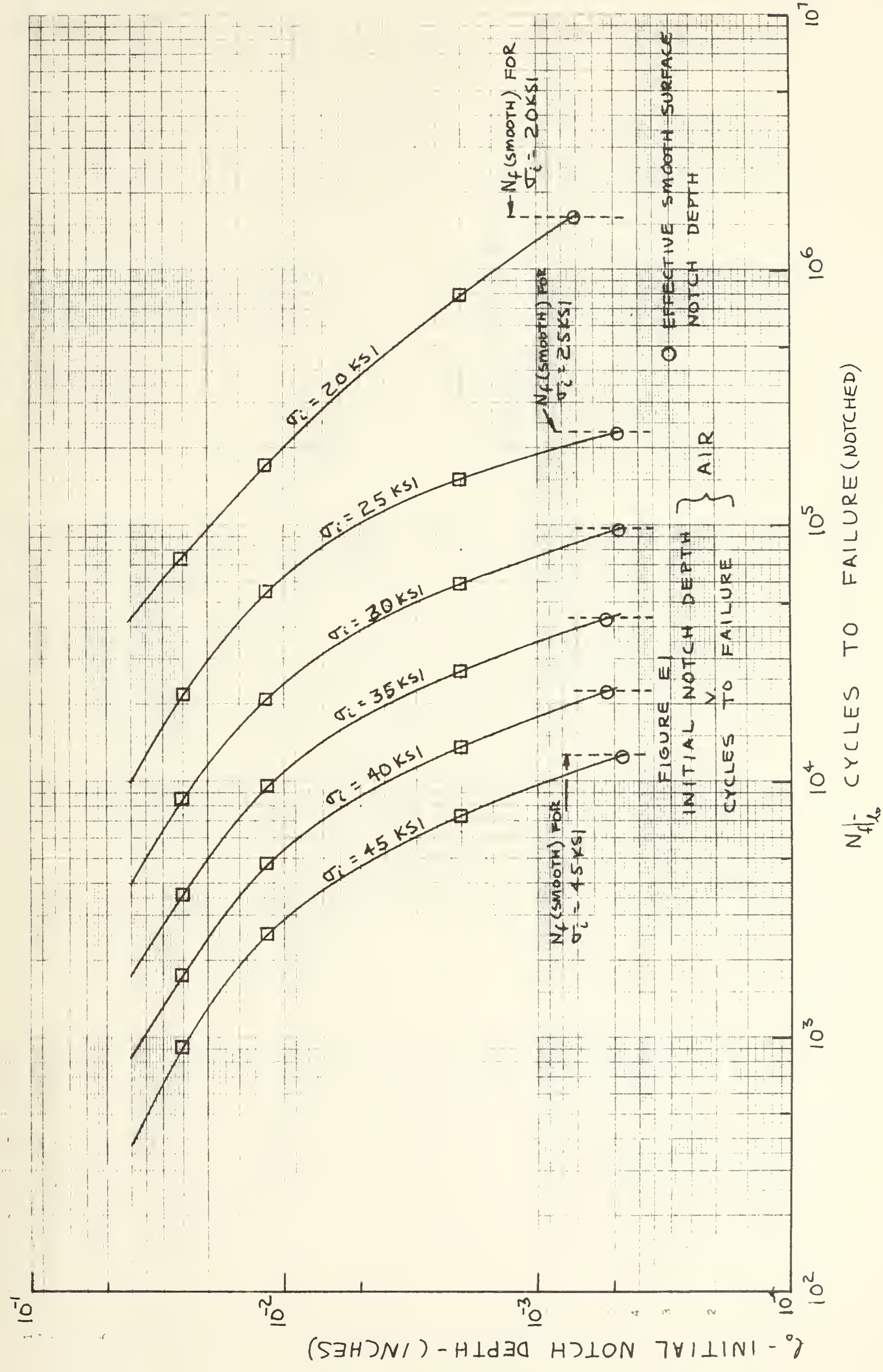

FIGURE E1
INITIAL NOTCH DEPTH v. CYCLES TO FAILURE } AIR

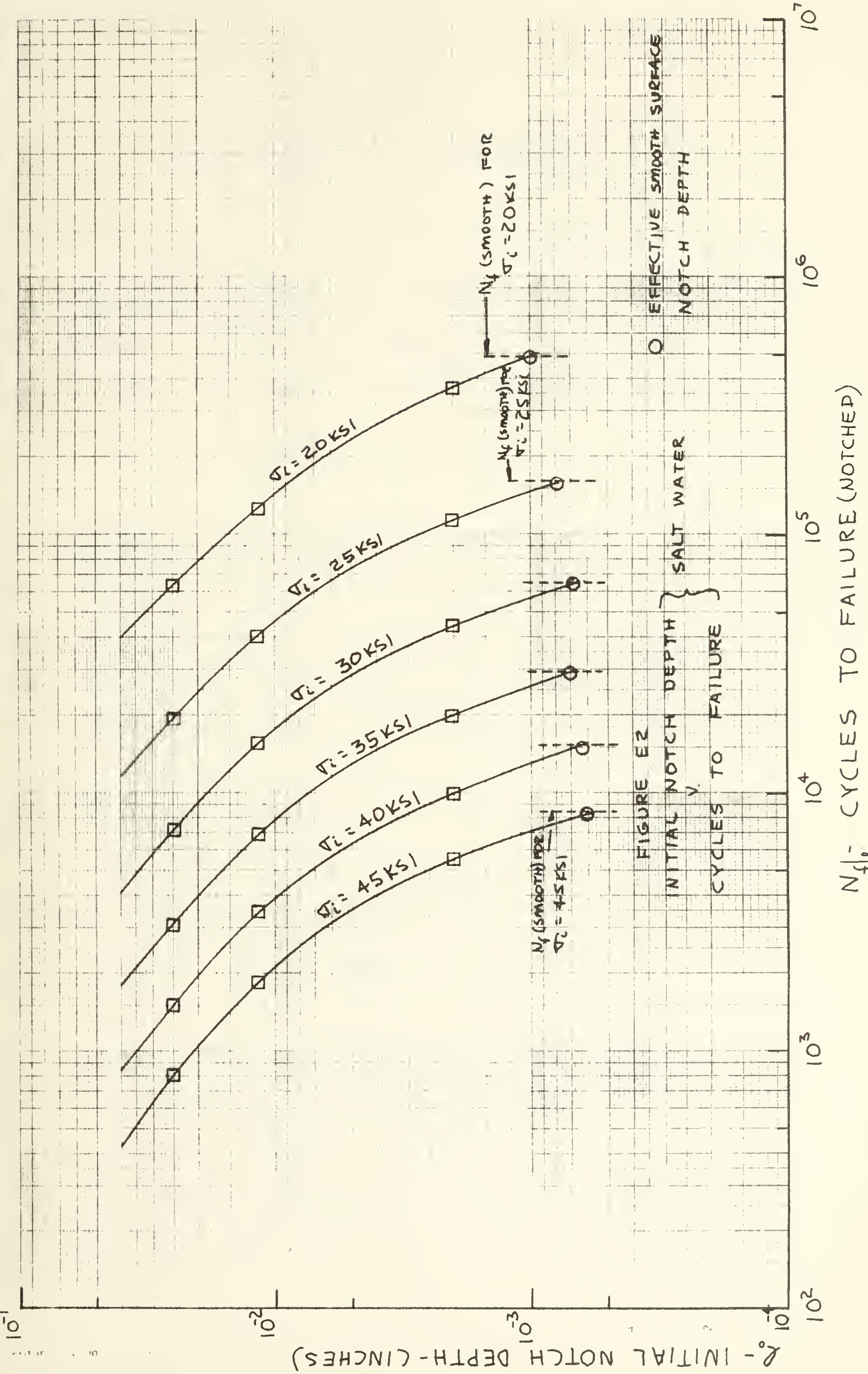

FIGURE E2
INITIAL NOTCH DEPTH v. CYCLES TO FAILURE } SALT WATER

APPENDIX F

Crack Propagation Rate Analysis

The σ_i v N_f and ℓ_o v N_f curves were used to develop σ_i v $N_p|_s^\ell$ curves where $N_p|_s^\ell$ is the number of cycles required to propagate a crack from a smooth surface condition to a depth ℓ. The following expression was used to determine $N_p|_s^\ell$

$$N_p|_s^\ell = N_f|_s - N_f|_{\ell_o} \qquad (6)$$

Equation (6) was used to directly determine σ_i v $N_p|_s^\ell$ for crack depths of .002 in., .0115 in., and .025 in. Additional curves for crack depths of .0015 in., .006 in., and .040 in. were determined by interpolation and extrapolation.

Intermediate steps and calculational results for the σ_i v $N_p|_s^\ell$ evaluation are given in Tables F1 and F2 for air and salt water, respectively.

Plots of σ_i v $N_p|_s^\ell$ are presented in Figures F1 and F2 for air and salt water, respectively.

The plots of σ_i v $N_p|_s^\ell$ were used to construct curves of ℓ v $N_p|_s^\ell$ for various constant values of σ_i over the range 20 - 45 Ksi. The points used to construct the ℓ v $N_p|_s^\ell$ curves in Figures F3 and F4 are presented in Tables F3 and F4 for air and salt water, respectively.

The slope of the ℓ v $N_p|_s^\ell$ curves which correspond to $d\ell/dn$ ($n = N_p|_s^\ell$) was then found graphically for various

Table F1

Calculational Results for σ_i v $N_P|_s^{\ell}$ (Air)

σ_i	N_{fs}	$N_{f\ .002}$	$N_{f\ .0115}$	$N_{f\ .025}$	$N_s - N_{f.002} = N_{P.002}$	$N_s - N_{f.0115} = N_{P.0115}$	$N_s - N_{f.0115} = N_{P.025}$
45	12.5×10^3	7.4×10^3	2.55×10^3	$.92\times10^3$	5.1×10^3	9.95×10^3	11.6×10^3
40	22.5×10^3	13.7×10^3	4.8×10^3	1.75×10^3	8.8×10^3	17.7×10^3	20.8×10^3
35	45.0×10^3	27×10^3	9.6×10^3	3.6×10^3	18×10^3	35.4×10^3	41.4×10^3
30	95.0×10^3	59×10^3	21×10^3	8.3×10^3	36×10^3	74×10^3	86.7×10^3
25	230×10^3	150×10^3	55×10^3	22×10^3	80×10^3	175×10^3	208×10^3
20	1600×10^3	800×10^3	173×10^3	75×10^3	800×10^3	1427×10^3	1525×10^3
19.2	10000×10^3	2000×10^3	225×10^3	97×10^3	8000×10^3	9775×10^3	9903×10^3
21	650×10^3	380×10^3	133×10^3	59×10^3	270×10^3	517×10^3	591×10^3

σ_i (Ksi) N(cycles) ℓ(in.)

σ_i	N_{fs}	$N_{f.0015}$	$N_{f\ .006}$	$N_{f\ .040}$	$N_{P.0015}$	$N_{P\ .006}$	$N_{P\ .040}$
45	12.5×10^3	8.2×10^3	4.3×10^3	$.38\times10^3$	4.3×10^3	8.2×10^3	12.1×10^3
40	22.5×10^3	15.3×10^3	7.8×10^3	$.84\times10^3$	7.2×10^3	14.7×10^3	21.7×10^3
35	45.0×10^3	30×10^3	15.6×10^3	1.73×10^3	15×10^3	29.4×10^3	43.3×10^3
30	95.0×10^3	65×10^3	34.5×10^3	4×10^3	30×10^3	60.5×10^3	91×10^3
25	230×10^3	162×10^3	92×10^3	10×10^3	68×10^3	138×10^3	220×10^3
20	1600×10^3	970×10^3	345×10^3	43×10^3	630×10^3	1255×10^3	1557×10^3
19.2	10000×10^3	2750×10^3	520×10^3	46.5×10^3	7250×10^3	9480×10^3	9954×10^3
21	650×10^3	420×10^3	223×10^3	30.3×10^3	230×10^3	427×10^3	620×10^3

Table F2

Calculational Results for σ_i v $N_P|_s^{\ell}$ (Salt Water)

σ_i	σ_i (Ksi) N_{fs}	N(cycles) $N_{f.002}$	ℓ (in.) $N_{f.0115}$	$N_{f.025}$	$N_s - N_{f.002}$ $N_{P.002}$	$N_s - N_{f.0115}$ $N_{P.0115}$	$N_s - N_{f.025}$ $N_{P.025}$
45	8.4×10^3	5.5×10^3	1.85×10^3	$.81 \times 10^3$	2.9×10^3	6.55×10^3	7.59×10^3
40	15×10^3	10×10^3	3.42×10^3	1.5×10^3	5×10^3	11.58×10^3	13.5×10^3
35	29.2×10^3	20×10^3	6.9×10^3	3.1×10^3	9.2×10^3	22.3×10^3	26.1×10^3
30	65×10^3	44.2×10^3	15.5×10^3	7.2×10^3	20.8×10^3	49.5×10^3	57.8×10^3
25	158×10^3	112×10^3	40.2×10^3	19.2×10^3	46×10^3	117.8×10^3	138.8×10^3
20	490×10^3	373×10^3	126×10^3	64×10^3	117×10^3	364×10^3	426×10^3
17.5	1350×10^3	730×10^3	251×10^3	130×10^3	620×10^3	1099×10^3	1220×10^3
15.2	10000×10^3	2300×10^3	530×10^3	280×10^3	7700×10^3	9470×10^3	9770×10^3

σ_i	N_{fs}	$N_{f.0015}$	$N_{f.006}$	$N_{f.040}$	$N_{P.0015}$	$N_{P.006}$	$N_{P.040}$
45	8.4×10^3	6.1×10^3	3.15×10^3	$.43 \times 10^3$	2.3×10^3	5.25×10^3	7.97×10^3
40	15×10^3	11.1×10^3	5.7×10^3	$.84 \times 10^3$	3.9×10^3	9.3×10^3	14.16×10^3
35	29.2×10^3	22.5×10^3	11.5×10^3	1.81×10^3	6.7×10^3	17.7×10^3	27.39×10^3
30	65×10^3	50×10^3	26×10^3	4.1×10^3	15×10^3	39×10^3	60.9×10^3
25	158×10^3	125×10^3	66.5×10^3	11.5×10^3	33×10^3	91.5×10^3	146.5×10^3
20	490×10^3	418×10^3	210×10^3	40×10^3	72×10^3	280×10^3	450×10^3
17.5	1350×10^3	830×10^3	410×10^3	79×10^3	520×10^3	940×10^3	1271×10^3
15.2	10000×10^3	3000×10^3	940×10^3	195×10^3	7000×10^3	9060×10^3	9805×10^3

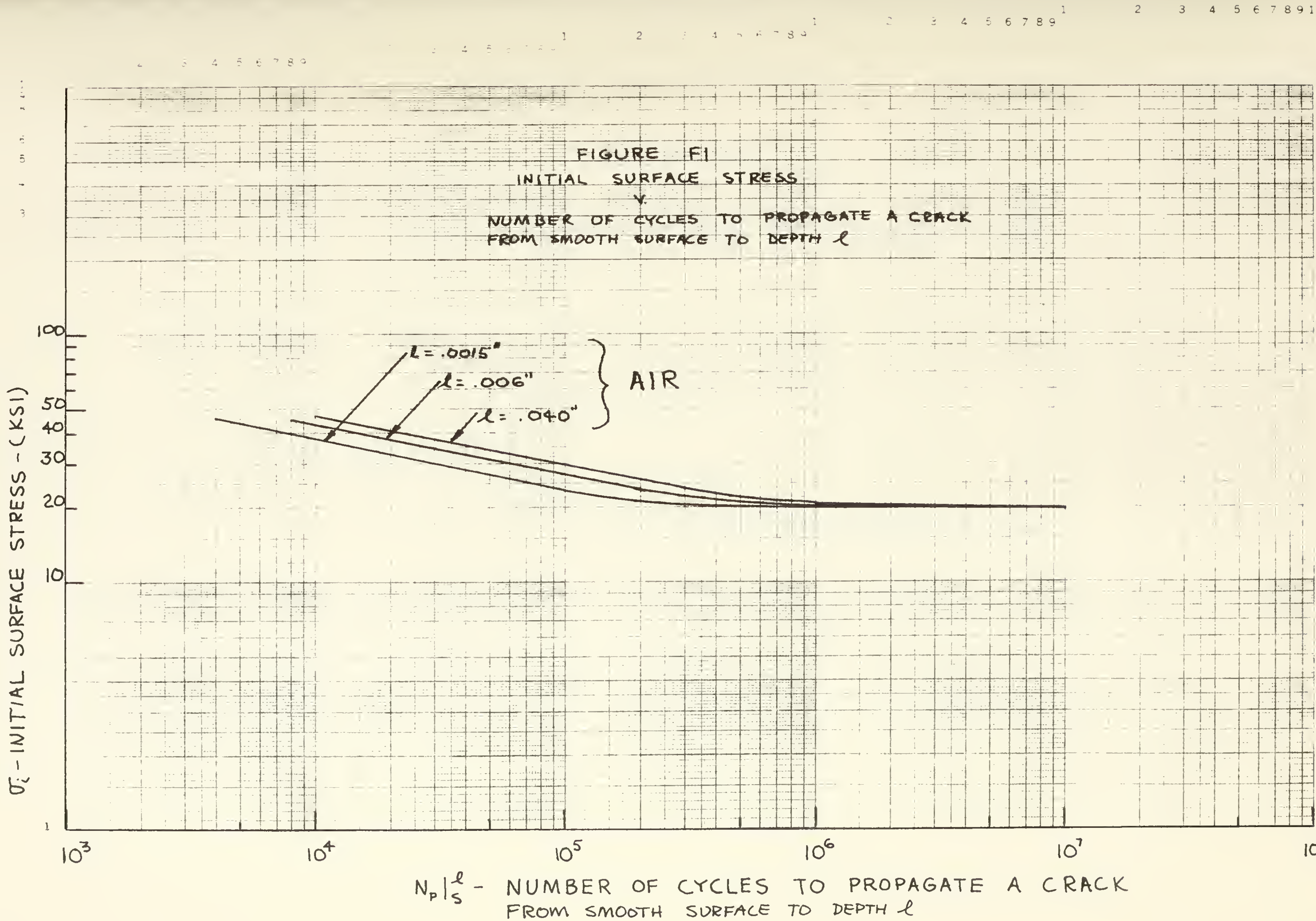
FIGURE F1
INITIAL SURFACE STRESS
v.
NUMBER OF CYCLES TO PROPAGATE A CRACK
FROM SMOOTH SURFACE TO DEPTH ℓ
ℓ = .0015"
ℓ = .006"
ℓ = .040"
AIR
100
50
40
30
20
10
1
σi - INITIAL SURFACE STRESS - (KSI)
10^3
10^4
10^5
10^6
10^7
10^8
Np|ℓs - NUMBER OF CYCLES TO PROPAGATE A CRACK
FROM SMOOTH SURFACE TO DEPTH ℓ

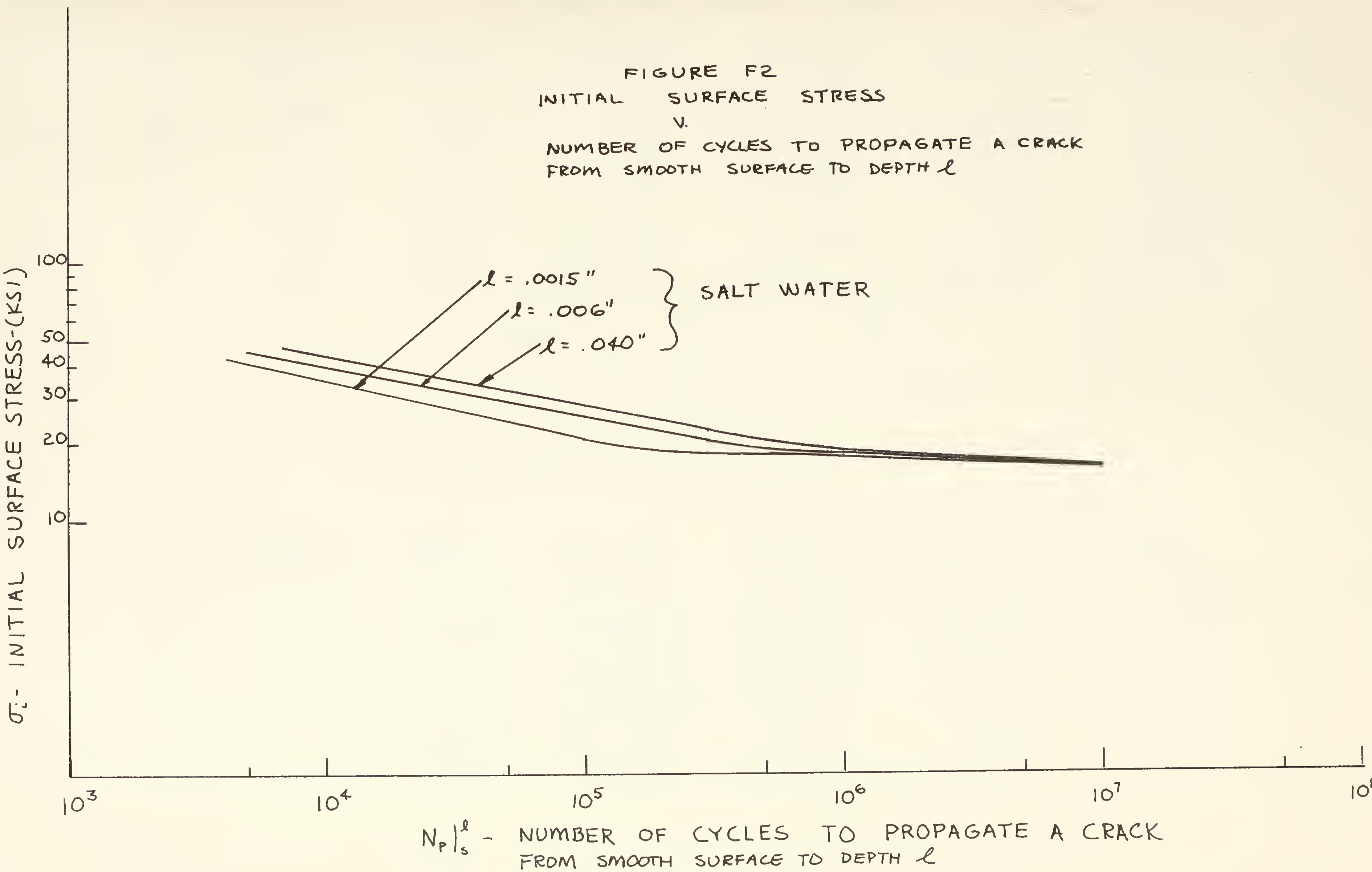

FIGURE F2
INITIAL SURFACE STRESS
V.
NUMBER OF CYCLES TO PROPAGATE A CRACK
FROM SMOOTH SURFACE TO DEPTH ℓ

Table F3

ℓ v $N_P|_s^\ell$ for Constant σ_i (Air)

σ_i/ℓ	N_P@.0015	N_P@.002	N_P@.006	N_P@.0115	N_P@.025	N_P@.040
45	4,250	5,100	8,000	10,000	11,800	12,700
40	7,500	9,000	14,300	17,700	20,600	22,300
35	14,200	17,000	28,000	34,400	40,200	43,300
30	30,000	37,000	60,300	74,000	87,000	91,000
25	71,000	88,000	147,000	183,000	211,000	221,000
20	630,000	800,000	1,255,000	1,427,000	1,525,000	1,557,000

σ_i(Ksi) N(cycles) ℓ(in.)

Table F4

ℓ v $N_P|_s^\ell$ for Constant σ_i (Salt Water)

σ_i/ℓ	N_P@.0015	N_P@.002	N_P@.006	N_P@.0115	N_P@.025	N_P@.040
45	2.25×10^3	2.8×10^3	5.12×10^3	6.55×10^3	7.6×10^3	8×10^3
40	3.83×10^3	4.85×10^3	9.13×10^3	1.18×10^4	1.35×10^4	1.43×10^3
35	7.25×10^3	9.32×10^3	1.78×10^4	2.33×10^4	2.61×10^4	2.8×10^4
30	1.5×10^4	2×10^4	3.85×10^4	5.03×10^4	5.8×10^4	6.1×10^4
25	3.53×10^4	4.8×10^4	9.5×10^4	1.22×10^5	1.38×10^5	1.47×10^5
20	1×10^5	1.4×10^5	2.8×10^5	3.65×10^5	4.3×10^5	4.5×10^5

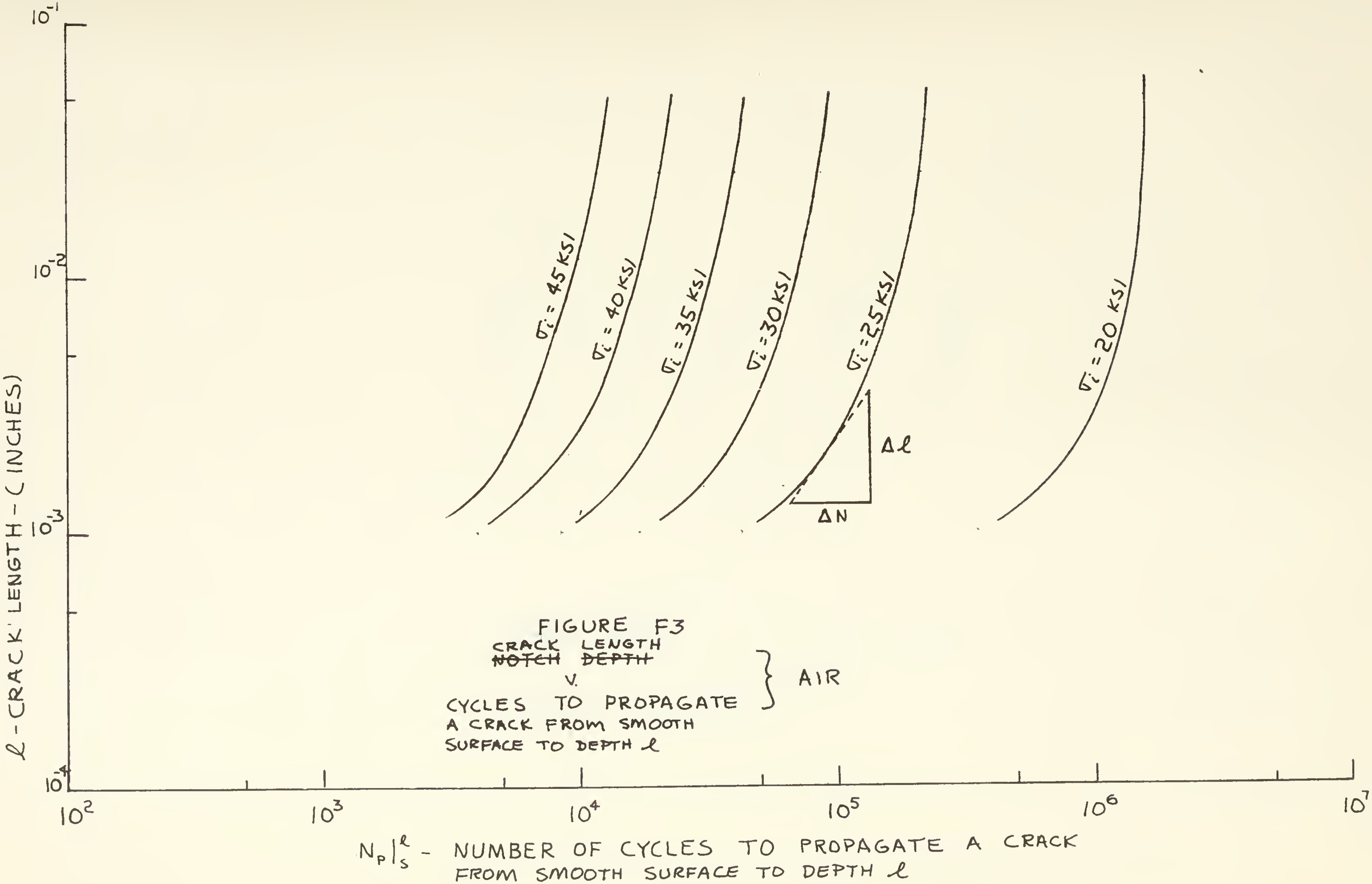

FIGURE F3

CRACK LENGTH ~~NOTCH DEPTH~~ v. CYCLES TO PROPAGATE A CRACK FROM SMOOTH SURFACE TO DEPTH ℓ } AIR

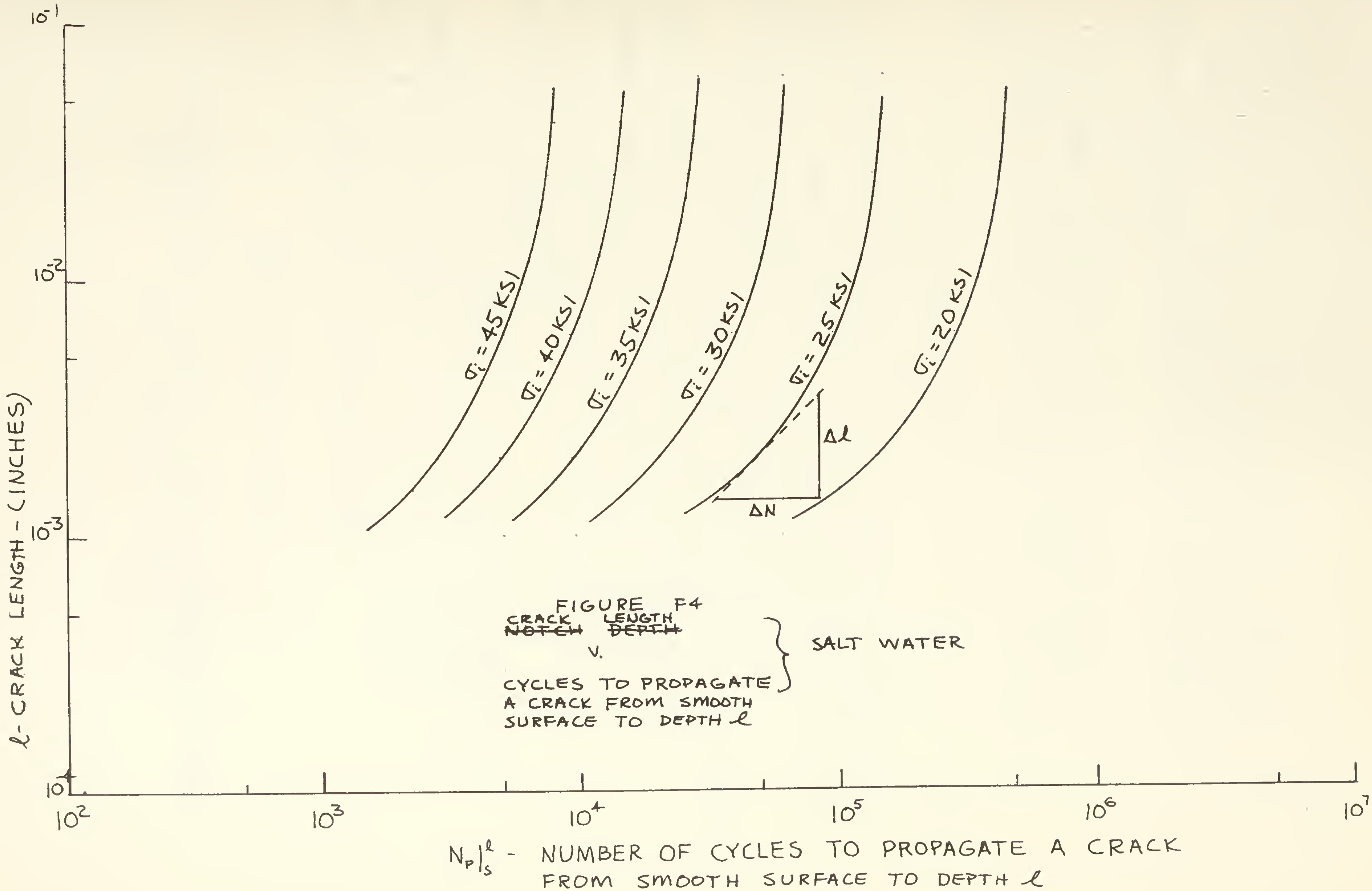

FIGURE F4

CRACK LENGTH ~~NOTCH DEPTH~~ V. CYCLES TO PROPAGATE A CRACK FROM SMOOTH SURFACE TO DEPTH ℓ

values of ℓ = .0015 in., .002 in., .006 in., .0115 in., .025 in., and .040 in. The intermediate results for finding $d\ell/dn$ are presented in Tables F5 and F6 for air and salt water, respectively.

For each value of ℓ for which a $d\ell/dn$ value was determined, a corresponding stress intensity was calculated using

$$\Delta K_i = \gamma \sigma_i \sqrt{\pi \ell} \tag{7}$$

The method used to determine stress intensity is explained in Appendix G. The intermediate results for determining ΔK_i for the various values of ℓ are presented in Table F7.

The values of ΔK_i were then plotted against corresponding values of $d\ell/dn$ to see whether fracture mechanics would correlate the data of this investigation. The plots of ΔK_i v $d\ell/dn$ are presented in Figures F5 and F6 for air and salt water, respectively.

A safe crack propagation curve was drawn using the lowest ΔK_i value for each value of $d\ell/dn$. The following modified form of the Paris Law was used to develop a predictor equation for these safe curves.

$$\frac{d\ell}{dn} = A(\Delta K_i - \Delta K_{th})^n \tag{8}$$

Trial and error was used to find the empirical values for A, n, and ΔK_{th}. These values are summarized in Table F8.

Table F5

Determination of $\frac{d\ell}{dn}$ (Air)

ℓ	$\Delta\ell$	ΔN $\sigma_i=45$	$\Delta\ell/\Delta N$	ΔN $\sigma_i=40$	$\Delta\ell/\Delta N$	ΔN $\sigma_i=35$	$\Delta\ell/\Delta N$
.0015	.001	3.07×10^{3}	3.26×10^{-7}	4.8×10^{3}	2.08×10^{-7}	7.5×10^{3}	1.333×10^{-7}
.002	.002	3.6×10^{3}	5.56×10^{-7}	5.2×10^{3}	3.85×10^{-7}	9.7×10^{3}	2.06×10^{-7}
.006	.003	1.1×10^{3}	2.73×10^{-6}	2×10^{3}	1.5×10^{-6}	4.3×10^{3}	6.98×10^{-7}
.0115	.01	1.6×10^{3}	6.25×10^{-6}	2.5×10^{3}	4×10^{-6}	6.8×10^{3}	1.47×10^{-6}
.025	.02	1.6×10^{3}	1.25×10^{-5}	2.8×10^{3}	7.14×10^{-6}	7.3×10^{3}	2.74×10^{-6}
.040	.03	1.3×10^{3}	2.31×10^{-5}	2.7×10^{3}	1.11×10^{-5}	7×10^{3}	4.29×10^{-6}

σ_i (Ksi) N(cycles) ℓ(in.)

ℓ	$\Delta\ell$	ΔN $\sigma_i=30$	$\Delta\ell/\Delta N$	ΔN $\sigma_i=25$	$\Delta\ell/\Delta N$	ΔN $\sigma_i=20$	$\Delta\ell/\Delta N$
.0015	.001	19.7×10^{3}	5.08×10^{-8}	46×10^{3}	2.17×10^{-8}	4.3×10^{5}	2.32×10^{-9}
.002	.002	21×10^{3}	9.52×10^{-8}	51×10^{3}	3.92×10^{-8}	4.9×10^{5}	4.08×10^{-9}
.006	.003	9×10^{3}	3.33×10^{-7}	27×10^{3}	1.11×10^{-7}	1.4×10^{5}	2.14×10^{-8}
.0115	.01	12×10^{3}	8.33×10^{-7}	31×10^{3}	3.23×10^{-7}	1.4×10^{5}	7.14×10^{-8}
.025	.02	10×10^{3}	2×10^{-6}	20×10^{3}	1×10^{-6}	6×10^{4}	3.33×10^{-7}
.040	.03	5×10^{3}	6×10^{-6}	17×10^{3}	1.76×10^{-6}	5×10^{4}	6×10^{-7}

Table F6

Determination of $\frac{d\ell}{dn}$ (Salt Water)

ℓ	$\Delta\ell$	ΔN $\sigma_i=45$	$\Delta\ell/\Delta N$	ΔN $\sigma_i=40$	$\Delta\ell/\Delta N$	ΔN $\sigma_i=35$	$\Delta\ell/\Delta N$
.0015	.001	1280	7.81×10^{-7}	2370	4.22×10^{-7}	4600	2.17×10^{-7}
.002	.002	1730	1.16×10^{-6}	3150	6.35×10^{-7}	6000	3.33×10^{-7}
.006	.003	1100	2.73×10^{-6}	1800	1.67×10^{-6}	4000	7.5×10^{-7}
.0115	.010	1300	7.69×10^{-6}	2300	4.35×10^{-6}	5000	2×10^{-6}
.025	.020	850	2.35×10^{-5}	1800	1.11×10^{-5}	3500	5.71×10^{-6}
.040	.030	450	6.67×10^{-5}	900	3.33×10^{-5}	1700	1.77×10^{-5}

σ_i (Ksi) N(cycles) ℓ(in.)

ℓ	$\Delta\ell$	ΔN $\sigma_i=30$	$\Delta\ell/\Delta N$	ΔN $\sigma_i=25$	$\Delta\ell/\Delta N$	ΔN $\sigma_i=20$	$\Delta\ell/\Delta N$
.0015	.001	11400	8.77×10^{-8}	28000	3.57×10^{-8}	85500	1.17×10^{-8}
.002	.002	15300	1.31×10^{-7}	38500	5.19×10^{-8}	125000	1.6×10^{-8}
.006	.003	8500	3.53×10^{-7}	20000	1.5×10^{-7}	63000	4.76×10^{-8}
.0115	.010	11000	9.09×10^{-7}	26000	3.85×10^{-7}	80000	1.25×10^{-7}
.025	.020	6000	3.33×10^{-6}	11000	1.82×10^{-6}	32000	6.25×10^{-7}
.040	.030	2300	1.3×10^{-5}	10000	3×10^{-6}	25000	1.2×10^{-6}

Table F7

Determination of ΔK_i

ℓ/σ_i	$\sqrt{\pi\ell}$	45 Ksi $\gamma/\Delta K_i$	40 Ksi $\gamma/\Delta K_i$	35 Ksi $\gamma/\Delta K_i$	30 Ksi $\gamma/\Delta K_i$	25 Ksi $\gamma/\Delta K_i$	20 Ksi $\gamma/\Delta K_i$
.0015	.0686	1.104/3.41	1.085/2.97	1.067/2.56	1.052/2.17	1.038/1.79	1.029/1.41
.002	.0793	1.082/3.88	1.063/3.37	1.045/2.91	1.032/2.46	1.018/2.02	1.009/1.60
.006	.1373	1.054/6.51	1.036/5.69	1.018/4.90	1.005/4.14	.991/3.40	.983/2.70
.0115	.1901	1.006/8.6	.988/7.51	.972/6.46	.959/5.47	.946/4.49	.938/3.56
.025	.2802	.885/11.2	.870/9.74	.855/8.39	.844/7.10	.833/5.83	.825/4.62
.040	.3545	.777/12.4	.763/10.8	.752/9.32	.741/7.85	.732/6.49	.725/5.14

ℓ(in.)

Table F8

Crack Propagation Equation Empirical Constants

	A(in./cycle)	n	ΔK_{th}(Ksi$\sqrt{\text{in.}}$)
Air	1×10^{-7}	2.2	1.25
Salt Water	1.1×10^{-7}	2.6	1

The curves predicted by these equations are shown in Figures F5 and F6.

FIGURE F5

INITIAL STRESS INTENSITY v CRACK PROPAGATION RATE AIR

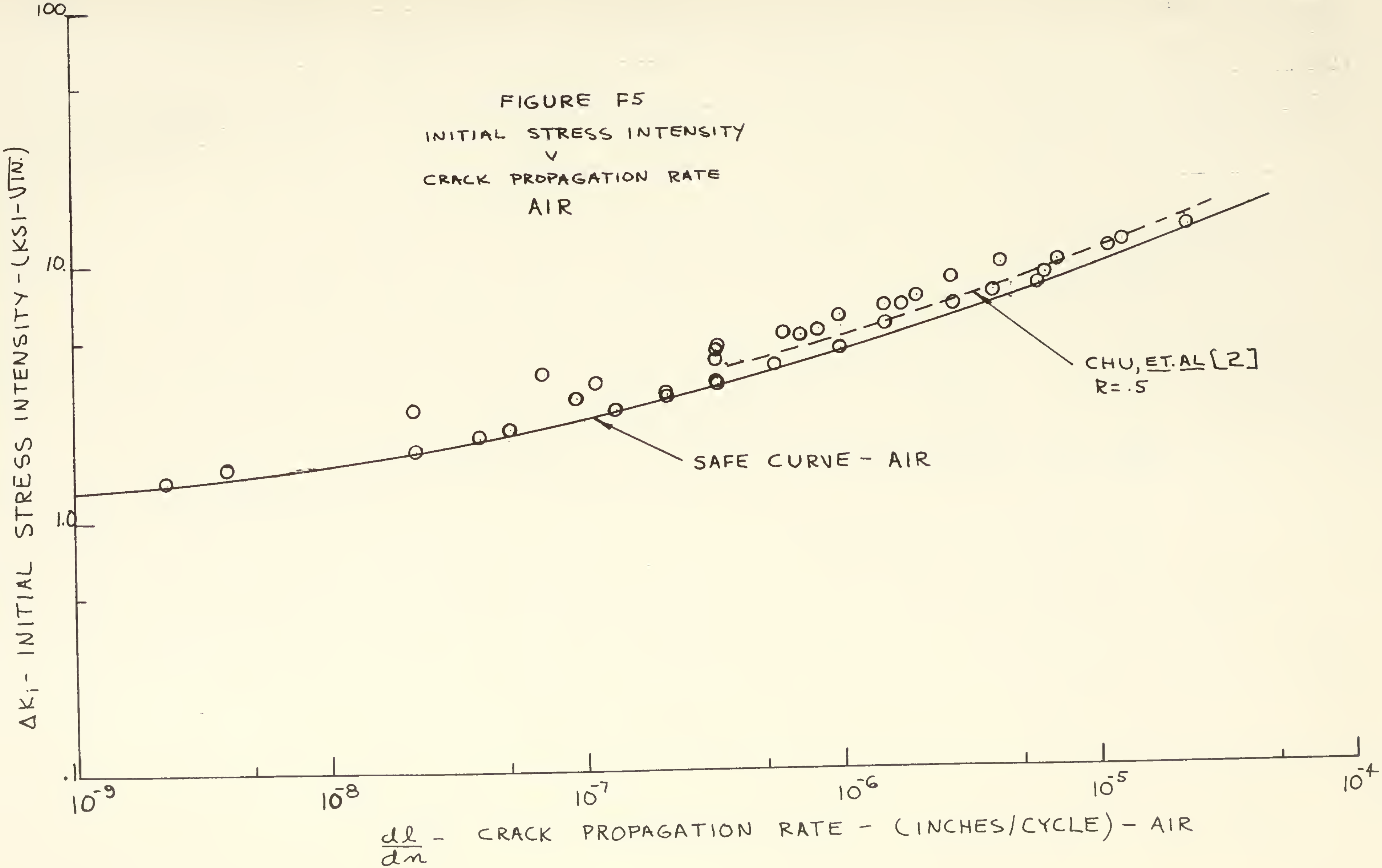

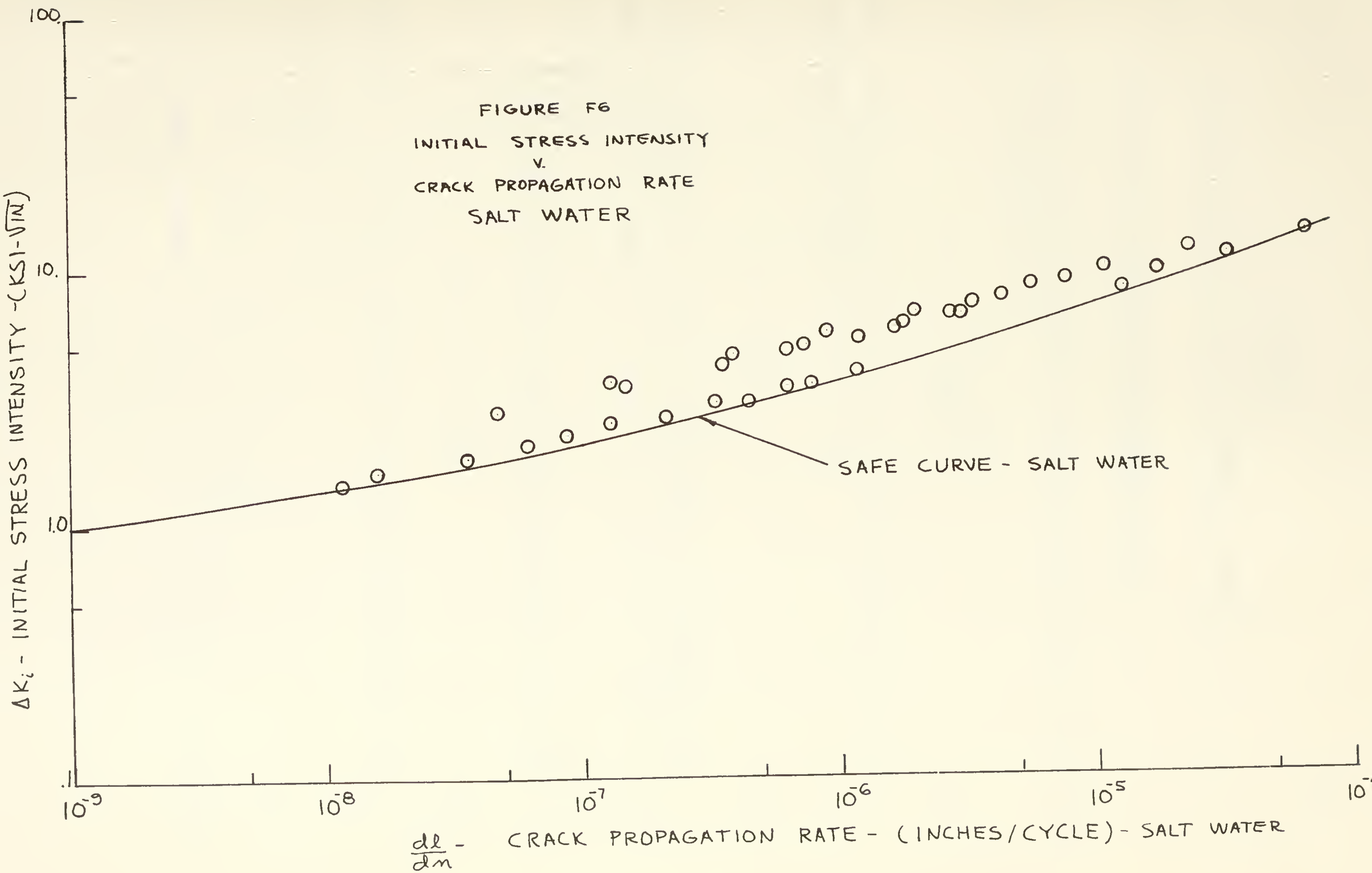

FIGURE F6

INITIAL STRESS INTENSITY

V.

CRACK PROPAGATION RATE

SALT WATER

APPENDIX G

Determination of Stress Intensity Factor

1. Correction for Surface Intensification

Stress intensity factors were calculated using the method of Shah and Kobayashi [7]

$$\Delta K_i = \frac{M_B \sigma_i \sqrt{\pi \ell}}{E(k)} \qquad (G1)$$

where values for M_B (correction for front and back surface) were taken from Figure 14 of [7] and

$$\sigma_i = \frac{Mt}{2I} \qquad (G2)$$

σ_i rather than $2\sigma_i$ was used to calculate ΔK_i because crack propagation was assumed to occur only during the tension part of a cycle.

E(k) is an elliptic integral of the second kind where

$$k = \left(1 - \frac{\ell^2}{a^2}\right) \qquad (G3)$$

Broek [17] provides an equation for approximating E(k) and it was used for this work.

$$E(k) = \frac{\pi}{2} \{1 - \frac{1}{4}k - \frac{3}{64}k^2 - \ldots \} \qquad (G4)$$

The following stress intensity correction parameter was defined

$$\gamma_G = \frac{M_B}{E(k)} \quad \text{(G5)}$$

The calculational results for determining γ_G are summarized in Table G1.

Table G1

Stress Intensity Correction Parameters for

Surface Intensification (γ_G)

Crack length	a	ℓ	ℓ/a	ℓ/t	M_B	E(k)	γ_G
.0015	.0275	.0015	.0545	.0120	1.115	1.106	1.01
.002	.0315	.002	.0635	.0160	1.095	1.107	.99
.004	.0445	.004	.0899	.0320	1.087	1.109	.98
.0115	.075	.0115	.1533	.0920	1.030	1.117	.92
.025	.109	.025	.2294	.2000	.9175	1.133	.81
.040	.136	.040	.2941	.320	.819	1.151	.712

2. Correction for Plastic Zone Size

Presence of a plastic zone modifies the elastic stress field as if the crack were longer. Broek [17] states:

$$\ell_{effective} = \ell_{actual} + r_p^* \quad \text{(G6)}$$

where

$$r_p^* = \frac{(\Delta K)^2}{4\pi\sqrt{2}\,\sigma_y^2} \quad \text{(G7)}$$

Defining

$$\gamma_p = \frac{(\Delta K)_{corrected}}{(\Delta K)_{uncorrected}} \quad \text{(G8)}$$

$$\gamma_p = \frac{\gamma_G \sigma \sqrt{\pi \ell_{effective}}}{\gamma_G \sigma \sqrt{\pi \ell actual}} = \sqrt{\frac{\ell_{eff}}{\ell_{act}}} \quad \text{(G8)}$$

This parameter depends upon both σ and ℓ. However, the dependence on ℓ is so weak that it can be ignored. Calculated values for γ_P are presented in Table G2.

Table G2

Stress Intensity Correction Parameters for

Plastic Zone Size (γ_P)

γ_P/σ	10Ksi	15Ksi	20Ksi	25Ksi	30Ksi	35Ksi	40Ksi	45Ksi
γ_P	1.005	1.012	1.019	1.028	1.042	1.056	1.074	1.093

3. Stress Intensity Factor Correction Parameter (γ)

A stress intensity correction parameter that accounts for both surface intensification and plastic zone size was defined

$$\gamma = \gamma_G \gamma_P \tag{G9}$$

This parameter was then used to determine the stress intensity factors used for this investigation. The calculated values for γ are given in Table G3. The intermediate values were obtained by graphical interpolation. These factors were then used to calculate stress intensity factors using

$$\Delta K = \gamma \sigma \sqrt{\pi \ell} \tag{7}$$

Table G3

σ_i (Ksi) ℓ(in.)

σ_i/ℓ	.0005	.0015	.002	.006	.0115	.020	.025	.040
10	1.045	1.015	.995	.968	.925	.855	.814	.715
15	1.048	1.022	1.002	.975	.931	.860	.820	.720
20	1.055	1.029	1.009	.983	.938	.867	.825	.725
25	1.070	1.038	1.018	.991	.946	.875	.833	.732
30	1.082	1.052	1.032	1.005	.959	.887	.844	.741
35	1.107	1.067	1.045	1.018	.972	.898	.855	.752
40	1.125	1.085	1.063	1.036	.988	.914	.870	.763
45	1.140	1.104	1.082	1.054	1.006	.930	.885	.777
50	1.155	1.123	1.102					
53.5	1.160							

APPENDIX H

Fatigue Design/Failure Criterion

The σ_i v N_f curves were used to develop ℓ_o v σ_i data for various constant values of N_f equal to 1×10^7, 1×10^6, 1×10^5, 1×10^4, and 5×10^3 cycles. Points for ℓ_o equal to .0005 (smooth) in., .002 in., .0115 in., and .025 in. were used to construct the plots in Figures H1 and H2 for air and salt water, respectively. These curves were then used to find values for additional notch depths of .0015 in., .006 in., .020 in., and .040 in. These values were determined by interpolation/extrapolation. Straight line extrapolation was used to find the values for ℓ_o = .040 in. A summary of the ℓ_o v σ_i data is presented in Tables H1 and H2 for air and salt water respectively.

Table H1

ℓ_o v σ_i for Constant N_f (Air)

N(cycles) σ_i(Ksi) ℓ(in.)

N_f/ℓ_o	.0005 smooth	.0015	.002	.006	.0015	.020	.025	.040
5×10^3	53.5	50.8	49	44	39.5	35	33	29
1×10^4	47	44	42.3	38.5	34.5	30.3	29	26
1×10^5	29.5	28	27.2	25	22.2	20	19	17.2
1×10^6	20.2	20	19.8	17.8	17.6(16.2)	14.5	14	13
1×10^7	19.2	18.6	18.5	16.6	17.1(15.3)	14	13.2	12

Table H2

ℓ_o v N_f for Constant N_f (Salt Water)

N(cycles) σ_i(Ksi) ℓ(in.)

N_f/ℓ_o	.0005 smooth	.0015	.002	.006	.0115	.020	.025	.040
$5x10^3$	49.8	47	46	41	37.2	33.7	32	28.3
$1x10^4$	43.3	41	40	35.3	32.3	29.3	28.1	25.3
$1x10^5$	27.3	26	25.3	22.6	21	19.2	18.4	17
$1x10^6$	18	17	16.6	15	13.5	12.5	12	10.8
$1x10^7$	15.2	14	13.7	12.2	11.3	10.2	9.4(10)	9

On plotting the data, it was noted that three points were off the curves predicted by the other points. It was concluded that this was probably due to experimental error and therefore the associated stress for these points was slightly modified as indicated in Table H3.

Table H3

ℓ_o v N_f for Constant N_f Data Modification

Environment	ℓ_o	N_f	σ_i (original)	σ_i (modified)
air	.0115	1×10^6	17.8	16.2
air	.0115	1×10^7	17.1	15.3
salt water	.025	1×10^7	9.4	10

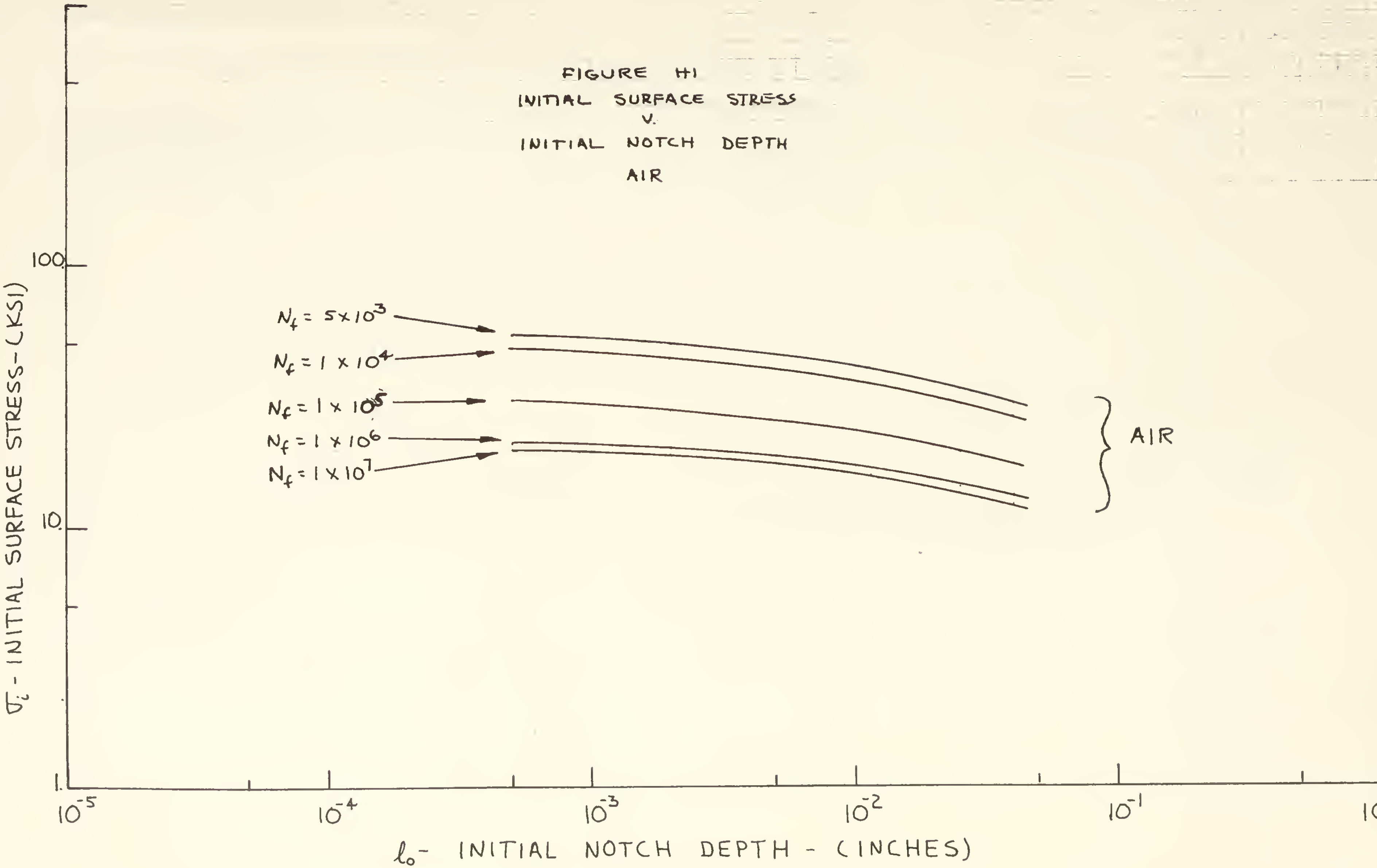

FIGURE H1
INITIAL SURFACE STRESS
V.
INITIAL NOTCH DEPTH
AIR

FIGURE H2
INITIAL SURFACE STRESS
V.
INITIAL NOTCH DEPTH
SALT WATER

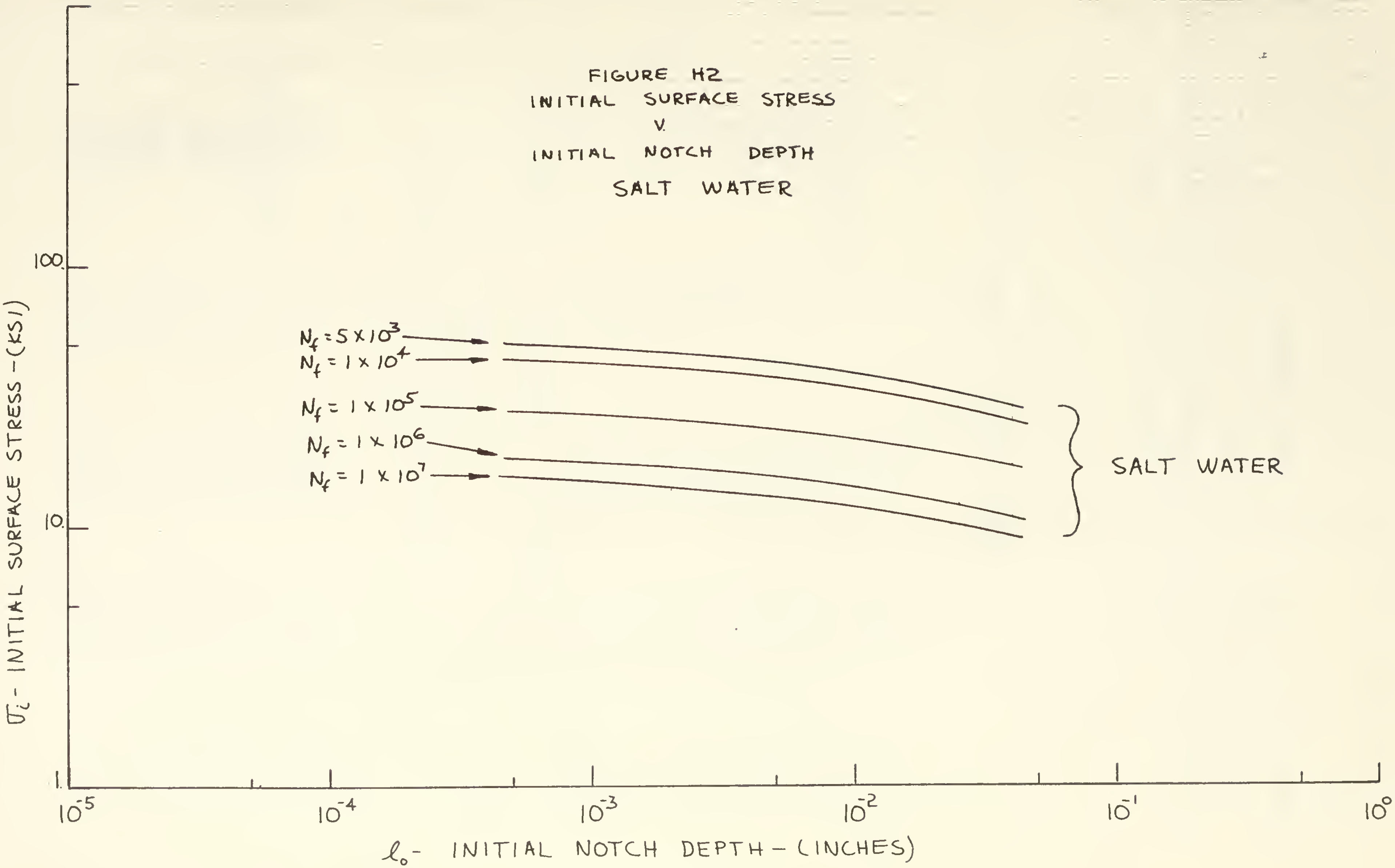

Using this data, a stress intensity (ΔK_i) was calculated for each corresponding value of σ_i and ℓ_o. The intermediate calculations and results are presented in Tables H4 through H8 for air and Tables H9 through H13 for salt water.

Table H4

Stress Intensity Results (Air)

$N_f = 5 \times 10^3$

σ_i	ℓ_o	γ	$\sqrt{\pi \ell_o}$	$\gamma\sigma_i$	ΔK_i
53.5	.0005(smooth)	1.16	.0396	62.1	2.46
50.2	.0015	1.112	.0686	55.8	3.83
49	.002	1.102	.0793	54.0	4.28
44	.006	1.050	.1373	46.2	6.34
39.5	.0115	.988	.1901	39.0	7.42
34.6	.020	.898	.2507	31.1	7.79
33	.025	.851	.2802	28.1	7.87
29	.040	.741	.3545	21.5	7.62

σ_i(Ksi) N(cycles) ℓ(in.)

Table H5

Stress Intensity Results (Air)

$N_f = 1 \times 10^4$

σ_i	ℓ_o	γ	$\sqrt{\pi \ell_o}$	$\gamma\sigma_i$	ΔK_i
47	.0005(smooth)	1.140	.0396	53.6	2.12
44	.0015	1.104	.0686	48.6	3.33
42.3	.002	1.073	.0793	45.4	3.60
38.5	.006	1.028	.1373	39.6	5.43
34.5	.0115	.972	.1901	33.5	6.37
30.3	.020	.887	.2507	26.9	6.74

Table H5 (cont'd)

σ_i	ℓ_o	γ	$\sqrt{\pi \ell_o}$	$\gamma \sigma_i$	ΔK_i
29	.025	.844	.2802	24.5	6.86
26	.040	.734	.3545	19.1	6.77

Table H6

Stress Intensity Results (Air)

$N_f = 1 \times 10^5$

σ_i	ℓ_o	γ	$\sqrt{\pi \ell_o}$	$\gamma \sigma_i$	ΔK_i
29.5	.0005(smooth)	1.082	.0396	31.9	1.26
28	.0015	1.045	.0686	29.3	2.01
27.2	.002	1.025	.0793	27.9	2.21
25	.006	.991	.1373	24.8	3.40
22.2	.0115	.942	.1901	20.9	3.98
20	.020	.867	.2507	17.3	4.35
19	.025	.824	.2802	15.7	4.39
17.2	.040	.699	.3545	12.02	4.26

σ_i (Ksi) N(cycles) ℓ(in.)

Table H7

Stress Intensity Results (Air)

$N_f = 1 \times 10^6$

σ_i	ℓ_o	γ	$\sqrt{\pi \ell_o}$	$\gamma \sigma_i$	ΔK_i
20.2	.0005(smooth)	1.055	.0396	21.3	.84
20	.0015	1.029	.0686	20.6	1.41
19.8	.002	1.009	.0793	20	1.58
18	.006	.978	.1373	17.6	2.42
16.2	.0115	.934	.1901	15.1	2.88
14.4	.020	.862	.2507	12.41	3.11

Table H7 (cont'd)

σ_i	ℓ_o	γ	$\sqrt{\pi \ell_o}$	$\gamma\sigma_i$	ΔK_i
14	.025	.820	.2802	11.5	3.22
12.9	.040	.695	.3545	8.97	3.18

Table H8

Stress Intensity Results (Air)

$N_f = 1 \times 10^7$

σ_i	ℓ_o	γ	$\sqrt{\pi \ell_o}$	$\gamma\sigma_i$	ΔK_i
19.2	.0005(smooth)	1.055	.0396	20.3	.802
18.6	.0015	1.028	.0686	19.1	1.31
18.5	.002	1.005	.0793	18.6	1.47
16.6	.006	.979	.1373	16.3	2.23
15.3	.0115	.934	.1901	14.3	2.72
14	.020	.860	.2507	12.0	3.01
13.2	.025	.817	.2802	10.8	3.02
12	.040	.694	.3545	8.33	2.95

σ_i(Ksi) N(cycles) ℓ(in.)

Table H9

Stress Intensity Results (Salt Water)

$N_f = 5 \times 10^3$

σ_i	ℓ_o	γ	$\sqrt{\pi \ell_o}$	$\gamma\sigma_i$	ΔK_i
49.8	.0005(smooth)	1.154	.0396	57.5	2.28
47	.0015	1.112	.0686	52.3	3.59
46	.002	1.086	.0793	50	3.96
41	.006	1.040	.1373	42.6	5.85
37.2	.0115	.979	.1901	36.4	6.92
33.7	.020	.895	.2507	30.2	7.56
32	.025	.848	.2802	27.1	7.60
28.3	.040	.734	.3545	20.9	7.40

Table H10

Stress Intensity Results (Salt Water)

$N_f = 1 \times 10^4$

σ_i	ℓ_o	γ	$\sqrt{\pi \ell_o}$	$\gamma\sigma_i$	ΔK_i
43.3	.0005(smooth)	1.135	.0396	49.1	1.95
41	.0015	1.089	.0686	44.6	3.06
40	.002	1.063	.0793	42.5	3.37
35.3	.006	1.019	.1373	36.0	4.94
32.3	.0115	.965	.1901	31.2	5.93
29.3	.020	.885	.2507	25.9	6.5
28.1	.025	.840	.2802	23.6	6.61
25.3	.040	.733	.3545	18.5	6.57

σ_i (Ksi) N(cycles) ℓ (in.)

Table H11

Stress Intensity Results (Salt Water)

$N_f = 1 \times 10^5$

σ_i	ℓ_o	γ	$\sqrt{\pi \ell_o}$	$\gamma\sigma_i$	ΔK_i
27.3	.0005(smooth)	1.076	.0396	29.4	1.16
26	.0015	1.041	.0686	27.1	1.86
25.3	.002	1.019	.0793	25.8	2.04
22.6	.006	.987	.1373	22.3	3.06
21	.0115	.940	.1901	19.7	3.75
19.2	.020	.866	.2507	16.6	4.17
18.4	.025	.823	.2802	15.1	4.24
17	.040	.722	.3545	12.3	4.35

Table H12

Stress Intensity Results (Salt Water)

$N_f = 1 \times 10^6$

σ_i	ℓ_o	γ	$\sqrt{\pi \ell_o}$	$\gamma\sigma_i$	ΔK_i
18	.0005(smooth)	1.052	.0396	18.9	.750
17	.0015	1.025	.0686	17.4	1.20
16.6	.002	1.004	.0793	16.7	1.32
15	.006	.975	.1373	14.6	2.00
13.5	.0115	.929	.1901	12.5	2.38
12.5	.020	.858	.2507	10.7	2.69
12	.025	.816	.2802	9.79	2.74
10.8	.040	.716	.3545	7.73	2.74

Table H13

Stress Intensity Results (Salt Water)

$N_f = 1 \times 10^7$

σ_i	ℓ_o	γ	$\sqrt{\pi \ell_o}$	$\gamma\sigma_i$	ΔK_i
15.2	.0005(smooth)	1.048	.0396	15.9	.631
14	.0015	1.021	.0686	14.3	.981
13.7	.002	1.0	.0793	13.7	1.09
12.2	.006	.971	.1373	11.8	1.63
11.3	.0115	.927	.1901	10.5	1.99
10.2	.020	.855	.2507	8.72	2.19
10	.025	.814	.2802	8.14	2.28
9	.040	.715	.3545	6.44	2.28

These results were then plotted using corresponding values of σ_i v ℓ_o for constant N_f and ΔK_i v ℓ_o for constant N_f. The plots are presented in Figures H3 and H4 for air and salt water, respectively.

These plots can be used to predict failure given either σ_i or ΔK_i and ℓ_o. They can also be used for design purposes. Design for both infinite ($N_f \geq 1 \times 10^7$ cycles) and finite ($N_f \leq 1 \times 10^7$ cycles) fatigue life can be accomplished. σ_i is shown to be independent of initial notch depth (ℓ_o) for $\ell_o < .001$ in. and increasingly dependent for larger ℓ_o. ΔK_i is independent of initial notch depth (ℓ_o) for $\ell_o > .020$ in. and increasingly dependent for smaller ℓ_o.

This information was used to determine allowable fatigue strengths (σ_{iALL}) and stress intensities (ΔK_{iALL}) for initial notch depths $\ell \tilde{<} .001$ in. and $\ell_o \tilde{>} .020$ in. for both air and salt water. The allowable values are presented in Figure H5. Figures H3 and H4 are used directly to determine fatigue life for $.001 \text{ in.} < \ell_o < .020$ in.

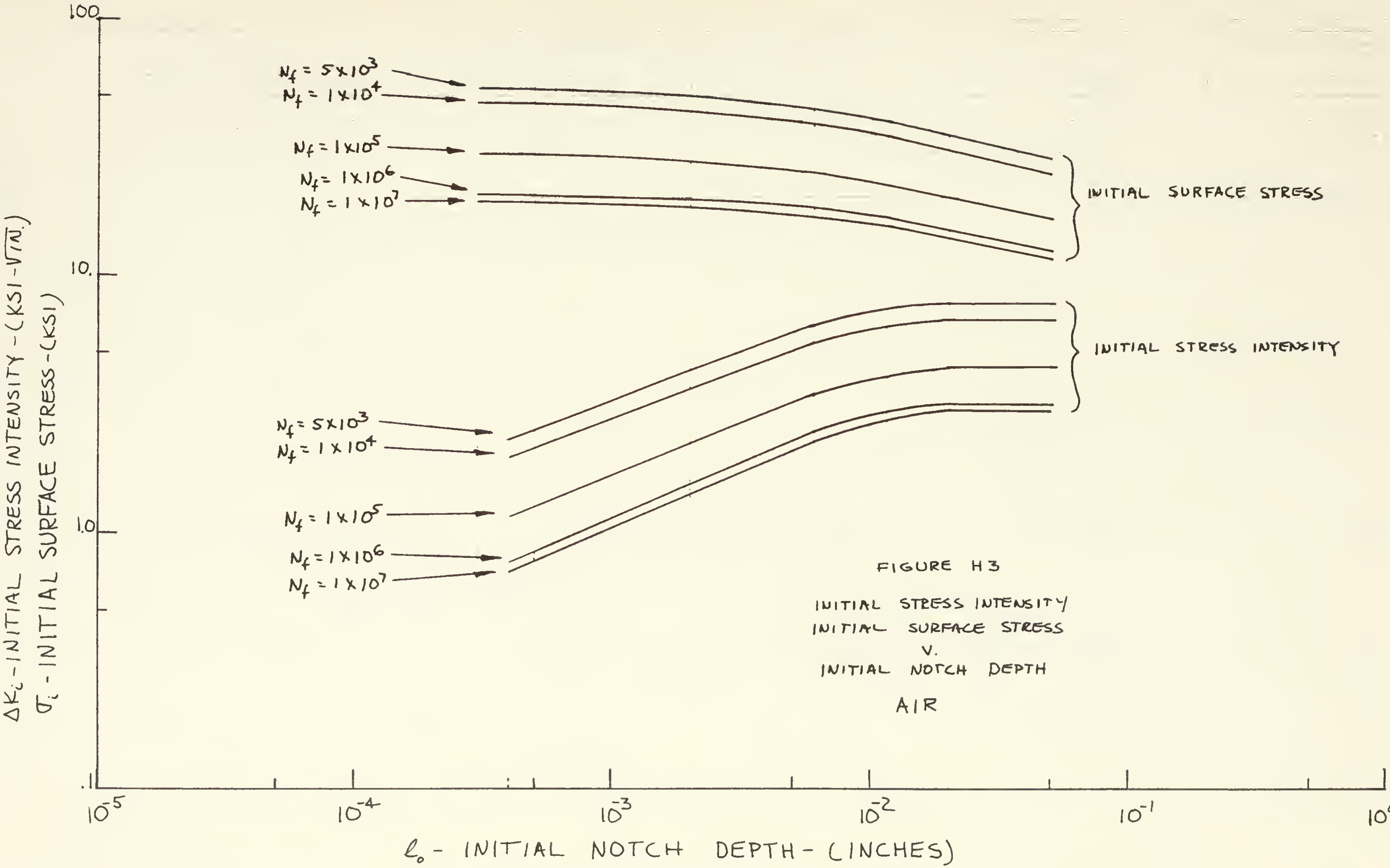

FIGURE H3

INITIAL STRESS INTENSITY/
INITIAL SURFACE STRESS
V.
INITIAL NOTCH DEPTH

AIR

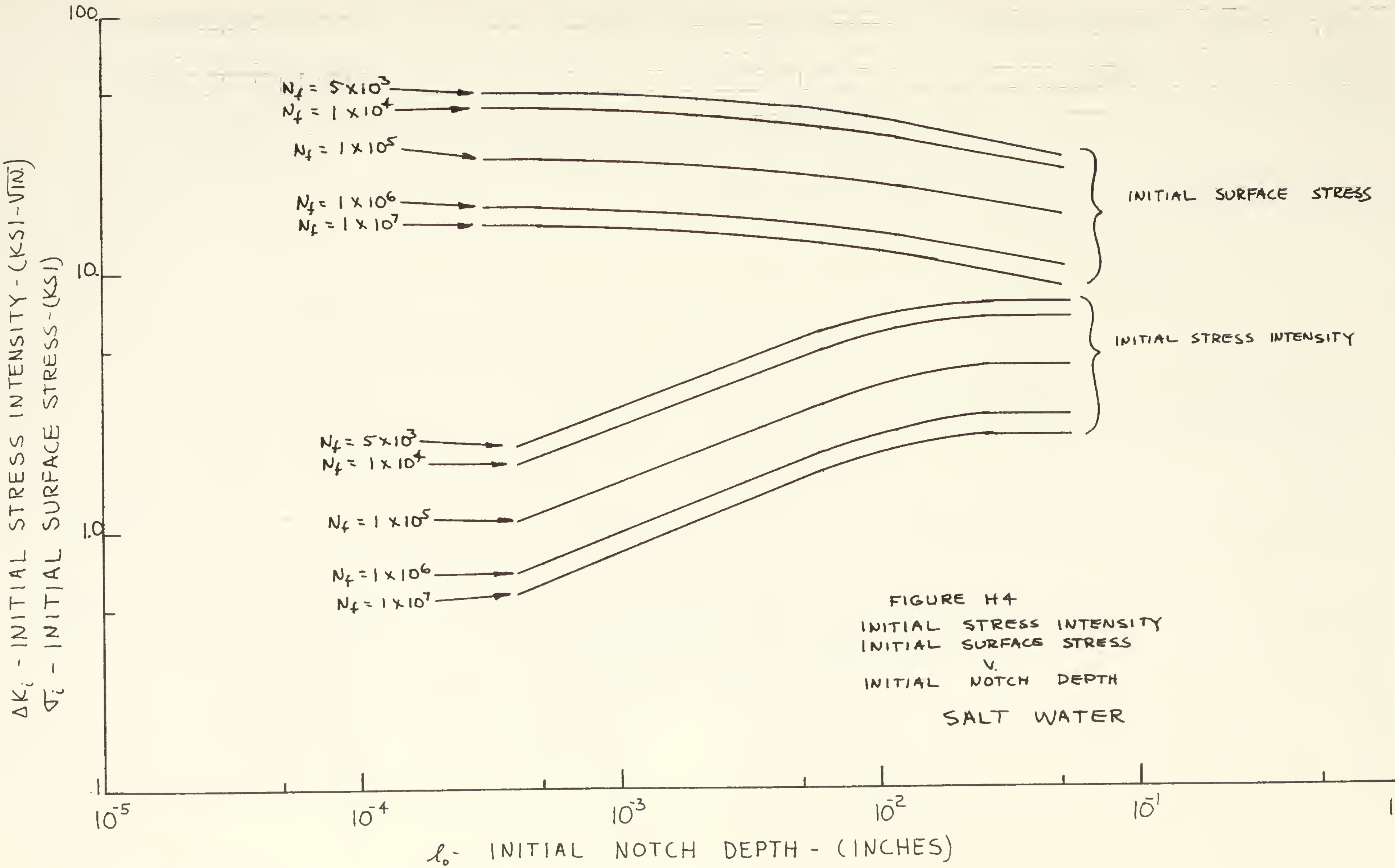

FIGURE H4

INITIAL STRESS INTENSITY
INITIAL SURFACE STRESS
V.
INITIAL NOTCH DEPTH

SALT WATER

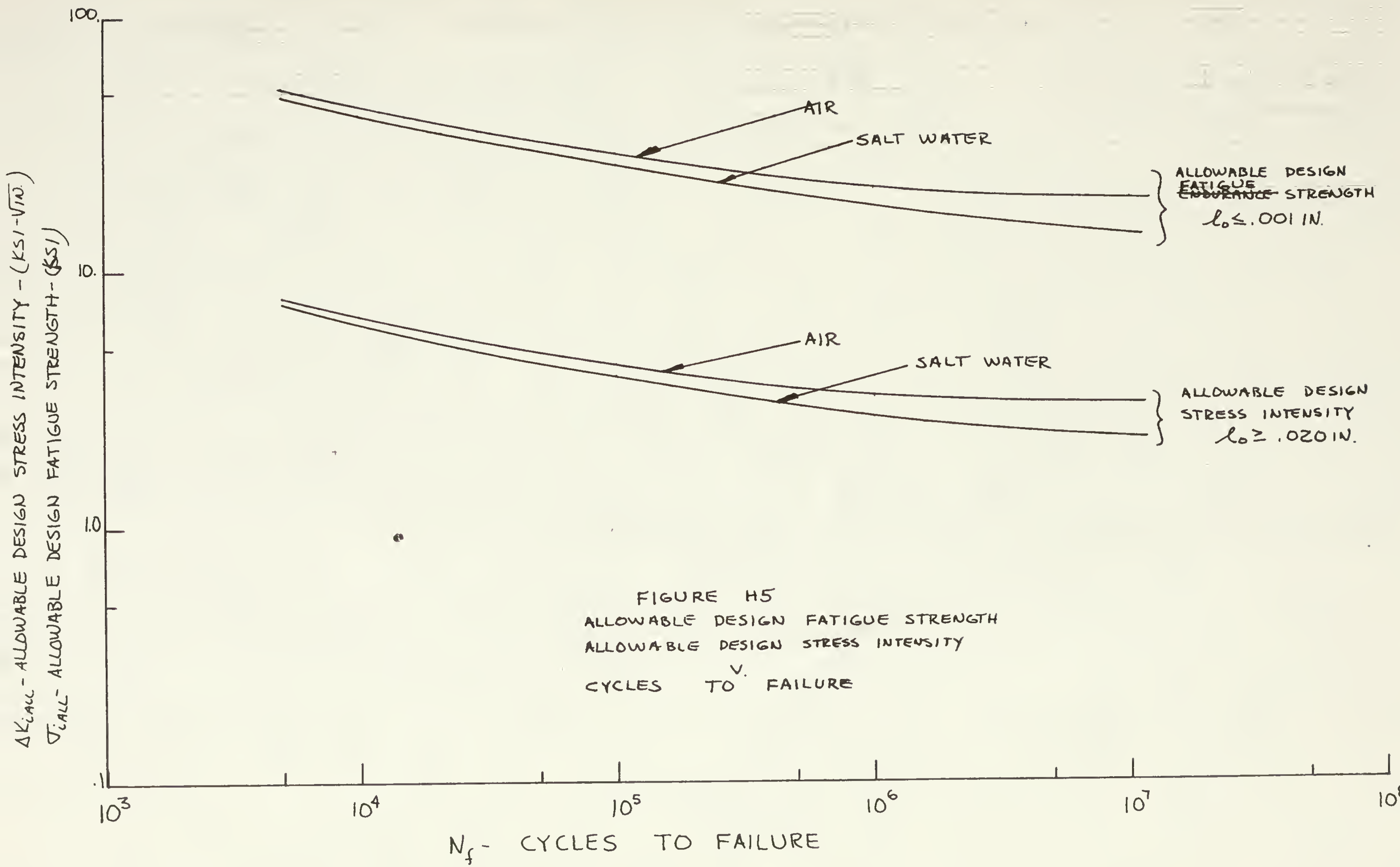

FIGURE H5
ALLOWABLE DESIGN FATIGUE STRENGTH
ALLOWABLE DESIGN STRESS INTENSITY
V.
CYCLES TO FAILURE